Dynamic Modelling and Control of MEA Absorption Processes for CO_2 Capture from Power Plants

by

Thanita Nittaya

A thesis
presented to the University of Waterloo
in fulfillment of the
thesis requirement for the degree of
Master of Applied Science
in
Chemical Engineering

Waterloo, Ontario, Canada, 2014

Author's Declaration

I hereby declare that I am the sole author of this thesis. This is a true copy of the thesis, including any required final revisions, as accepted by my examiners.

I understand that my thesis may be made electronically available to the public.

Abstract

Greenhouse gas (GHG) emission control has been extensively studied over the past decade. One GHG mitigation alternative is post-combustion carbon dioxide (CO_2) capture using chemical absorption, which is a promising alternative due to its proven technology and the relative ease to install on existing coal-fired power plants. Nevertheless, the implementation of commercial-scale CO_2 capture plants faces several challenges, such as high energy consumption, commercial availability, and geological CO_2 storage. Therefore, there is a great incentive to develop studies that provide insights needed to design and dynamically operate industrial-scale CO_2 capture plants for coal-fired power plants.

This work presents a mechanistic dynamic model of a pilot plant of a post-combustion CO_2 capture plant using the monoethanolamine (MEA) absorption processes. This model was implemented in gPROMS. The process insights gained from the sensitivity analysis, on six manipulated variables and six potential controlled variables, was used to determine promising control schemes for this pilot plant. This study then proposed three decentralized control structures. The first control scheme was designed based on the traditional-RGA (Relative Gain Array) analysis, whereas the other two control schemes were designed using heuristics. The performance evaluation of those control structures were conducted under eight scenarios, e.g. changes in flue gas composition, set point tracking, valve stiction, reboiler heat duty constraint, and flue gas flow rate. Under the condition where the reboiler temperature is to be controlled, a control scheme obtained from the heuristic showed faster response to achieve the process control objectives (90% CO_2 capture rate and 95 mol% CO_2 purity in the CO_2 product stream) than the RGA-based control scheme.

Furthermore, this study describes a step-by-step method to scale-up an MEA absorption plant for CO_2 capture from a 750 MW supercritical coal-fired power plants. This industrial-scale CO_2 capture plant consists of three absorbers (11.8 m diameter, 34 m bed height) and two strippers (10.4 m diameter, 16 m bed height) to achieve 87% CO_2 captured rate and 95% CO_2 purity in the CO_2 product stream. It was calculated that the reboiler heat duty of 4.1GJ is

required to remove 1 tonne of CO_2 at the base case condition (20 kmol/s of flue gas flow rate with 16.3 mol% of CO_2). The mechanistic model of an industrial-scale CO_2 capture plant including a proposed control structure was evaluated using different scenarios. The performance evaluation result revealed that this plant can accommodate a maximum flue gas flow rate of +22% from the nominal condition due to absorbers' flooding constraints. Moreover, it is able to handle different disturbances and offers prompt responses (After a plant is disturbed by an external perturbation, control variables in that plant are able to return to their set points in timely fashion using the adjustment of manipulated variables.) without significant oscillating signal or offset. In addition, this study highlights that the poor wetting in the strippers can be avoided by the implementation of a process scheduling, which has not been presented in any publications.

Based on the above, the mechanistic models of CO_2 absorption plants and proposed control structures provide insights regarding dynamic behaviour and controllability of these plants. In addition, the industrial-scale CO_2 capture plant model can be used for future studies, i.e. integration of power plant and CO_2 capture plant, feasibility of plant operation, and controllability improvement.

Acknowledgements

I would like to thank my supervisors, Prof. Peter L. Douglas, Prof. Eric Croiset, Assistant Prof. Luis-Ricardez Sandoval, for my opportunity to pursue the MASc degree in University of Waterloo and their invaluable guidance and support throughout my study.

I am especially grateful to my beloved family, Tawatchai and Bunruean Nittaya, for unconditional love and encouragement. I also own my special appreciation to my Canadian parents, Dallas and Irene Thill, for valuable advice and wholehearted love. I also appreciate great hospitality, friendliness, and help from my fellows, Sutham Hengsuwan, Atchariya Chansomwong, Noorlisa Harun, Lena Ahmadi, Kritsada Thammasiri, and the Thai Student Association of the University of Waterloo.

Finally, I appreciate for the financial support from the Natural Sciences and Engineering Research Council of Canada (NSERC).

Thanita Nittaya

Dedicated to my beloved parents

Table of Contents

List of Figures

List of Tables

Nomenclature

List of English symbols

a_s	Shell-side of the bundle cross flow area (m^2)
a_w	Interfacial area per unit volume (m^2/m^3)
A_{tube}	Crossectional area of a tube(m^2)
A_T	Crossectional area of a tank(m^2)
B	Baffle spacing (m)
$C^{'}$	Clearance between tubes (m)
C_p	Heat capacity (J/mol.K)
C_s	Flooding velocity(ft/s)
C_t	Ratio of the density of MEA solution to its molecular weight ($kmol/m^3$)
C_v	Valve sizing coefficient (m^2)
CH_4	Methane
CV	Controlled variable
CCS	Carbon capture and storage
CO_2	Carbon dioxide
CP	Capacity parameter
D	Diameter (m)
D_c	Diameter of the packed column (m)
D_e	Wetted perimeter (m)
E_{cond}	Accumulated energy in condenser (J)
E_{reb}	Accumulated energy in reboiler (J)
f_{Leak}	Leakage fraction of a valve
F_G	Gas molar flow rate (kmol/s)
F_{in}	Inlet molar flow rate (kmol/s)
F_L	Liquid molar flow rate (kmol/s)
$F_{L,m}$	Liquid mass flow rate (kg/s)
F_p	Packing factor (ft^{-1})
FP	Flow parameter
G_m	Mass velocity of gas stream (kg/m^2s)
G_s	Mass velocity (kg/m^2s)
GHG	Greenhouse gas
$GPDC$	Generalized Pressure Drop Correlation
h	Film coefficient for fluids in tube (w/m^2K)
h_T	Liquid level in a tank (m)
$H_{in,cond}$	Enthalpy of vapour stream entering condenser (J/mol)
$H_{V,cond}$	Enthalpy of vapour stream leaving condenser (J/mol)
$H_{L,cond}$	Enthalpy of liquid stream leaving the condenser(J/mol)
$H_{in,reb}$	Enthalpy of liquid stream entering reboiler (J/mol)
$H_{V,cond}$	Enthalpy of vapour stream leaving reboiler (J/mol)
$H_{L,cond}$	Enthalpy of liquid stream leaving reboiler (J/mol)
H_{OG}	Height of the transfer unit (m)

H_G	Film transfer unit height in gas
H_L	Film transfer unit height in liquid
HHV	High heating value (kJ/kg)
HETP	Height equivalent of a theoretical stage (m)
ISE	Integrated-Squared-Error
IMC	Internal model control
k	Conductive heat transfer coefficient (w/m^2)
k_G	Gas film mass transfer coefficient ($kmol/s.m^2kPa$)
k_L	Liquid film mass transfer coefficient (m/s)
K_Ga	Overall volumetric mass transfer coefficient for gas phase (1/h)
K_{ij}	Steady state gain between controlled variable *i* and manipulated variable *j*
K_p	Steady state process gains
m	Total MEA solution flowing in a single tube
m_{coal}	Mass flow rate of coal (kg/s)
mw_L	Molecular weight of the outlet liquid stream from valve (g/mol)
$M_{t=0}$	Value of manipulated variables at $t = 0$
$M_{new,ss}$	Value of manipulated variables at the new steady state
MEA	Monoethanolamine
MV	Manipulated variable
L	Length (m)
L_c	Total length of packed column (m)
L_m	Mass velocity of liquid stream (kg/m^2s)
L/G	Liquid – to – gas ratio
L_c/D_c	Length-diameter (L_c/D_c) ratio for a vertical vessel
n_{tube}	Number of tubes in single shell
N_{OG}	Number of overall transfer unit
N_2O	Nitrous oxide
Nu	Nusselt number
P	Operating pressure in the packed column (kPa)
P_T	Pitch size (m)
Pr	Prandtl number
PI	Proportional-Integral
ΔP	Pressure drop (Pa)
$\Delta P_{flood,tot}$	Total pressure drop in the packed column (inH_2O/ ft of packing)
Q_e	Electrical energy (MW)
Q_{cond}	Heat duty required in a condenser (watt)
Q_{reb}	Heat duty required in a reboiler (watt)
Q_{tank}	Heat duty required in a buffer tank (watt)
RGA	Relative gain array
r	Radius (m)
Re	Reynolds number
T	Temperature (K)
t	Time (h)
u	Velocity of liquid flowing in cross heat exchanger (m/s)

u_o	Operating superficial velocity (m/s)
U	Overall heat transfer coefficient
V_{SP}	Valve stem position
V_{SP}^{act}	Actual valve stem position
$y_{t=0}$	Value of a controlled variable at the initial condition
$y_{new,ss}$	Value of a controlled variable at the new steady state
Z_c	Packed bed height (m)
%CC	Percentage of CO_2 captured
%flood	Percentage of flooding velocity

Subscripts

Abs	Absorber
cond	Condenser
in	Inlet
i	Component i
mkpH2O	Makeup water
mkpMEA	Makeup MEA
i	Liquid phase
LM	Log mean
reb	Reboiler
sh	Shell
SP	Set point
tot	Total
tu	Tube
out	Outlet
v	Vapour phase

Greek symbols

α	Fractional valve opening
μ	Viscosity (kg/m.s)
y_1	Mole fraction of CO_2 in the flue gas and in the vent gas streams
y_2	Mole fraction of CO_2 in the vent gas streams
λ	Ratio of gas to liquid molar flow rate
λ_{ij}	Elements of the relative gain array matrix
Λ	Relative gain array matrix
η_{comb}	Combustion efficiency (%)
ρ_g	Density of gas
ρ_l	Density of liquid
υ	Kinematic viscosity of the liquid (centistoke)
τ_p	Open loop time constants (min)
τ_v	Valve's time constant (min)

Chapter 1
Introduction

1.1 Greenhouse gas emissions and current actions

The past century has seen many global warming effects, i.e. an increase in globally average temperature, sea level, and melting of ice. Major contributors causing these environmental impacts are anthropogenic greenhouse gas (GHG) emissions (IPCC, 2007). Carbon dioxide (CO_2), a greenhouse gases, was used to represent the qualitative GHG emission rate from emission sources. Due to economic growth and increase in energy consumption, the total world CO_2 emissions have been continuously increasing since 1980, as shown in Fig. 1.1. The primary CO_2 emission sources are coal industries, especially the electricity generation sector (IEA, 2012), since coal is a low-price fossil fuel and provides high flexibility for power plant operation.

Several greenhouse gas agreements have been set to reduce CO_2 emissions mostly from power plants. For instance, the European Union Emissions Trading System (EU ETS) aims to reduce 20% of GHG emissions from 1999 to 2020 (EU ETS, 2013) whereas the Environmental Protection Agency (EPA), in the United States, proposed a standard of CO_2 emissions from power plants with respect to the power plant technologies (EPA, 2013). Likewise, the Government of Canada issued a regulation on greenhouse gas emissions, i.e. the level of CO_2 emissions from power stations needs to be less than 420 tCO_2/GWh (Department of Justice, 2012). In order to successfully reduce GHG emissions from the electrical generation sector, several mitigation alternatives have been proposed, i.e., life cycle changes, efficiency improvement, and carbon capture and storage (CCS) technologies.

The improvement in power plants' energy efficiency can be promptly performed, i.e., process design and heat integration; nevertheless, the CO_2 reduction resulting from the efficiency improvement is quantitatively low when compared to other alternatives. That is, in addition to the efficiency improvement, the integration of the carbon capture and storage (CCS) technology to power plants should be considered as this technology offers a high level of reduction in CO_2 emissions (>90% CO_2 removal). The CCS technology is a method in which CO_2 is removed

from the flue gas stream prior to venting into the atmosphere. The captured CO_2 is then permanently stored or used for particular purposes such as enhanced oil recovery (EOR). Three potential technologies used to capture CO_2 from flue gas have been extensively studied. A pre-combustion approach, i.e. Integrated Gasification Combined Cycle (IGCC) power plant, is a technology which is able to generate electricity comparable to traditional pulverized-coal power plan but with less GHG emissions. Oxy-fuel power plant is also an attractive option as it provides high partial pressure of CO_2 in flue gas stream resulting in the ease of CO_2 removal. IGCC and Oxy-fuel power plants are considered for green field power plan due to the significant retrofit cost for existing power plants' facilities. To capture CO_2 in flue gas produced from existing power plants, a promising alternative is post-combustion capture in which CO_2 is removed from flue gas stream after coal combustion occurs.

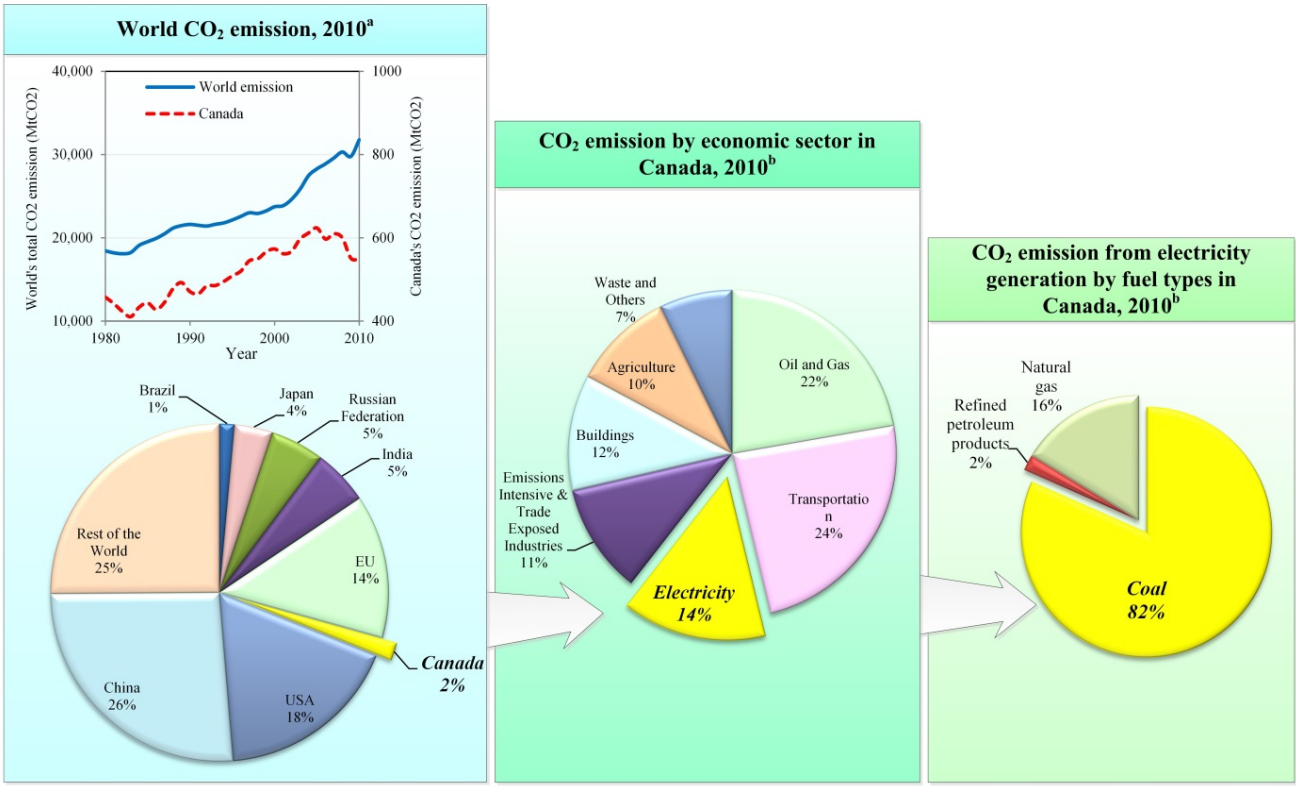

Figure 1.1 Overview of CO_2 emissions in 2010 ([a]IEA, 2012; [b]Environment Canada,2012)

1.2 Post-combustion CO_2 capture technology

Several CO_2 separation techniques can be used in post-combustion technology (see Fig. 1.2). Although the adsorption and membrane-based separations are proven technologies, they provide low selectivity and require high CO_2 concentration in the inlet gas stream (the average CO_2 concentration in the flue gas produced from coal-fired power plant is only about 13 – 15 mol%.). Physical absorption and membrane absorption offer high selectivity; however, to increase the driving force resulting in an increase in CO_2 removal, they are more suitable for high pressure flue gas streams, which leads to the requirement of additional compression unit. Because of the low CO_2 partial pressure in the flue gas stream from pulverized combustion, cryogenic separation is unlikely to be implemented in post-combustion capture. Due to low CO_2 partial pressure in the flue gas, chemical absorption is more suitable for removing CO_2 than other applications. Post-combustion CO_2 capture using chemical absorption can be connected to an existing power plant and a CO_2 compression train, as presented in Fig. 1.3.

Prior to entering the CO_2 capture plant, the particulate matter, sulfur dioxide (SO_2) and nitrogen oxide (NO_x) in the flue gas leaving the furnace are removed since those species are detrimental to the absorption process. Post-combustion CO_2 capture using chemical absorption consists of six major process units: (i) absorber; (ii) stripper; (iii) cross heat exchanger; (iv) reboiler; (v) condenser; (vi) cooler.

Moreover, additional process units may be included to improve CO_2 capture capability and minimize solvent deficiency. For example, a reclaimer is used to remove non-volatile solvent waste (Wang et al. 2011) whereas the enhancement of chemical reaction in an absorber can be achieved using the absorber with an intercooler (Schach et al. 2010). Monoethanolamine (MEA) solution is used as a sorbent in state-of-the-art CO_2 capture plants since it is readily available in the market with low price and possesses high absorption capability (over 95% CO_2 captured (Dugas, 2006)). However, MEA possesses several disadvantages (Rao and Rubin, 2002; Knudsen et al., 2009), such as internal equipment corrosion, loss of solvent due to evaporation, and oxidative degradation.

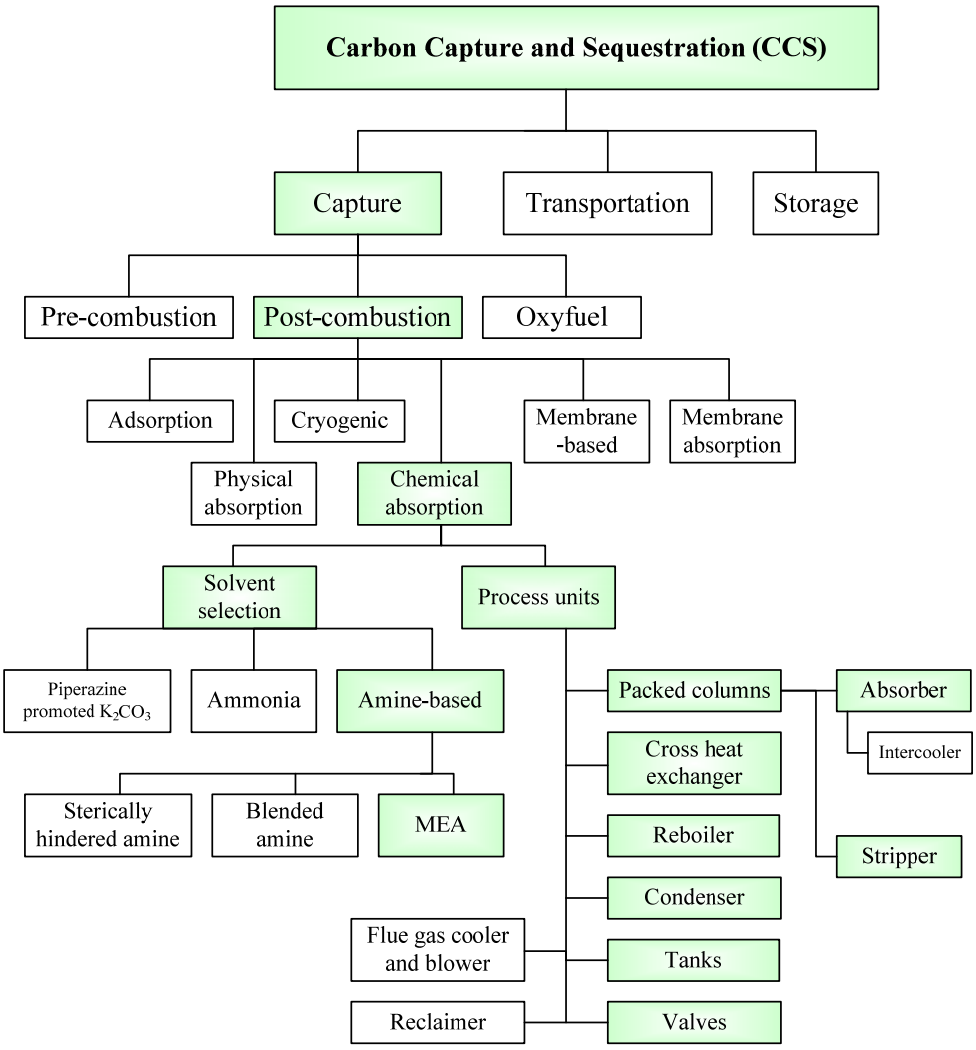

Figure 1.2 Flowsheet of carbon capture technologies (modified from Rao and Rubin, 2012 and DNV, 2010)

The key drawback of the chemical absorption is the high energy penalty, in particular to regenerate the solvent in the stripper column. Many experimental research studies on the CO_2 scrubbing process together with modelling works have been conducted and alternatives to minimize the energy impact have been proposed, for example:

i) Solvent improvement, e.g. blended amines (Aroonwilas and Veawab, 2004) and sterically hindered amine (Kansai Electric Power).
ii) Process design change, e.g. modified absorber with an intercooler, and matrix strippers (Schach et al. 2010).

iii) Process optimization, e.g. Ali et al. (2004) proposed the optimum lean loading in which the regeneration energy was minimum (in the range of 0.25 – 0.30), whereas Moser et al. (2009) presented that the operating temperature of the amine solvent entering the absorber was optimal at 314 K.

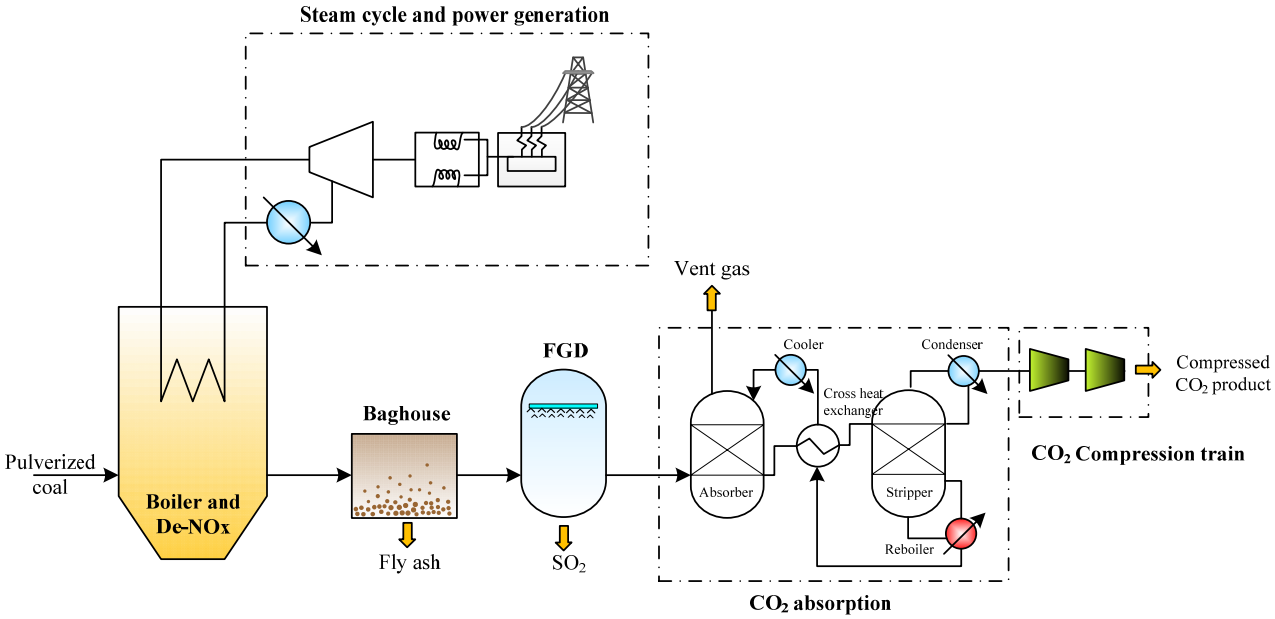

Figure 1.3 Power plant and post-combustion carbon capture processes

Also, CO_2 capture pilot plants have been built to determine the process performance (Dugas, 2006; Posch and Haider, 2010; Idem et al., 2006; Kishimoto et al., 2009 (MHI); CO2CRC, 2009). A number of modelling studies, based on experimental data provided by pilot plants were validated using mostly steady-state data, but in some cases dynamic conditions. However, only a few published papers investigated process control strategies for a CO_2 capture plant and the dynamic modelling of a commercial-scale CO_2 capture plant.

1.3 Research objectives and contribution

1) To improve the dynamic model of a MEA absorption processes for CO_2 capture from flue gas produced from the coal-fired power plant originally proposed by Harun et al. (2012) in order to represent realistic condition.
   - Several process units have been added in the process flowsheet proposed in this study. For instance, a condenser is used to attain the high CO_2 purity in CO_2 product stream entering CO_2 compression train whereas an absorber sump tank acts as the accumulator of liquid at the bottom of an absorber.
   - Additional process streams, i.e., cooling medium in a buffer tank and makeup streams of water and MEA, have been considered in this study.
2) To propose a promising control structure for CO_2 capture plant
   - Based on the insight gained from open loop dynamic response, different control schemes have been developed based on RGA analysis and heuristics.
   - Those control schemes were tested using different scenarios to analyse their controllability performance and the best control scheme was identified.
3) To develop a model of an industrial-scale CO_2 capture plant with the implementation of a promising control system.
   - Major process units' dimension and process streams' flow rates were determined based on the given power plant capacity and market availability. An industrial-scale CO_2 capture plant was then modelled.
   - A potential control scheme obtained from controllability analysis for the pilot plant model was used as a guideline for controlling an industrial-scale CO_2 removal plant.
   - The plant's performance was evaluated using different changes in operating conditions.

1.4 Outline of thesis

Chapter 2 Literature review

The studies relevant to pilot plants and industrial-scale CO_2 capture plants using amine absorption technique and process controllability analysis for CO_2 capture plant are summarised in this chapter.

Chapter 3 Pilot plant modelling and process controllability analysis

The mechanistic model development for the pilot plant of CO_2 capture processes using MEA absorption is described. Furthermore, this chapter shows the controllability study on this plant. As a result, three control schemes were proposed. The performance of each control scheme was tested using different scenarios. The content in this chapter has been published in Fuel:

- Nittaya, T., Douglas, P.L., Croiset, E., and Ricardez-Sandoval, L.A. (2014) Dynamic modelling and control of MEA absorption processes for CO_2 capture from power plants. *Fuel*. 116, 672 – 691.

Chapter 4 Industrial-Scale CO_2 capture plant modelling

The description of a scale-up methodology of an industrial-scale CO_2 captured plant with the implementation of a proposed control structure is presented. Moreover, the results of performance evaluation of this plant are shown and discussed in this chapter.

Chapter 5 Conclusions and recommendations

The key findings regarding process controllability analysis and study on a commercial-scale CO_2 capture plant are concluded in this chapter. Moreover, the Recommendation Section shows potential future research topics which can be extended from this work.

Chapter 2
Literature Review

This chapter presents an overview of published studies related to pilot plants and industrial-scale CO_2 capture plants using amine absorption technique in terms of process unit design and process controllability, which are presented in Sections 2.1 and 2.2.

2.1 Pilot plants and commercial-scale CO_2 capture plants

For decades, multiple parametric studies on the CO_2 removal process from flue gas using solvent absorption have been conducted in pilot plants, which have the capability of CO_2 capture in the range of 2 – 10 tonne of CO_2 captured per day (tCO_2/d). Example of such pilot plants are CO_2 capture pilot plant at University of Texas at Austin, the United State (Dugas, 2006), the pilot plant at RWE's Niederaussem power plant, Germany (Moser et al., 2009), the pilot plant at J-Power Matsushima Power Station, Japan (MHI, 2009), and the Boundary Dam CO_2 Pilot plant, Canada (Idem et al., 2006). Furthermore, experimental data obtained from pilot plants which were generally reported under steady state condition were used as a data input for many studies on the process modelling of CO_2 capture plant using different model implementation tools, such as ASPEN Plus, gPROMS, and MATLAB (Ziaii et al., 2009; Kvamsdal et al., 2009; Harun et al., 2010; Lawel et al., 2010).

Currently, studies on the post-combustion CO_2 capture from flue gas produced by fossil fuel power plants have been extended to commercial-scale plants. For example, Singh et al. (2003) estimated that, in order to achieve a 90% CO_2 capture from a typical 400 MW sub-critical power plant, which is approximately 7,800 tCO_2/d, a single-train CO_2 absorber's with a column diameter of 19 m is required. Therefore, in order to ensure the process operability and accelerate the implementation of full-scale CO_2 capture plants, process modelling is the most effective approach to specify the possible requirements of large-scale CO_2 capture plants. Accordingly, a few process modelling studies have proposed commercial-scale CO_2 capture plant model and used them to investigate different aspects such as economic feasibility (Singh et al., 2003; Rao and Rubin, 2006; Dowel and Shah, 2013), process integration to an existing power plant and

process optimization (Ali et al., 2005; Abu-Zahra et al., 2007; Sanpasertparnich et al., 2010) and plant performance (Lawal et al., 2012; Lin et al., 2012).

Also, a few studies have focused on the design of the absorber unit for commercial-scale plants. The low CO_2 concentration in the flue gas emitted from a pulverized coal-fired power plant (approximately 13 – 15 mol%) is a key factor that determines an absorber's diameter. Due to the fabrication limitation and a heavy support structure required for a cylinder tower, a maximum diameter of a cylinder-based absorber column of 12 – 15 m has been reported in many studies (Chapet et al., 1999; Reddy et al., 2003; Singh et al., 2003; Steeneveld et al., 2006; Ramezon and Skone, 2007; Lawal et al., 2012). Mitsubishi Heavy Industries (MHI) has proposed that a rectangular absorption tower may be appropriate for a full-scale CO_2 capture plant, i.e. 1,000 tCO_2/day capacity (MHI, 2009). Moreover, for a 500 MW sub-critical coal-fired power plant, Lawal et al. (2012) presented the effect of an absorber's height on the energy requirement and suggested that an absorber with a diameter and bed height of 9 and 27 m, respectively, may provide the minimum plant energy consumption. Furthermore, several studies have shown that the sorbent used in the chemical absorption processes also impacts the size of the process units, i.e. solvents with high CO_2 absorption capabilities might lead to small recycled amine flow rates, energy penalties and thereby size of packed columns (Aroonwilas and Veawab, 2007; Wang et al. 2011; Lawal et al. 2012).

Nevertheless, most of the previous works presented were based on steady state plant models. It is until very recently that a few dynamic modelling studies on commercial-scale CO_2 capture plants have emerged in the open literature. Lin et al. (2012) modeled an integrated flowsheet of a 580 MW coal-fired power plant, CO_2 absorption processes and CO_2 compression train using ASPEN Plus and ASPEN Dynamics. Two control structures were proposed and aimed at providing the feasibility of the plant operation based on the fractional capacity in packed columns. Lawal et al. (2012) presented a mechanistic model of the integration of a 500 MW sub-critical coal-fired power plant with an industrial-scale CO_2 capture using monoethanolamine (MEA) absorption as well as the implementation of the control scheme for that plant. That work recommended that an improvement in the tuning parameters, i.e. controller gains and time constants, might decrease the interaction between the CO_2 capture plant and the power plant.

The previous works have not provided a systematic description of the scale-up methodology of a large-scale CO_2 capture plant. In addition, the study of the dynamic behaviour of a large-scale CO_2 capture plant using a mechanistic model and its appropriate process control strategy have not been explicitly presented in the open literature.

2.2 Process control for CO_2 capture processes

Plant operability and flexibility is a key factor for industry to consider appropriate methodologies to minimize the release of greenhouse gas. Process modelling is a powerful tool to evaluate the readiness of CO_2 capture technology to be implemented at industrial scale. However, most of previous studies on the process modelling of post-combustion CO_2 capture plant were based on steady state conditions. In order to fully comprehend the operation of a CO_2 capture plant, the study of the dynamic behaviour is essential (Chikukwa et al., 2012). In addition, the implementation of control strategies and its responses to changes in the operating condition will benefit the design of an industrial-scale CO_2 capture plant.

Bedelbayev et al. (2008) presented a mechanistic model of a standalone absorber controlled by a Model Predictive Controller (MPC). The lean solution velocity was a primary manipulated variable to control the CO_2 content in the vent gas stream. The proposed control strategy displayed smooth and prompt response to the changes in the set point and the flue gas stream. Posch & Haider (2010) presented the validation of a dynamic absorber model against pilot plant data obtained from the CO_2SEPPL pilot plant at the Dürnrohr power plant in Austria. The process units in this model included an absorber, an absorber sump tank, 2 heat exchangers and 3 control valves. Three general feedback control loops were implemented for the disturbance rejection, i.e. swings of flue gas temperature and its flow rate. This study pointed out that the liquid-to-gas ratio (the ratio of the lean amine flow rate to the flue gas flow rate entering an absorber) should be maintained at the given value. However, the impact of the recycled lean solvent on the CO_2 capture effectiveness was not considered in this work. To minimize the energy consumption in the reboiler, Ziaii et al. (2009) proposed to control the amine regeneration system using a ratio between the rich amine flow rate to the reboiler heat duty to maintain the CO_2 capture rate at its set point during high electricity demands. After a step test of the reduction

of the reboiler heat duty, this control strategy improved by 1% the CO_2 capture and provided faster response to the change.

The previous published studies presented only standalone unit operation; therefore, the impact of recycle lean solvent in terms of composition, temperature and flow rate was not considered in those controllability studies. In recent years, several studies on the controllability of the complete CO_2 capture process have been published (Robinson and Luyben, 2010; Schach et al., 2010; Lawal et al., 2010; Lin et al., 2011, Panahi and Skogestad, 2011). Most of those studies implemented a *general control structure* and monitored the system's dynamic performance in the presence of typical process disturbances. There are four key variables involved in the general control structure:

i) Reboiler heat duty
ii) Lean amine flow rate
iii) Reboiler temperature
iv) Percentage of CO_2 captured

By *general control structure*, the author means two control loops of those four variables: the reboiler heat duty controlling the reboiler temperature, and the percentage of CO_2 removal adjusted by the lean solution flow rate. The other remaining control loops in the CO_2 scrubbing plant follow the principle of direction of flow, e.g. a liquid level in a tank is controlled using an outlet flow rate.

Part of an integrated gasification combined cycle (IGCC) dynamic model studied by Robinson & Luyben (2010) was the amine absorption process with the feedback control scheme. There are 4 major control loops using Proportional (P) and Proportional-Integral (PI) controllers and the setting of the individual control parameter was determined by the Tyreus-Luyben method. The process controllability was evaluated by observing the plant's response to the change in the flue gas flow rate and its CO_2 content. This study reported that the plan took 2-3 h to achieve final stable condition after the introduction of the disturbance. However, the step of control structure design and other unexpected scenarios were not discussed in this work.

Lin et al. (2011) simulated the complete plant of the CO_2 capture process including the feedback control system, based on the control objective of 90% CO_2 removal. In general, this control scheme is similar to that reported by Robinson & Luyben (2010), except the location of the makeup stream. This study pointed out that three significant process variables are required to be controlled: water makeup, amine solvent flow rate, and lean loading (the ratio of mole of CO_2 to MEA in the lean solution (moles of CO_2/ moles of MEA)). In addition, Lin et al. (2012) scaled up the CO_2 capture plant model and integrated the steam cycle and the CO_2 compression train. Also, they proposed a control scheme for handling the fluctuations in the flue gas flow rate by minimizing the change in the percentage of flooding (%flood). To achieve this, the liquid flow rate entering the absorber was maintained at a given value using the absorber's liquid inlet valve whereas the variation in the gas flow rate in the stripper was controlled using the control loop of the recycle stream of CO_2 product.

The mechanistic process model of the CO_2 capture plant, validated against pilot plant data (Dugas, 2006), was proposed by Lawal et al. (2010a). The generic PI control structure was implemented in this model and the process' transient responses to various disturbances were presented. For example, in the case of 10% reduction in the reboiler heat duty, they found the time constant of approximately 1 h and a ratio of change in reboiler heat duty to CO_2 capture of 1:1.2. Moreover, they pointed out two key operational parameters which were the impact of water makeup stream to the process efficiency and the sensitivity of CO_2 captured rate to liquid-gas ratio. Lawal et al. (2010b) scaled up the CO_2 capture plant to an industrial size with integration to the steam cycle process while using a similar control structure proposed by Robinson & Luyben (2010).

Panahi and Skogestad (2011, 2012) presented a comprehensive study of plant-wide control for the amine absorption process for CO_2 captured using the self-optimization method. In that study, the absorber and the stripper were modelled as tray columns using Unisim®; the model was validated using data obtained from the CO_2 absorption pilot plant located at the Esbjerg coal-fired power plant (Knudsen et al., 2007). Panahi and Skogestad (2011, 2012) proposed four control alternatives using RGA and dynamic RGA. The best control scheme proposed in that work, which was able to operate in two different regions of the flue gas load with low energy

consumption, consists of 10 control loops. The performance of each control structure proposed in that study was only evaluated using changes in the flue gas flow rate. Schach et al. (2010) proposed to integrate the intercooler to the absorber tower to minimize the investment costs for the CO_2 absorption process using monoethanolamine (MEA) as a sorbent. A control structure for the CO_2 scrubbing process with an intercooler based on the self-optimization method was proposed by Schach et al. (2011). However, that control structure is different from that proposed by Panahi and Skogestad (2011, 2012) and the general control structures proposed by Robinson & Luyben (2010), Lawal et al. (2010), and Lin et al. (2011). For instance, Schach et al. (2011) proposed to control the temperature set point of tray 18 in the absorber by using the inlet lean amine flow rate, and the flue gas mass flow rate was adjusted by using the rich amine flow rate and the steam flow rate fed to the reboiler.

Based on the above, a control structure design for the complete CO_2 capture process and its corresponding evaluation based on a mechanistic process model have not explicitly addressed in the published literature.

Chapter 3
Pilot Plant Modelling and Process Controllability Analysis

This chapter describes the mathematic models of process units considered in a pilot plant (Dugas, 2006). In addition, the process controllability study aiming at proposing a promising control scheme for this plant is presented. The structure of this chapter is organized as follows: Section 3.1 describes the model development of each units present in the CO_2 capture process flowsheet, i.e. packed columns, reboiler, condenser, cross heat exchanger, tanks, and valves. Section 3.2 provides the description of the operation of the CO_2 capture process at the base case condition and presents the equipment specifications. Section 3.3 identifies the process operational parameters, which were considered during the process controllability analysis, i.e. the percentage of CO_2 removal, reboiler temperature, lean amine temperature, and condenser temperature. Section 3.4 shows the open-loop responses of the process to different changes in the operating conditions, and provides a discussion corresponding to their responses. Section 3.5 describes the systematic design of the process control structure. Moreover, three control schemes for the pilot plant of CO_2 capture processes are proposed. Section 3.6 covers the performance evaluation of the proposed control structures using different scenarios, and the performance of each control structure is discussed. Finally, Section 3.7 summarises the process controllability analysis of the CO_2 scrubbing pilot plant.

3.1 Mechanistic process models

This section presents the mechanistic CO_2 capture process models used in this work to conduct the controllability analysis for this system. The process model used in this study is based on a mechanistic model proposed by Harun et al. (2012) in which the predicted temperature profiles in the absorber and stripper were successfully validated against the pilot plant data, presented in Dugas (2006), using gPROMS and Aspen Plus. The process flowsheet of the pilot plant model considered in this work is shown in Fig. 3.1. The main difference regarding the process between the present work and the work of Harun et al. (2012) is the addition of some process units, that are essential to represent the actual operation of the CO_2 capture plant, i.e., condenser (C1), absorber sump tank (A102), and reboiler surge tank (R102), and the addition of some process

streams (makeup streams of water and MEA and cooling medium in the buffer tank (T1). The importance of the additional units and process streams is described as follows:

(i) The condenser (C1) is mainly used to attain the desired CO_2 composition in the product stream and to minimize the compression power requirements downstream of the CO_2 capture process.

(ii) The absorber sump tank (A102) stores the accumulation of liquid at the bottom of the absorber (A101) tower whereas the reboiler surge tank (R102) acts as the lean solution collector in the kettle reboiler (R101).

(iii) The loss of water and MEA that occurs in the absorber (A101) and in the condenser (C1) may cause variability in the sorbent concentration in the system (material balance). Regarding the temperature bulge profile inside an absorber (Harun, 2012), two processes are occurring simultaneously:
   (a) The exothermic reaction causing an increase in temperature of the gas and liquid phases from the top towards the bottom of the column and resulting in the evaporation of water and MEA.
   (b) The condensation of water and MEA vapour by contacting with the lower temperature of the lean solution fed at the top of column (Kvamsdal et al., 2010).

   However, the net amounts of water and MEA in the vapour phase increases and results in the loss of sorbent to the vent gas stream. The loss of water and MEA also occurs in the condenser (C1). The purity of the concentrated CO_2 product stream at the base case condition is about 95 mol%; hence, the remaining contents of the product stream are water and MEA. Therefore, water and MEA makeup streams at ambient temperature (293 K) added to the buffer tank (T1) have been included in the present mechanistic process model.

(iv) A cooling medium in the buffer tank (T1) is used to maintain the lean solution temperature, which is a key factor that affects the performance of CO_2 removal in terms of thermodynamics and kinetics.

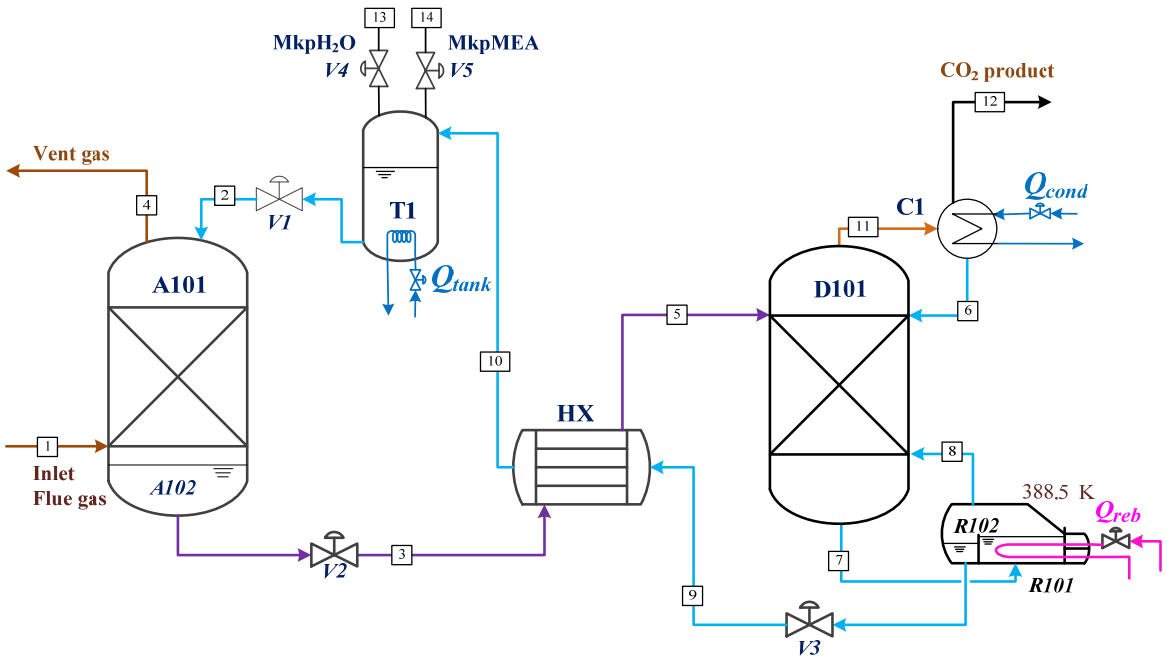

Figure 3.1 Flowsheet of the CO_2 capture pilot plant

Table 3.1 Base case operating conditions (open-loop)

Stream	Phase	Flow rate (mol/s)	Temperature (K)	Pressure (kPa)	Mole fraction			
					CO_2	H_2O	MEA	N_2
1	Gas	4.01	319.7	103.5	0.180	0.025	-	0.795
2[a]	Liquid	32.9	314	103.5	0.029	0.871	0.100	-
3[a]	Liquid	33.4	327.8	103.5	0.049	0.853	0.098	-
4	Gas	3.4	313	101.3	0.009	0.062	6E-5	0.929
5	Liquid	33.4	350	160	0.049	0.853	0.098	-
6	Liquid	0.2	314	159.5	0.041	0.956	0.003	-
7	Liquid	36.1	378.7	160	0.032	0.876	0.092	-
8	Gas	3.4	388.4	160	0.067	0.931	0.002	-
9	Liquid	32.7	388.4	160	0.029	0.870	0.101	-
10	Liquid	32.7	366.5	160	0.029	0.870	0.101	-
11	Gas	0.9	350.7	159.5	0.770	0.230	6E-4	-
12	Gas	0.7	314	159.5	0.950	0.046	1E-6	-
13	Liquid	0.2	298	103.5	-	1	-	-
14	Liquid	2E-4	298	103.5	-	-	1	-

[a] The lean loading is 0.29 whereas the rich loading is 0.5.

As shown in Fig. 3.1, the process flowsheet considered in the present analysis, represents a major improvement to that proposed in Harun et al. (2012) and provides a more realistic description of the CO_2 capture plant's dynamic behaviour. In addition, the input information for the normal operating condition in the pilot plant was based on the condition studied by Harun et al. (2012), i.e. the flue gas flow rate (Stream 1) is 4.01 mol/s, and its composition is 18 mol% CO_2 whereas the absorbent entering the absorber (Stream 2) is the MEA solution with the concentration of 10 mol% MEA. That is, the operating conditions of other process streams at the base case condition, presented in Table 3.1, were estimated using the mechanistic model of the pilot CO_2 capture plant.

Moreover, the key novelty introduced in the present study is the development, implementation and testing of three different control strategies on the CO_2 capture plant; such a controllability study was not performed in Harun et al. (2012). Therefore, the present study aims at providing insight regarding the dynamic operation of a CO_2 capture plant in closed-loop in the presence of several scenarios that reflect more accurately the true operating conditions for this process. The mechanistic process model used in this study is described next.

3.1.1 Packed columns

The absorber and stripper towers were modelled using the rate-based approach considering the mass transfer between the gas and liquid phases based on the two-film theory. The difference between the absorber and the stripper models was the assumption of the chemical reaction complexity. The absorber model considered the kinetics reaction based on the exothermic reaction at moderate operating temperature (~320K). Moreover, the enhancement factor, which describes the actual mass transfer rate in this unit, was considered in the absorber model. On the other hand, the instantaneous reaction occurring at high operating temperatures (~380 K) was assumed in the stripper model. Accordingly, the stripper model was developed based on the equilibrium reaction. More details regarding the mathematic models of the packed columns can be found in Harun et al. (2012).

3.1.2 Reboiler and condenser

The reboiler and condenser units were modelled as flash drums where the outlet vapor and outlet liquid flow rate were determined based on the equilibrium condition at given operating conditions (Harun et al., 2012). Both models were the same except for the sign on the heat duty as shown in Equations 3.1 and 3.2, the negative sign on ($-Q_{cond}$) indicates energy removal and the positive sign on ($+Q_{reb}$) indicates the energy required in the reboiler (Harun et al., 2012).

$$\frac{dE_{cond}}{dt} = F_{in,cond}H_{in,cond} - F_{V,cond}H_{V,cond} - F_{L,cond}H_{L,cond} - Q_{cond} \tag{3.1}$$

$$\frac{dE_{reb}}{dt} = F_{in,reb}H_{in,reb} - F_{V,reb}H_{V,reb} - F_{L,reb}H_{L,reb} + Q_{reb} \tag{3.2}$$

From Equations 3.1 and 3.2, E_{cond} (J) and E_{reb} (J) are the accumulated energy in the condenser and the reboiler, respectively; Q_{cond} (watt) and Q_{reb} (watt) represent the heat duties required in the condenser and the reboiler, respectively. In the condenser, $F_{in,cond}$ (mol/s) stands for the inlet vapour stream, and two outlet streams are the vapour flow rate, $F_{V,cond}$ (mol/s), and the liquid flow rate, $F_{L,cond}$ (mol/s). The enthalpy of inlet and outlet vapour streams is represented by $H_{in,cond}$ (J/mol) and $H_{V,cond}$ (J/mol), respectively; whereas, $H_{L,cond}$ (J/mol) is the enthalpy of liquid leaving the condenser. Likewise, in the reboiler, the inlet stream is in the liquid phase, $F_{in,reb}$ (mol/s), whereas the outlet streams are the lean amine flow rate, $F_{L,reb}$ (mol/s), and the vapour flow rate entering the stripper, $F_{V,reb}$ (mol/s). The enthalpy of the liquid stream entering the reboiler is $H_{in,reb}$ (J/mol). The enthalpies of the product streams are: $H_{L,reb}$ (J/mol), the enthalpy of outlet liquid, and $H_{V,reb}$ (J/mol), the enthalpy of outlet vapour.

3.1.3 Cross heat exchanger

The cross heat exchanger, HX in Fig. 3.1, is used to conserve the heat duty of the fluids by heating the cold rich amine solution with the hot lean solution stream. The hot lean stream flows inside the shell whereas the cold rich stream flows through the tubes to prevent corrosion and ease the heat exchanger's maintenance, e.g. tube repair. In case of a tube leakage, one merely plugs the failed tube or replaces the tube bundle if needed. The heat exchanger was modelled as a one-tube-pass counter-current shell and tube heat exchanger. The outlet liquid streams'

temperature of the fluids on the shell and tube sides are selected by providing the upstream conditions.

The assumptions made in the model development of this unit are:

1. Counter current shell and tube heat exchanger
2. Pressure drop is negligible
3. No phase change

The energy balance equations for a single shell and tube are as follows:

$$\frac{\partial T_{tube}}{\partial t} = \frac{-u_{tube}}{L}\frac{\partial T_{tube}}{\partial z} + UT_{LM}\frac{\pi D_{tube}}{\rho_{tube}A_{tube}C_{p,tube}} \tag{3.3}$$

$$\frac{\partial T_{shell}}{\partial t} = \frac{-u_{shell}}{L}\frac{\partial T_{shell}}{\partial z} - UT_{LM}\frac{n_{tube}\left(\pi D_{tube}\right)}{\rho_{shell}A_{shell}C_{p,shell}} \tag{3.4}$$

where T_{tube} (K) and T_{shell} (K) describe the temperature profiles in a single tube and shell, respectively; the liquid velocity flowing in the tube and shell is represented by u_{tube} (m/s) and u_{shell} (m/s), respectively; ρ_{tube} (mol/m^3) and ρ_{shell} (mol/m^3) are the liquid densities in the tube and in the shell, respectively; heat capacities of the liquids are represented by $C_{p,shell}$ (J/mol.K) and $C_{p,tube}$ (J/mol.K); n_{tube} is the number of tubes in a single shell. The size of a single tube is described by the tube's cross-sectional area, A_{tube} (m^2) and the tube's diameter, D_{tube} (m), respectively. Likewise, A_{shell} (m^2) and D_{shell} (m) stand for the cross-sectional area and the diameter of the shell, respectively; L (m) represents the length of tube and the shell is assumed to be the same for both sides.

The overall heat transfer coefficient (U, W/m^{2}K) describes the total mass transfer coefficient of the conductive heat transfer coefficient of the tube metal (k_{tu}, W/m^2), the film coefficient for fluids in tube (h_{tu}, w/m^{2}K) and in shell (h_{sh}, w/m^{2}K), i.e., (Incropera and Dewitt, 2002)

$$U = \frac{1}{\frac{1}{h_{sh}} + \frac{r_{tu,i}}{k_{tu}}\ln\frac{r_{tu,o}}{r_{tu,i}} + \frac{1}{h_{tu}}} \tag{3.5}$$

where $r_{tu,i}$ (m) and $r_{tu,o}$ (m) are the internal and outer radius of a tube, respectively. Assuming that the liquid flow characteristic in a tube is turbulent flow and no phase change occurs in a tube, a film coefficient for fluids in the tube (h_{tu} ,w/m^{2}K) is estimated from the Nusselt number (Nu) using the equation, as follows (Incropera and Dewitt, 2002):

$$Nu = \frac{h_{tu} D_{in,tu}}{k} = 0.027\,\mathrm{Re}^{0.8}\,\mathrm{Pr}^{1/3}\left(\frac{\mu}{\mu_w}\right)^{0.14} \tag{3.6}$$

where k (kg/m.s) is the thermal conductivity at the bulk fluid temperature; $D_{tu,in}$ (m) is the internal diameter of a tube; μ (kg/m.s) is the viscosity at the bulk fluid temperature; μ_w (kg/m.s) is the viscosity of the fluid at the wall temperature; Re is Reynolds number ($Re=4m/\mu\pi D_{tu,in}$); m is the total MEA solution flowing in a single tube; and Pr is the Prandtl number ($Pr = \mu C_p/k$). Likewise, the film coefficient for fluids on a shell side (h_{sh}) is also determined using Nusselt number (Nu) as follows (Kern, 1965):

$$Nu = \frac{h_{shell} D_e}{k} = 0.36\left(\frac{G_s D_e}{\mu}\right)^{0.55}\mathrm{Pr}^{1/3}\left(\frac{\mu}{\mu_w}\right)^{0.14} \tag{3.7}$$

where G_s (kg/m^{2}s) is the liquid mass velocity ($G_s = F_{L,m}/a_s$); $F_{L,m}$ (kg/s) is the mass flow rate of liquid on shell side; a_s (m^2) is the cross flow area on a shell side ($a_s = D_{in,sh}\,C'B/P_T$); B (m) is the baffle spacing (the number of baffles can be increased to improve heat transfer); C' (m) is the clearance between the tubes (about 0.25 $D_{out,tu}$); $D_{in,sh}$ (m) and $D_{out,tu}$ (m) are the internal diameters of shell and the outer diameter of a tube, respectively; P_T (m) is the pitch size (approximately 1.25 $D_{out,tu}$). The tube clearance and the pitch size depend on the layout of the tubes (see Fig. 3.2), i.e. square pitch and triangular pitch. The triangle pitch was used in this work as this tube arrangement provides greater heat transfer rate and higher tube density (number of tubes in a single shell) in a shell when comparing to the square pitch (Mukherjee, 1998; Branan, 2005). Similarly, D_e (m) is the wetted perimeter which is expressed as follows (Kern, 1965):

$$D_e = \frac{4\left(P_T^2 - \frac{\pi}{4}D_{tu,out}^2\right)}{\pi D_{tu,out}} \tag{3.8}$$

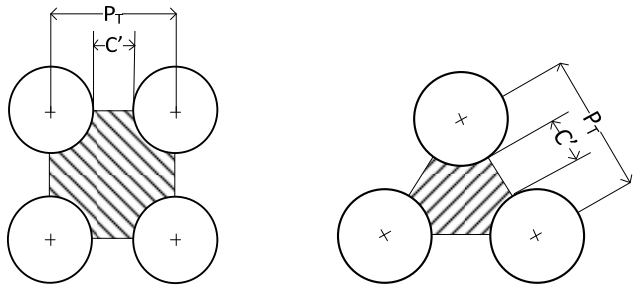

(a) Square pitch (b) Triangular pitch

Figure 3.2 Equivalent diameter of each tube arrangement (Kean, 1965)

3.1.4 Tanks

3.1.4.1. Buffer tank

The buffer tank, T1 in Fig. 3.1, acts to dampen fluctuations in the lean MEA flow rate prior to entering the absorber. As shown in Fig. 3.1, this tank has a cooler as well as water and MEA makeup streams. The water and MEA makeup flow rates are calculated based on the overall material balance in the CO_2 capture process, i.e.

$$F_{mkpH_2O} = F_{v,out,Cond,H_2O} + F_{v,out,Abs,H_2O} - F_{v,in,Abs,H_2O} \tag{3.9}$$

$$F_{mkpMEA} = F_{v,out,Cond,MEA} + F_{v,out,Abs,MEA} - F_{v,in,Abs,MEA} \tag{3.10}$$

where F_{mkpH2O} (mol/s) and F_{mkpMEA} (mol/s) are the makeup liquid flow rates of water and MEA, respectively; $F_{v,out,Cond,H2O}$ (mol/s) and $F_{v,out,Cond,MEA}$ (mol/s) are the vapour flow rates of water and MEA leaving the condenser, respectively; $F_{v,out,Abs,H2O}$ (mol/s) and $F_{v,out,Abs,MEA}$ (mol/s) are the vapour flow rates of water and MEA leaving the absorber, respectively; $F_{v,in,Abs,H2O}$ (mol/s) and $F_{v,in,Abs,MEA}$ (mol/s) are the vapour flow rates of water and MEA in the flue gas stream entering the absorber, respectively.

The material balance equation for the buffer tank is expressed as follows:

$$A_T \frac{dh_T}{dt} = \frac{F_{in,tot}}{\rho_{in}} - \frac{F_{out,tot}}{\rho_{out}} \tag{3.11}$$

where A_T (m^2) is the crossectional area of a tank; h_T (m) is the liquid level in a tank; ρ_{in} (kmol/m^3) and ρ_{out} (kmol/m^3) represent the liquid densities of the inlet and outlet streams; and

$F_{in,tot}$ (kmol/s) is the total liquid flow rate entering a tank. The total molar flow rate leaving a tank ($F_{out,tot}$, kmol/s) depends on the valve sizing coefficient (C_v, m^2) and the fractional valve opening (α), also called *flow characteristic*, i.e.,

$$F_{out,tot} = \frac{C_v \alpha}{mw_L} \sqrt{\rho_{out} \Delta P} \tag{3.12}$$

where ΔP (Pa) is the pressure drop across the valve and mw_L (g/mol) is the molecular weight of the outlet liquid stream.

In order to maintain the temperature in the lean amine stream entering the absorber, the energy removal term (- Q_{tank}) was included in the energy balance equation for the buffer tank, i.e.,

$$\frac{dE_{tank}}{dt} = F_{in,tank} H_{in,tank} + F_{mkpH_2O} H_{mkpH_2O} + F_{mkpMEA} H_{mkpMEA} - F_{out,tank} H_{out,tank} - Q_{tank} \tag{3.13}$$

where E_{tank} (J) is the energy accumulated in the buffer tank; $F_{in,tank}$ (mol/s) and $F_{out,tank}$ (mol/s) are the lean amine flow rates entering and leaving the buffer tank, respectively; Q_{tank} (W) is the heat duty removed from the buffer tank. Moreover, $H_{in,tank}$ (J/mol) represents the enthalpy of the lean amine inlet stream; H_{mkpH2O} and H_{mkpMEA} (J/mol) represent the enthalpy of the makeup water and MEA, respectively, whereas $H_{out,tank}$ (J/mol) denotes the enthalpy of liquid leaving the buffer tank.

3.1.4.2. Absorber sump tank and reboiler surge tank

The absorber sump tank (A102 in Fig. 3.1) model describes the liquid accumulated at the bottom of the absorber due to changes in the inlet flue gas flow rate or in the lean amine flow rate. Likewise, the reboiler surge tank (R102 in Fig. 3.1) acts as the lean amine solution collecting compartment in the kettle reboiler (R101) (Fig. 3.3). The level of the rich solution in the absorber must be controlled to ensure that the column will not flood or dry up. In addition, the sump tank ensures that the residence time in the absorber unit is sufficient to minimize foaming resulting from the solution contaminants (Kohl and Nielsen, 1997). The residence time is typically 3 – 5 min (GPSA, 1999) depending upon the process configuration. The absorber sump tank and the reboiler surge tank models neglect the loss of energy.

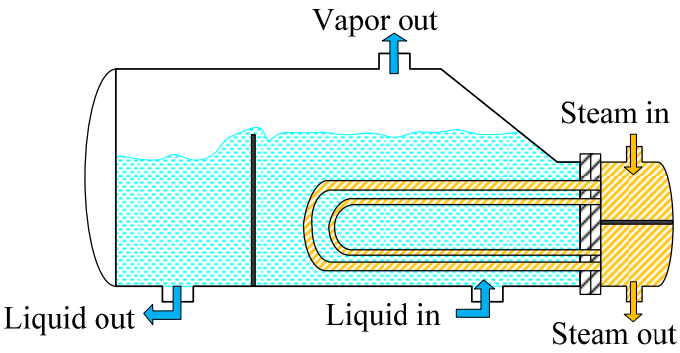

Figure 3.3 Kettle reboiler

3.1.5 Valves

The control valve is modelled using the correlation of valve's time constant (τ_v) and a valve stem position (V_{SP}) (Thomas, 1999). The valve time constant (τ_v) determines how fast an actual valve stem position (V_{SP}^{act}) achieves a stem position set point (V_{SP}), i.e. if the valve's time constant is high, the valve stem position approaches the desired point slowly. At steady state, the actual valve stem position (V_{SP}^{act}) is normally at the same position as the set point of the valve stem position (V_{SP}), $V_{SP}^{act} = V_{SP}$. The assumptions made to simulate the valve model are:

1) Globe valve
2) Linear valve characteristic
3) Very small liquid passing flow rate
4) No phase changes across a valve
5) No temperature change across a valve

The expression of an actual valve stem position (V_{SP}^{act}) is written as follows:

$$\tau_v \frac{dV_{SP}^{act}}{dt} = V_{SP} - V_{SP}^{act} \tag{3.14}$$

Moreover, the leakage fraction (f_{Leak}) of a valve was taken into account to determine the fractional valve opening (α) which is one of the variables used to calculate the outlet liquid flow rate of a valve, in Eq. (3.12). The leakage fraction represents the liquid flow rate passing through a valve although a valve stem position is at the fully closed position. The fractional valve opening (α) was determined using the equation as follows (gPROMS PML, 2012):

$$\alpha = \frac{V_{SP}^{act} + f_{Leak}}{1 + f_{Leak}} \tag{3.15}$$

In addition, the size of each valve was identified by the sizing valve coefficient (C_v) which was computed using Eq. (3.12) based on the estimated liquid flow rate flowing through such a valve to obtain the valve stem position of 50% opening at the normal operating condition (Seborg et al., 2012).

3.2 Base case operating condition

As shown in Fig. 3.1, the flue gas, assumed to be free of sulphur dioxide (SO_2) and low in moisture, flows to the bottom of the absorber whereas a lean amine solution containing approximately 10 mol% MEA (30 wt%) is fed at the top. The low temperature in the absorber enhances the exothermic reaction between the CO_2 contained in the flue gas and the MEA solution. Scrubbed flue gas, low in CO_2, is vented to the atmosphere. The rich amine solution (with 4.8 mol% of CO_2 content) leaves the absorber and flows to the cross heat exchanger. The lean amine solution, hot and less corrosive fluid entering the shell side, transfers heat to the cold rich amine stream flowing in the tube side. Then the hot rich amine solution enters the stripper column. Due to the relatively high operating temperature in the stripper, an instantaneous reversible reaction occurs that produces a liquid stream with 2.7 mol% CO_2 content and a rich CO_2 vapour stream. The concentrated CO_2 vapour stream leaves the stripper and flows to the condenser to remove any water and MEA prior to entering the compression train (not included in this flow sheet). The liquid stream, mostly water, condensed in the condenser flows to the top of the stripper and combine with the rich amine stream flowing from the outlet of the cross heat exchanger. The lean sorbent stream leaves the reboiler and enters the cross heat exchanger and the buffer tank thereafter. The sorbent concentration in the entire CO_2 absorption system is maintained by the two makeup streams of water and MEA mixed in the buffer tank. The lean solution is cooled in the buffer tank to enhance absorption efficiency prior to entering the absorber. The open-loop plant's energy required (total reboiler heat duty per tonne of CO_2 captured (Rao and Rubin, 2002)) at the base case condition was approximately 5 GJ/tCO_2. Considering a packing hydraulics using 1.5" random packings (Kister, 1992), the fractional

capacities, or the percentage of flood (*%flood*) in the absorber and the stripper were 33% and 23%, respectively. This indicates that the CO_2 capture pilot plant might run at the minimum plant capacity since the packed column is typically designed to operate in the range of 30% to 80% of flood (Tontiwachwuthikul, 1990). Likewise, the equipment specification and the operating conditions are shown in Table 3.1 and Table 3.2, respectively.

Table 3.2 Equipment specification and operating condition for pilot plant model

Parameter	**Value**	**Remark**
Absorber (A101)		
- Internal diameter (m)	0.43	(Dugas, 2006)
- Height (m)	6.1	(Dugas, 2006)
- Packing size (mm)	IMTP#40	(Dugas, 2006)
- Nominal packing size (m)	0.038	(Dugas, 2006)
- Specific area (m^2/m^3)	143.9	(Dugas, 2006)
- Operating temperature (K)	314 – 329	(Dugas, 2006)
- Operating pressure (kPa)	101.3 – 103.5	(Dugas, 2006)
Stripper (D101)		
- Internal diameter (m)	0.43	(Harun et al., 2012)
- Height (m)	6.1	(Harun et al., 2012)
- Packing size (mm)	IMTP#40	(Harun et al., 2012)
- Operating temperature (K)	350 – 380	(Harun et al., 2012)
- Operating pressure (kPa)	159.5 – 160	(Harun et al., 2012)
Reboiler (R101)		
- Operating temperature (K)	383 – 393	(Harun et al., 2012)
- Operating pressure (kPa)	160	(Harun et al., 2012)
Condenser (C1)		Additional unit in the present work
- Operating temperature (K)	312 – 315	
- Operating pressure (kPa)	159	
Cross heat exchanger (HX)		
- Internal diameter of shell (m)	0.305	(Edward, 2008)
- Internal diameter of tube (m)	0.148	(Edward, 2008)
- Outer tube diameter of tube (m)	0.190	(Edward, 2008)
Buffer tank (T1)		
- Internal diameter (m)	2	
Absorber sump tank (A102)		Additional unit in the present work
- Internal diameter (m)	0.43	
Reboiler surge tank (R102)		Additional unit in the present work
- Internal diameter (m)	0.43	

Parameter	Value	Remark
Valves		
C^*_v of V1 (m^2)[a]	1.01×10^{-3}	
C^*_v of V2 (m^2)[a]	0.85×10^{-3}	Additional unit in the present work
C^*_v of V3 (m^2)[a]	0.85×10^{-3}	

[a]Unit of sizing valve coefficient (C_v) is typically reported as either m^2 or $gpm/psi^{1/2}$ and the equation for unit conversion is $C_v\ (m^2) = 2.3837 \times 10^{-5}\ C^*_v (gpm/psi^{1/2})$

3.3 Process operational parameters

3.3.1 CO_2 removal (*%CC*)

The percentage of CO_2 captured (*%CC*) is defined as the amount of CO_2 captured per total CO_2 entering the plant. This metric is widely used to measure the performance of CO_2 removal process (Rao and Rubin, 2002; Panahi and Skogestad, 2011; Harun et al., 2012). The expression of the percentage of CO_2 captured is defined as follows:

$$\%CC(t) = 1 - \frac{y_{CO_2,out,Abs}(t)\,F_{v,out,abs}(t)}{y_{CO_2,in,Abs}(t)\,F_{v,in,abs}(t)} \tag{3.16}$$

where $y_{CO2,in,Abs}$ and $y_{CO2,out,Abs}$ are the mole fraction of CO_2 in the total flue gas stream and in the vent gas stream at a given time t, respectively, whereas $F_{v,in,Abs}$ (mol/s) and $F_{v,out,Abs}$ (mol/s) are the molar flow rate of the flue gas and the vent gas streams at time t, respectively.

3.3.2 Reboiler temperature (T_{reb})

The lean amine stream leaving the stripper is heated in the reboiler to promote the reversible chemical reactions that regenerate the amine solution. Overheating, however, in the reboiler causes carbamate polymerization, an MEA degradation product, produced in the stripping section due to the presence of CO_2 in the aqueous amine solution at high temperature (Chi and Rochelle, 2002). Thus, the operating temperature range in the reboiler (T_{reb}) needs to be maintained in the range of 383 – 393 K (Harun, 2012).

3.3.3 Lean amine temperature

Aroonwilas & Tontiwachwuthikul (2000) showed that an increase in the lean amine temperature from 298 K to 309 K resulted in a proportional increase of CO_2 captured due to the enhancement of the rate of the second-order reaction in the absorber. Nevertheless, a further increase in the temperature from 309 K to 318 K causes a reduction in the absorption efficiency as it is dominated by thermodynamics properties instead of kinetics. The solubility of CO_2 into amine solvent is explained by Henry's constant which increases with temperature. The higher Henry's constant value means that CO_2 tends to be in the gas phase rather than in the liquid phase. Accordingly, the operating temperature of the lean amine solution entering the absorber in this mechanistic model is maintained approximately at 314 K at which the optimum operating condenser temperature was proposed by Moser et al. (2009).

3.3.4 Condenser temperature

A high concentration of CO_2 in the product stream is desired to reduce the compression costs. As shown in Fig. 3.4, the condenser temperature is inversely related to the CO_2 content in the vapour phase; this relationship allows one to control the CO_2 purity in the product's stream using inferential control, i.e., controlling the condenser's temperature indirectly controls the CO_2 purity in the product's stream. The benefit of inferential control is that it avoids the need/expense for an online CO_2 gas analyzer, and instead uses an inexpensive thermocouple. In this case, the cooling water flow rate entering the condenser has a direct effect on the condenser's temperature and therefore is considered as a potential manipulated variable for this system. The correlation used in this work to determine the condenser temperature (T_{cond}, K) based on the mole fraction of CO_2 in the CO_2 product stream ($y_{CO_2,out,Cond}$) is as follows:

$$T_{cond} = -5{,}351.5(y_{CO_2,out,Cond})^2 + 9{,}777.7(y_{CO_2,out,Cond}) - 4{,}143.3 \qquad (3.17)$$

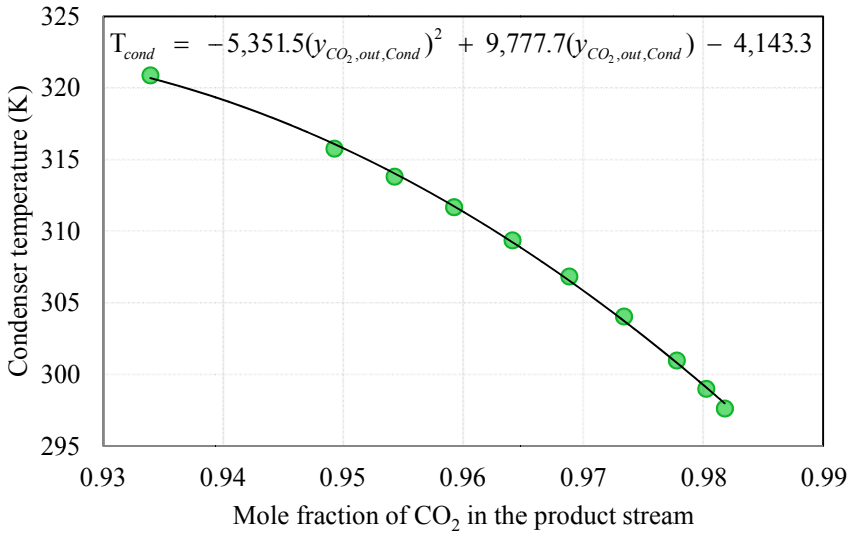

Figure 3.4 Effect of T_{cond} on the CO_2 purity in the product stream

3.4 Open-loop process analysis

Open-loop responses are the actions of process variables to a change in operating condition without the involvement of a controller's action. The analysis of the open-loop process responses aims to provide insights regarding the non-linear behaviour of key process variables during the transient condition, i.e. %CC, T_{reb}, and lean loading. Using the process flowsheet in Fig. 3.1, three scenarios were conducted, i.e., ramp change in the flue gas flow rate, sinusoidal change in the flue gas flow rate, and change in the reboiler heat duty. The results and discussions of these analyses are described as follows.

3.4.1 Ramp changes in the flue gas flow rate

This scenario represents the effect of changes in different magnitudes of the flue gas flow rates with respect to the base case condition (4.01 mol/s), on key process parameters, i.e. %CC, reboiler temperature and lean loading. Disturbances in the flue gas flow rate (±7.5% and ±10% of the flue gas flow rate at the base case condition) were introduced to the plant at the third hour of operation for 30 min (Fig. 3.5a). The increase (decrease) in the flue gas flow rate, which had lower temperature (319 K) when compared to the temperature of amine solution at the bottom of

the absorber (328.6K), caused the reduction (increase) in the rich amine stream's temperature leaving the absorber (stream 3 in Fig. 3.1) as shown in Fig.3.5c. Consequently, the decrease (increase) in T_{reb} (Fig. 3.5d) due to constant reboiler heat duty (Q_{reb}), led to an increase (decrease) in the lean loading, i.e. CO_2 concentration in the recycled lean solvent stream was increased (decreased) as shown in Fig. 3.5f. Therefore, the CO_2 capture rate in the absorber decreased (increased) (Fig. 3.5b) due to the increase (decrease) in the flue gas flow rate. Moreover, the non-linear relationship between %CC and the flue gas flow rate can be seen in Fig. 3.5b. For example, the disturbance in +10% of the flue gas flow rate resulted in a reduction in %CC by 11% and the plant took about 6 h to reach the new steady state condition whereas the plant required 3 h to achieve +3% of CO_2 capture rate increase due to the reduction in the flue gas flow rate of 10%.

In addition, Figures 3.5g and 3.5f present the effect of changes in the flue gas flow rates on the condenser temperature (T_{cond}) and the CO_2 concentration in the CO_2 product stream (stream 12 in Fig. 3.1). For instance, the increase in the flue gas flow rate resulted in a reduction in the reboiler temperature and the operating temperature in the stripper (D101). That is, the vapour flow rate leaving from the top of the stripper decreased. Since the constant condenser heat duty (Q_{cond}) was maintained, the reduction in the vapour flow rate entering the condenser (C1) led to the decrease in T_{cond} (Fig. 3.5g) and the increase in the CO_2 purity in the CO_2 product stream (Fig. 3.5h).

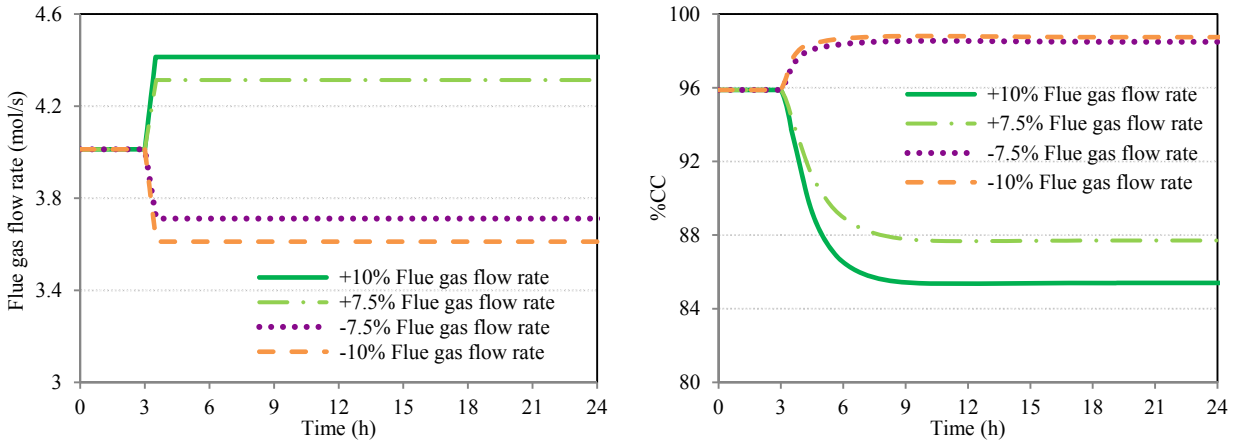

(a) (b)

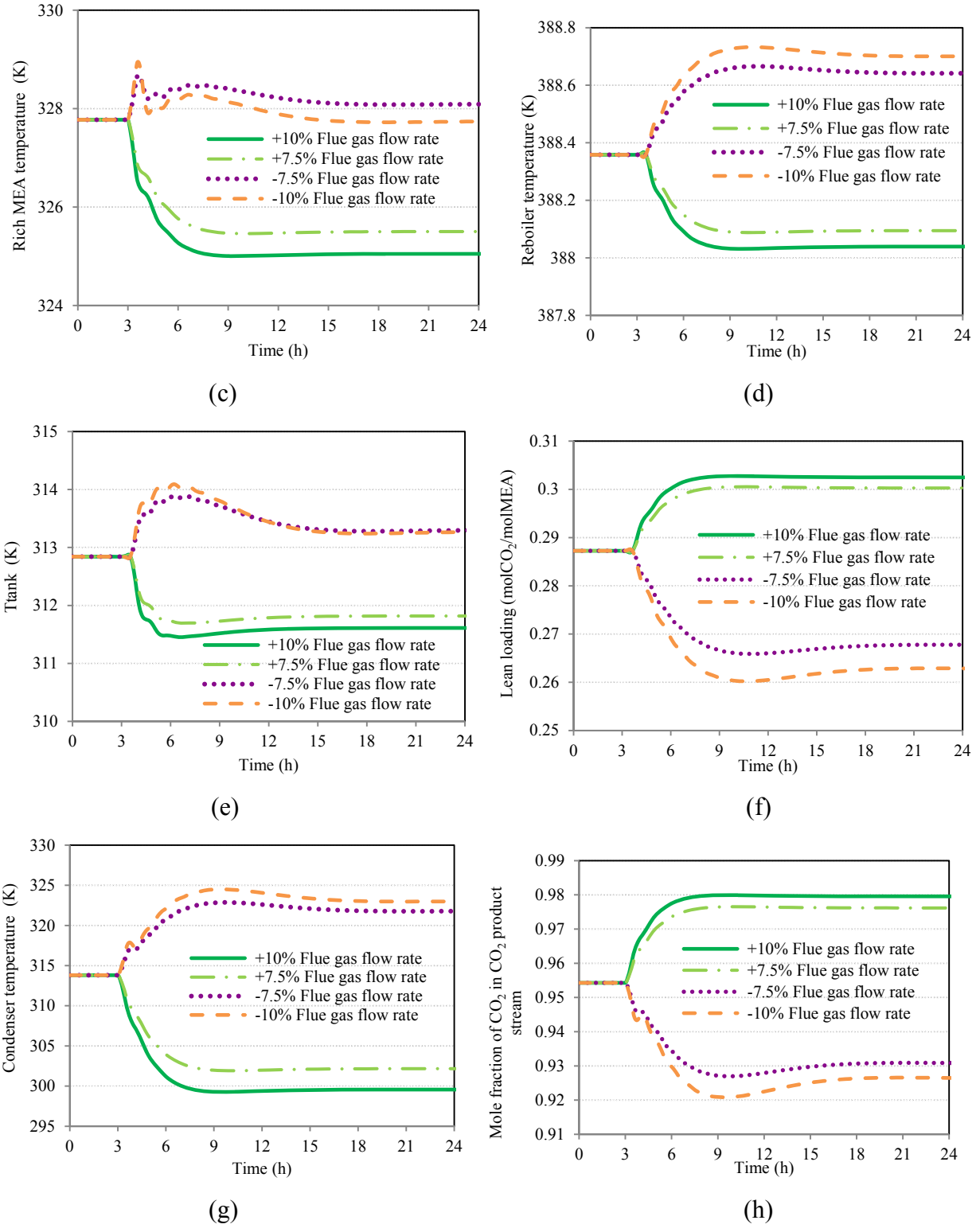

Figure 3.5 Open-loop responses of process variables to ramp changes in the flue gas flow rate: (a) Flue gas flow rate; (b) %CC; (c) Rich MEA temperature; (d) T_{reb}; (e) T_{tank} (Lean MEA temperature); (f) Lean loading; (g) T_{cond}; and (h) Mole fraction of CO_2 in CO_2 product stream

3.4.2 Sinusoidal change in the flue gas flow rate

Variation in the power demand over the course of the day results in changes in the flue gas flow rate. A sinusoidal change in the flue gas flow rate, with the maximum and minimum amplitudes of 4.4 mol/s and 3.6 mol/s was introduced to the plant for a period of 48 hours (2 days) (Fig. 3.6a). The oscillating response of %CC in the range of 86.5% to 98.7% which inversely related to the change in the flue gas flow rate was observed. A similar inversely proportional correlation was also observed in the response of the reboiler temperature which varied between 388.1 K and 388.7 K, as shown in Fig. 3.6b. However, the variation in the lean loading, between 0.26 and 0.30, was directly proportional to the change in the flue gas flow rate. That is, the lean loading decreased due to the reduction in the flue gas flow rate or vise-versa.

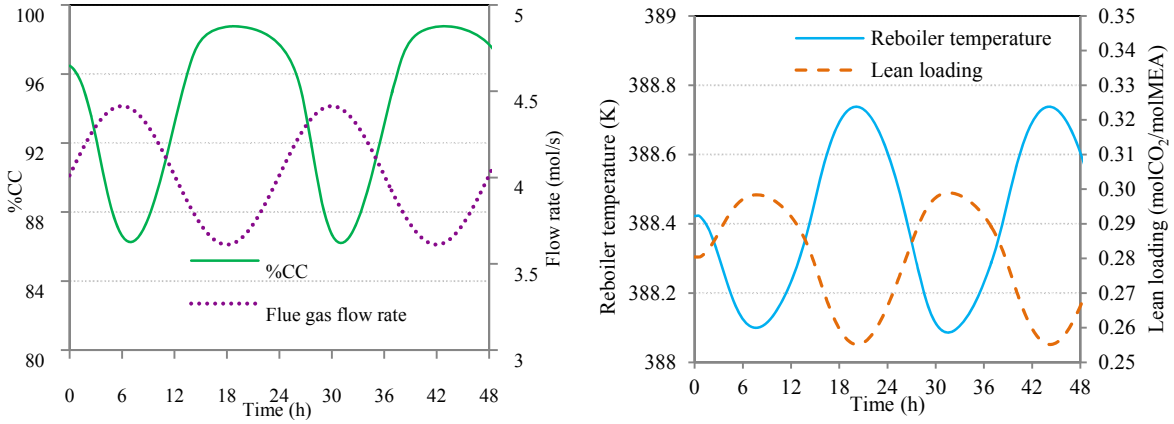

(a) (b)

Figure 3.6 Openloop responses of process variables to the change in the flue gas flow rate: (a) Flue gas flow rate and %CC; and (b) T_{reb} and lean loading

3.4.3 Changes in the reboiler heat duty

The analysis of changes in the reboiler heat duty (Q_{reb}) was conducted to determine the influence of the reboiler heat duty on the CO_2 removal performance (%CC) and the condenser temperature (T_{cond}). Disturbances in the reboiler heat duty were applied to the plant for 10 min after the plant had been operated for 3 h, as shown in Fig. 3.7a. Fig. 3.7b illustrates that the responses of the CO_2 removal rate (%CC) resulting from changes in Q_{reb} are a directly proportional and non-linear relationship. For example, an increase in Q_{reb} resulted in an increase in T_{reb} and vapour

flow rate leaving the reboiler; therefore, the CO_2 content in the reboiler's outlet liquid stream was decreased. In other words, the lean loading in the recycled lean MEA stream (Fig. 3.7c) was reduced, and the CO_2 absorption capability of the lean amine solution increased. However, as shown in Fig. 3.7b, the effect of the reboiler heat duty on %CC was relatively slow since the plant took about 7 h to converge to the new steady state after the change in the operating condition. The ratio of change in the reboiler heat duty to %CC was approximately 1:1.4.

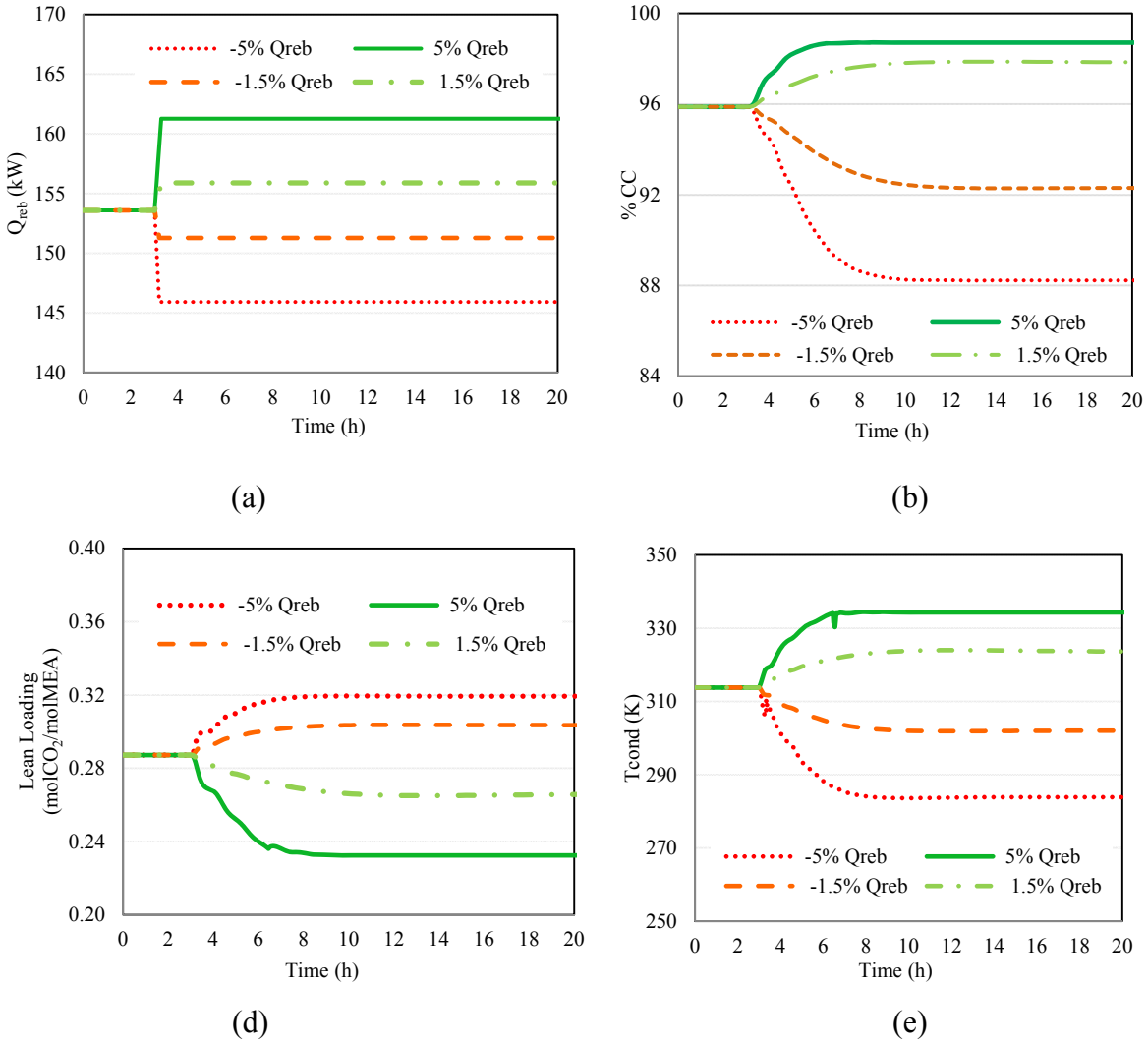

Figure 3.7 Openloop responses of process variables to changes in Q_{reb}:
(a) Q_{reb}; (b) %CC; (c) Lean loading; and (d) T_{cond}

3.5 Controllability analysis of the CO_2 capture process pilot plant

This section presents the methodologies used to specify the control structures proposed for the CO_2 scrubbing processes for the pilot plant described in the previous sections. The procedure used to design control schemes for this plant follows several steps (see Fig. 3.8 and additional description of the general design procedure of control system provided in Appendix A):

1) Specification of the process control objectives
2) Selection of manipulated and controlled variables
3) Sensitivity analysis
4) Relative gain array (RGA) analysis
5) Identification of a basic control scheme using RGA analysis
6) Specification of additional control structures based on process insights gained from different performance tests, known as heuristic approach.
7) The heuristic-based control structure was tested using the same scenarios and criteria as used to test the performance evaluation of the RGA-based control scheme.

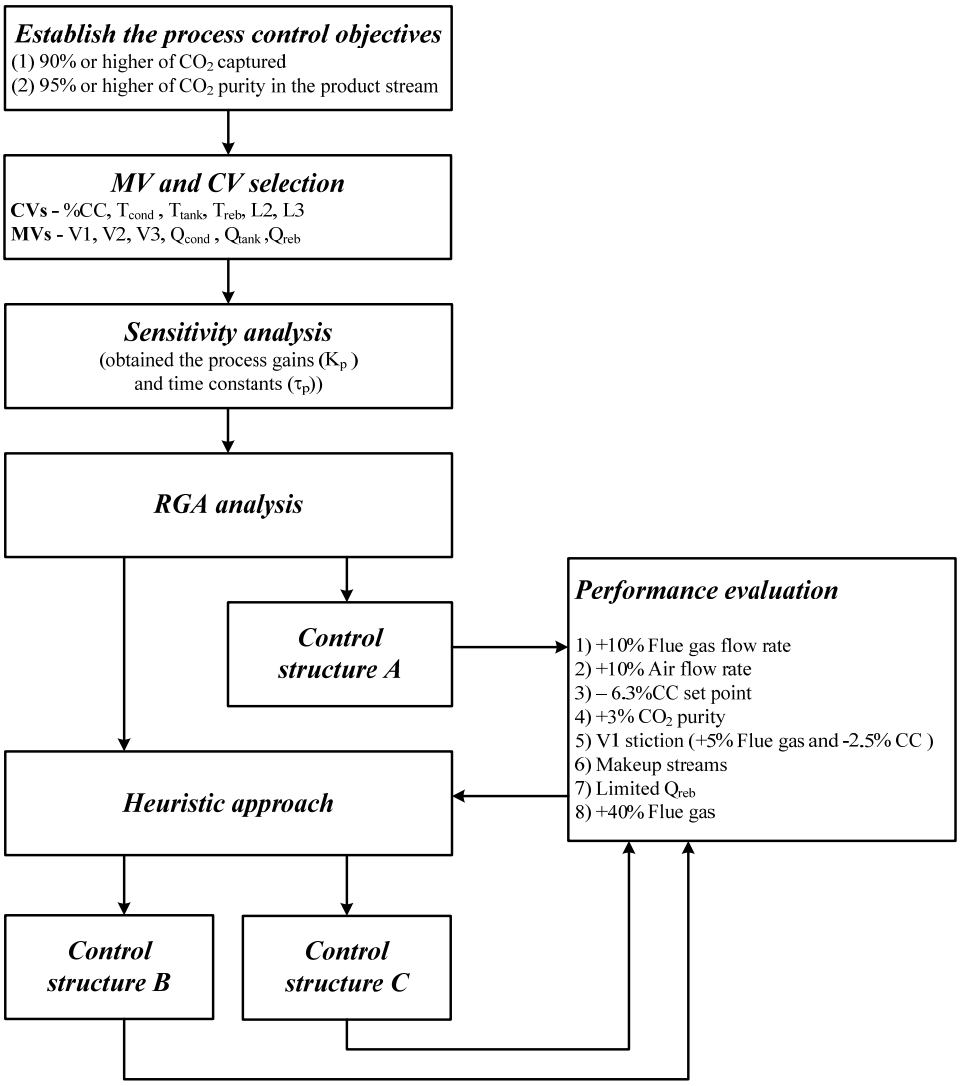

Figure 3.8 Controllability analysis methodology for the pilot plant

3.5.1 Process control objectives

The performance of the control structures was evaluated according to the following process control objectives:

(i) CO_2 removal of 90% or higher (see Eq. (3.16))
(ii) CO_2 composition in the gas product stream leaving the condenser at 95 mol% or higher.

3.5.2 Selection of manipulated and controlled variables

The next step in this analysis is the identification of the manipulated (MV) and controlled (CV) variables. As shown in Fig. 3.1, the CO_2 capture system has eight manipulated variables (valves) that can be used for control. Three of these valves can be used to regulate heating and cooling mediums, i.e., the reboiler heat duty (Q_{reb}), the condenser duty (Q_{cond}), and the buffer tank heat duty (Q_{tank}), whereas the other five valves adjust the process liquid flow rates, i.e., the outlet valve of the buffer tank (V1), the outlet valve of the absorber sump tank (V2), the outlet valve of the reboiler surge tank (V3), the water makeup valve (V4) and the MEA makeup valve (V5).

First, the controlled variables that need to be in closed-loop to maintain the inventories in the system need to be identified. For the present system, there are three liquid levels that need to be controlled, i.e., the absorber sump tank (A102), the reboiler surge tank (R102) and the buffer tank (T1). Gas inventory control was not considered in this analysis because linear pressure drop was assumed in both packed columns. Apart from the process operational constraints described in Section 3.3, there are other process variables that have a significant effect on the system's efficiency to capture CO_2, i.e. the MEA concentration in the lean stream, the lean loading, the liquid-to-gas ratio and the MEA flow rate in the lean stream.

Aroonwilas et al. (2001) emphasized that a high lean amine flow rate entering the absorber enhanced the wetted area of the packing elements in the absorber unit and eventually increased CO_2 absorption. Also, the amine concentration in the lean sorbent needs to be lower than 30 wt% MEA to mitigate corrosion in the system and the lean loading needs to be in the range of 0.25 – 0.30 to reduce energy consumption (Abu-Zahra et al., 2007; Alie et al., 2005). The variation in MEA concentration and the lean loading depends on the change in the reboiler temperature since an increase in the reboiler temperature reduces the CO_2 content in the lean amine stream, resulting in decreasing lean loading and increasing MEA concentration. The MEA concentration and lean loading are indirectly controlled by the control of T_{reb}. Table 3.3 summarizes the set of potential manipulated and controlled variables considered for this process.

Table 3.3 List of manipulated variables and controlled variables

Variable		Nominal steady state value
MV1	Condenser heat duty (Q_{cond})	8.6 kW
MV2	Buffer tank heat duty (Q_{tank})	164.3 kW
MV3	Reboiler heat duty (Q_{reb})	153.6 kW
MV4	Outlet valve position of the buffer tank (V1)	32 % opening
MV5	Outlet valve position of the absorber sump tank (V2)	50 % opening
MV6	Outlet valve position of the reboiler surge tank (V3)	50 % opening
CV1	Condenser temperature (T_{cond})	313.8 K
CV2	Lean amine temperature (T_{tank})	312.8 K
CV3	Reboiler temperature (T_{reb})	388.4 K
CV4	Percentage of CO_2 removal (%CC)	95.9 %
CV5	Liquid level in absorber sump tank (L2)	0.3 m
CV6	Liquid level in reboiler surge tank (L3)	0.3 m

Note that the water and the MEA makeup flow rates can either automatically control the level in the buffer tank or manually control the lean sorbent concentration in the buffer tank. In fact, the makeup flow rates are adjusted when the liquid level in the buffer tank is low and/or when a laboratory operator routinely analyses the sorbent properties, i.e. concentration, pH, foaming, and finds that it is off-specification, e.g., when MEA concentration is higher than 30 wt%. In the present work, makeup flow rates of water and MEA were computed based on the overall process material balance (see Eqs. (3.9) and (3.10)); that is, these flow rates are automatically controlled to maintain the amount of water and MEA in the system. A similar approach was used by Panahi and Skogestad (2012), i.e., the makeup stream of water is assigned to a manual control mode due to its low flow rate. Based on the above, the liquid level in the buffer tank and makeup stream valves for water (V4) and MEA (V5), as shown in Fig. 3.1, were not considered as either controlled or manipulated variables. Moreover, the flow rate and temperature of reflux stream coming from the condenser were approximately 0.2 mol/s and 314 K, respectively, whereas those of the hot rich MEA stream flowing from the cross heat exchanger to the stripper were about 33.5 mol/s and 350 K, respectively. The relatively high flow rate and temperature of the rich amine stream fed to the top of the stripper results in the reflux stream having little effect on the change in the regeneration efficiency of the stripper. That is, the stripper reflux stream was not included as a controlled variable in this study.

3.5.3 Sensitivity analysis

The next step in the controllability analysis was to perform a sensitivity analysis on the system using the mechanistic process model described in Section 3.1. Sensitivity analyses provide insight into the process dynamics and are also used to identify the process gains (K_p) and time constants (τ_p). Similarly, this analysis is essential for control structure selection. To perform the sensitivity analyses, all of the six manipulated variables shown in Table 3.3 were individually step changed by ±2.5% to ±10% of its nominal (steady-state) setting. The process gains and time constants between each manipulated variable and all the potential controlled variables were then calculated. The sensitivity analyses showed that there is an inversely proportional correlation between the condenser heat duty (Q_{cond}) and the condenser temperature (T_{cond}), shown in Fig. 3.9a the more heat removed from the condenser unit the lower the condenser temperature. A similar correlation exists in other pairs, i.e. the buffer tank heat duty (Q_{tank}) and the lean amine stream temperature (T_{tank}), the liquid level in the absorber sump tank (L2) and the valve stem position of V2, and the reboiler temperature (T_{reb}) and the valve stem position of V2 (Fig. 3.9b).

Likewise, the sensitivity analyses identified the directly proportional-related correlations, i.e. Figures 3.10a and 10b show the T_{reb} responses to changes in Q_{reb} and the variation in the liquid level in A102 due to changes in the valve stem position of V1.

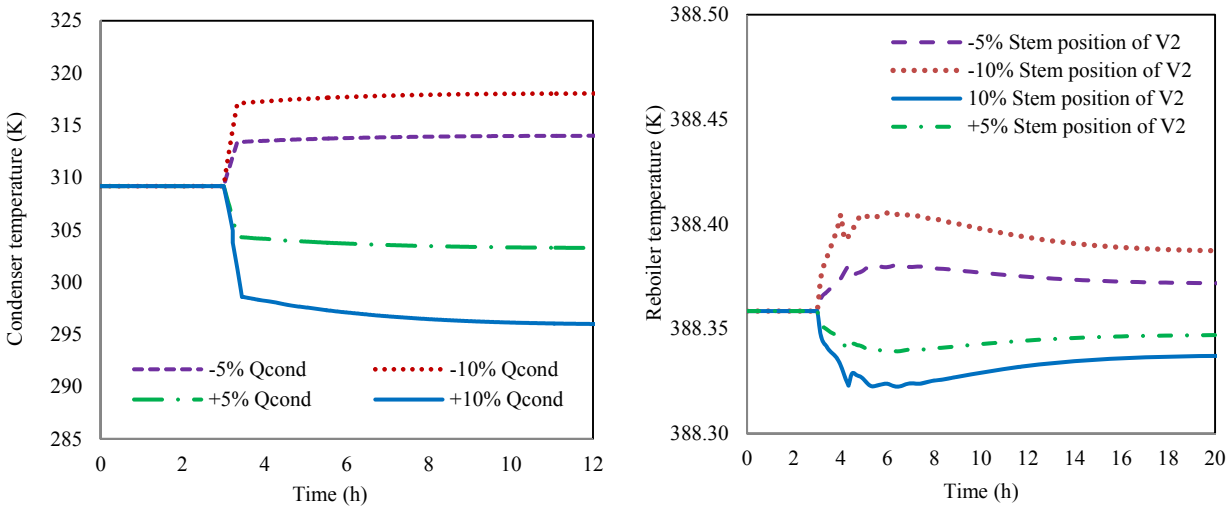

(a) (b)

Figure 3.9 Samples of inversely proportional correlations: (a) T_{cond} and Q_{cond} and (b) T_{reb} and V2

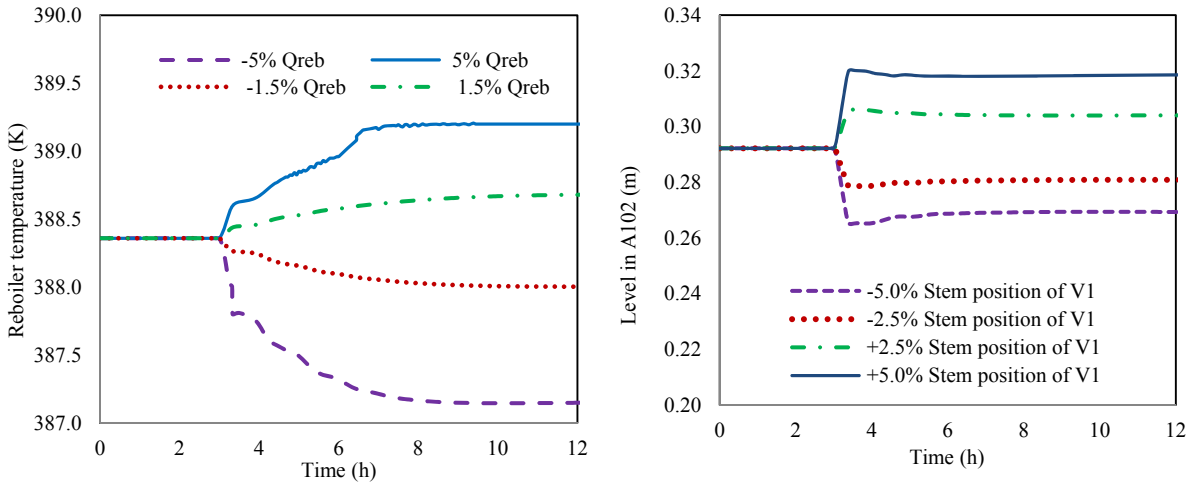

(a) (b)

Figure 3.10 Samples of directly proportional correlations:
(a) T_{reb} and Q_{reb} and (b) L2 and V1

In addition, Fig. 3.11a shows that the CO_2 removal (%CC) has the *inverse responds* to changes in the buffer tank's outlet valve (V1). Opening of V1 initially increases the CO_2 capture since an increase in the lean flow rate improves the CO_2 absorption by suddenly increasing the wetted area of packing elements in the absorber. However, after approximately half an hour, the CO_2 removal starts to decrease. At constant reboiler heat duty, the excessive amine solution flow rate results in an increase in the lean loading due to the high mole fraction of CO_2 remaining in the recycled amine stream returning to the absorber. In the present analysis, the response of CO_2 removal to the change in +2.5% and -2.5% change in the V1 stem position were fitted to a second-order model with numerator dynamic (Seborg et al., 2011) as described in Eqs. (3.18) and (3.19), respectively.

$$\Delta\%CC(t) = -276.51\left(\Delta V1(t)\right)\left(1 + 2.45e^{-t/16.8} - 3.45e^{-t/180}\right) \tag{3.18}$$

$$\Delta\%CC(t) = -180.10\left(\Delta V1(t)\right)\left(1 + 4.46e^{-t/16.8} + 3.46e^{-t/180}\right) \tag{3.19}$$

where $\Delta\%CC$ is the difference in the percentage of CO_2 capture in the time domain; $\Delta V1$ is the difference in the valve stem position (V1) in the time domain, and t is time. The fitting of the second-order models to CO_2 captured response gives a reasonably good prediction of the actual process output as depicted in Fig. 3.11b.

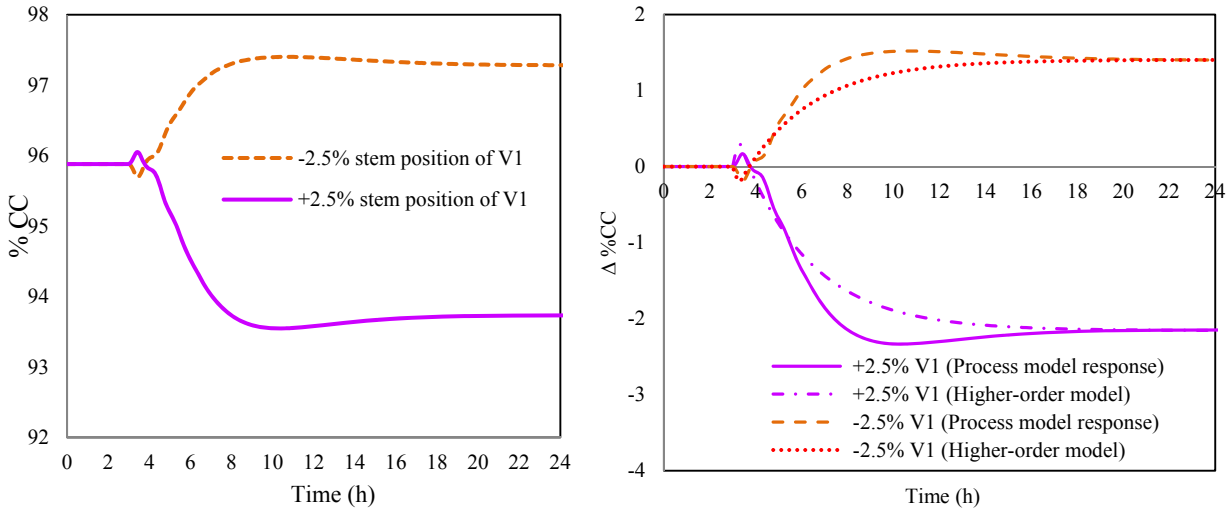

(a) (b)

Figure 3.11 Inverse responses of %CC and V1: (a) Sensitivity analysis of valve stem position of V1 on %CC; (b) Process model response and the second-order model for Δ%CC during +2.5% valve stem position increase.

The steady state process gains (K_p) and open loop time constants (τ_p) were then determined using the results obtained from the sensitivity analysis. The process time constant is the time at which the controlled variable achieves 63.2% of its total change, i.e. as shown in Fig. 3.10a the Q_{reb} reduction of 5% decreased T_{reb} by 1.21 K from the base case to the new steady state and the plant took about 86 min after the beginning of the change in Q_{reb} to achieve 378.6 K which was 63.2% of the total change in T_{reb}. However, the time constant of each pair presented in Table 3.4 was the average time constant from all magnitudes of changes in manipulated variables. The process gain of each pair based on the steady state values, also presented in Table 3.4, was calculated using the following equation:

$$K_p = \frac{\Delta y}{\Delta M} = \frac{y_{new,ss} - y_{t=0}}{M_{new,ss} - M_{t=0}} \tag{3.20}$$

where $y_{t=0}$ and $y_{new,ss}$ are values of a controlled variable at the initial condition and at the new steady state after the change in a manipulated variable, respectively. Likewise, $M_{t=0}$ and $M_{new,ss}$ are values of manipulated variables at $t = 0$ and at the new steady state.

Table 3.4 Process gains and time constants for the pilot plant model

MV / CV	Q_{reb}		Q_{con}		Q_{tank}		$V1$		$V2$		$V3$	
	K_P	τ_P (min)	K_P	τ_P (min)	K_P	τ_P (min)	K_P	τ_P (min)	K_P	τ_P (min)	K_P	τ_P (min)
%CC	0.94	105	-0.34	273.3	-0.23	127, 377 [a]	136.29	6.6, 160.2 [a]	-3.70	76.5	-4.07	43.2, 126.6 [a]
T_{cond}	3.98	101	-9.67	16.2	-1.44	397	-416.40	60.0	-10.69	90	-11.89	3.6, 40 [a]
T_{tank}	0.30	122	-0.06	228	-0.45	180	148.08	49.8, 246.6 [a]	1.63	23.4, 120 [a]	1.705	26.4, 178.2 [a]
L2	0.001	6.6, 73.2[a]	-0.0003	230	-0.0002	90, 543 [a]	1.57	13.3	-1.09	3.6	0.022	13.5
L3	0.001	220	0	30, 227 [a]	0	96.6, 424 [a]	1.71	20	0.02	6.6	-1.26	3.6
T_{reb}	0.14	108	-0.04	175	-0.04	376	-30.17	120	-0.46	20	-0.514	75

[a] The sensitivity analysis of these controlled and manipulated variables showed the inverse response.

Therefore, this table shows the overall process gain (K) and two values of time constants were reported (τ_{P1},τ_{P2}).

3.5.4 Control structure A: RGA analysis

Control structure A was determined based on an RGA analysis performed on the CO_2 capture plant (Bristol, 1966). The RGA method aims to identify the best pairing of controlled variables (CV) and manipulated variables (MV) in multiple-input, multiple-output (MIMO) processes to minimize the interaction between multiple control loops. Each of the elements of the relative gain array matrix (λ_{ij}) is described as follows:

$$\lambda_{ij} = K_{ij} H_{ij} \tag{3.21}$$

where K_{ij} is the steady state gain between controlled variable i and manipulated variable j, and H_{ij} denotes the i-j element of $H=(K^{-1})^T$.

The relative gains (λ_{ij}) are based on the process steady state gains (K_{ij}); that is, the dynamic response of system is not taken into account in the RGA analysis. This may result in poor closed-loop performance in highly non-linear systems. The process gains and time constants of each manipulated variable and controlled variable, considered in the present analysis, are presented in Table 3.4. Likewise, Eq. (3.22) shows the relative gain array matrix (Λ) obtained for the CO_2 scrubbing process, respectively. The most suitable pairings are highlighted in Eq. (3.22) and are schematically shown in Fig. 3.12. The RGA analysis suggests that the liquid levels in the units A102 (L2) and R102 (L3) need to be controlled using the rich amine flow rate leaving A102 (V2) and the lean amine flow rate leaving from R102 (V3), respectively. Also, the temperature in the condenser (T_{cond}) and that of the lean amine stream entering the absorber (T_{tank}) are controlled using Q_{cond} and Q_{tank}, respectively. As shown in Fig. 3.12, the temperature of the reboiler (T_{reb}) is controlled using V1 whereas the reboiler heat duty (Q_{reb}) is coupled with %CC. The CO_2 composition transmitters (AT) and flow transmitters (FT) located on the flue gas stream and the vent gas stream are used to determine the CO_2 inlet and outlet flow rates from the plant. The CO_2 captured rate (%CC) is then calculated according to Eq. (3.16). Furthermore, the RGA analysis indicated that the two liquid level control loops have less effect from the other control loops whereas the feedback control loops $T_{reb} - V1$ and $\%CC - Q_{reb}$ have a high interaction between the control loops.

$$\Lambda = \begin{array}{c} \\ \%CC \\ T_{cond} \\ T_{tank} \\ L2 \\ L3 \\ T_{reb} \end{array} \begin{array}{c} \begin{array}{cccccc} Q_{reb} & Q_{cond} & Q_{tank} & V1 & V2 & V3 \end{array} \\ \begin{bmatrix} \mathbf{4.524} & -0.118 & -1.631 & -1.624 & -0.074 & -0.077 \\ -0.341 & \mathbf{1.156} & 0.125 & 0.056 & 0.002 & 0.003 \\ -0.072 & -0.009 & \mathbf{0.897} & 0.178 & 0.003 & 0.003 \\ -0.005 & 0 & 0.002 & -0.006 & \mathbf{1.010} & -0.001 \\ -0.004 & 0 & 0.0 & -0.005 & -0.001 & \mathbf{1.010} \\ -3.101 & -0.028 & 1.607 & \mathbf{2.401} & 0.059 & 0.062 \end{bmatrix} \end{array} \tag{3.22}$$

The control pairing suggested by RGA represents the control structure A proposed in this work. PI controllers were used for each pairing; the controllers' parameters were initially tuned using Internal Model Control (IMC) (Seborg et al., 2011). As a preliminary test, the process response to a ramp change in the flue gas flow rate was used to retune the controllers' parameters such that the closed-loop system can recover quickly and smoothly. To simplify the analysis, reset windup was not included in the PI controllers. Table 3.5 shows the controllers' tuning parameters used to evaluate the system's closed-loop performance while using control structure A.

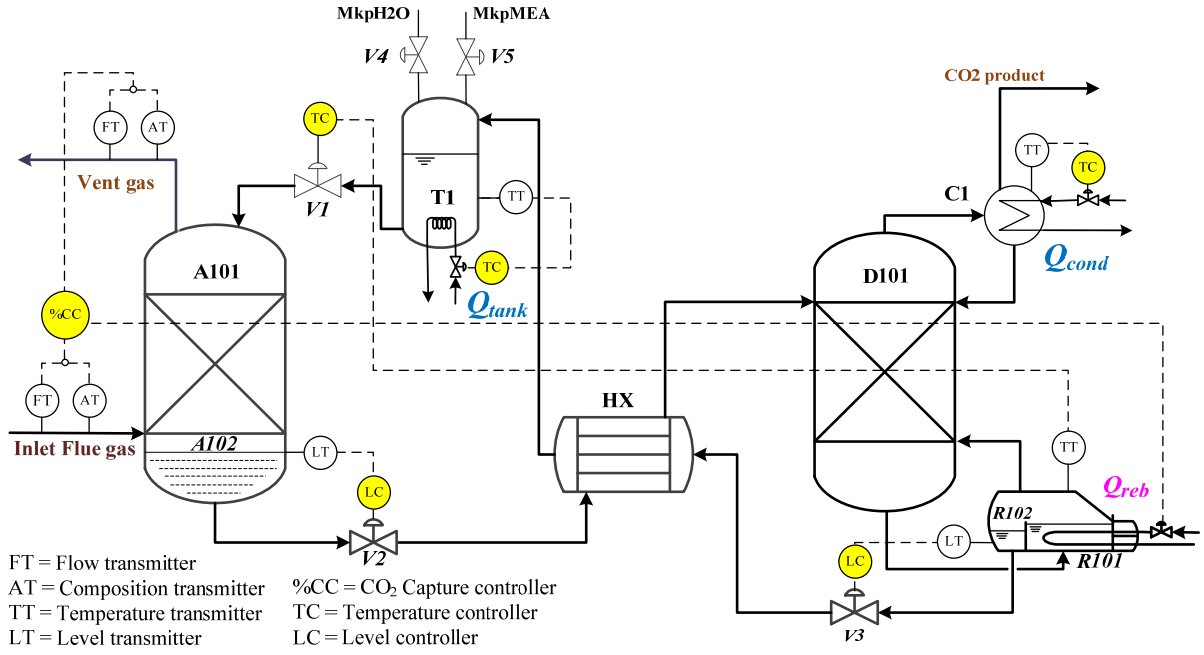

Figure 3.12 Control structure A

Table 3.5 Tuning parameters for control structure A

CV	MV	K_c	τ_I (min)	Set point
L2	*V2*	0.5	1.00	0.30 m
L3	*V3*	0.5	1.00	0.32 m
T_{cond}	Q_{cond}	12	1.62	315.4 K
T_{tank}	Q_{tank}	40	4.17	314K
%CC	Q_{reb}	80	4.17	96.3%
T_{reb}	*V1*	0.5	5.83	388.5 K

3.5.5 Control structure B: Heuristic-based approach

Control structure B was designed based on the insight gained from the process dynamics, i.e., a process heuristic approach. As shown in Fig. 3.11a, an inverse response was observed in %CC with changes in the stem position of the outlet valve of the buffer tank (V1). According to the sensitivity analysis, both the reboiler heat duty (Q_{reb}) and the lean amine flow rate (V1) significantly affect the CO_2 absorption performance. The latter variable has faster effect than the former because the change in the lean solution flow rate directly affects the absorption capability, by enhancing the mass transfer area, whereas changes in the reboiler heat duty has a slow effect on the CO_2 capture performance. For instance, in the presence of changes in the flue gas flow rate, an increase in the reboiler heat duty reduces the CO_2 concentration in the lean amine stream, and this lean MEA stream then flows through the cross heat exchanger and the buffer tank, respectively. The process to recycle this stream to the absorber may be slow to set the %CC back to its set point. In short, instead of increasing the reboiler heat duty; the %CC set point will be recovered faster by adjusting the lean amine flow rate using V1. As a result, control structure B, shown in Fig. 3.13, was implemented. Two key pairing loops were reversed in this scheme:

1) The percentage of CO_2 capture (%CC) was controlled by adjusting V1.
2) The reboiler temperature (T_{reb}) was maintained using Q_{reb}. The remainder of the control loops was similar to that shown for control structure A.

43

The PI controllers for the control loops *%CC-V1* and T_{reb}-Q_{reb} were tuned using process insights, described as follows:

(i) As shown in Fig. 3.11a, an excessive change in V1 may cause a reduction in the reboiler temperature, an increase in the lean loading and consequently the reduction of the CO_2 capture performance. Therefore, a small gain (K_c) and a large time constant (τ_I) for the *%CC-V1* control loop were considered; however, the control actions are still sufficiently fast so that the %CC can recover from a disturbance within an acceptable settling time.

(ii) The control parameters for the T_{reb}-Q_{reb} control loop were tuned to obtain a fast response to the amine solution regeneration. Note that control structure B requires T_{reb} to be under control. For example, in the case that Q_{reb} reached a saturation limit and T_{reb} is changing due to changes in the rich amine flow rate, e.g., due to an increase in the flue gas flow rate, V1 would increase to improve the absorption capability and attempt to recover %CC's set point. Although %CC may be improved during an initial increase of the lean flow rate, it would be not able to return to its %CC set point at the final steady state due to insufficient Q_{reb} to regenerate the lean amine stream and result in high lean loading. Therefore, to ensure that the lean loading is in an acceptable range, the T_{reb} needs to be tightly controlled using Q_{reb}. The tuning parameters for control structure B are shown in Table 3.6.

Table 3.6 Tuning parameters for control structure B

CV	**MV**	**K_c**	**τ_I** (min)	**Set point**
L2	V2	0.5	1.00	0.30 m
L3	V3	0.5	1.00	0.32 m
T_{cond}	Q_{cond}	12	1.62	315.4 K
T_{tank}	Q_{tank}	40	4.17	314K
T_{reb}	Q_{reb}	15	5.00	388.5 K
%CC	V1	0.01	33	96.3%

44

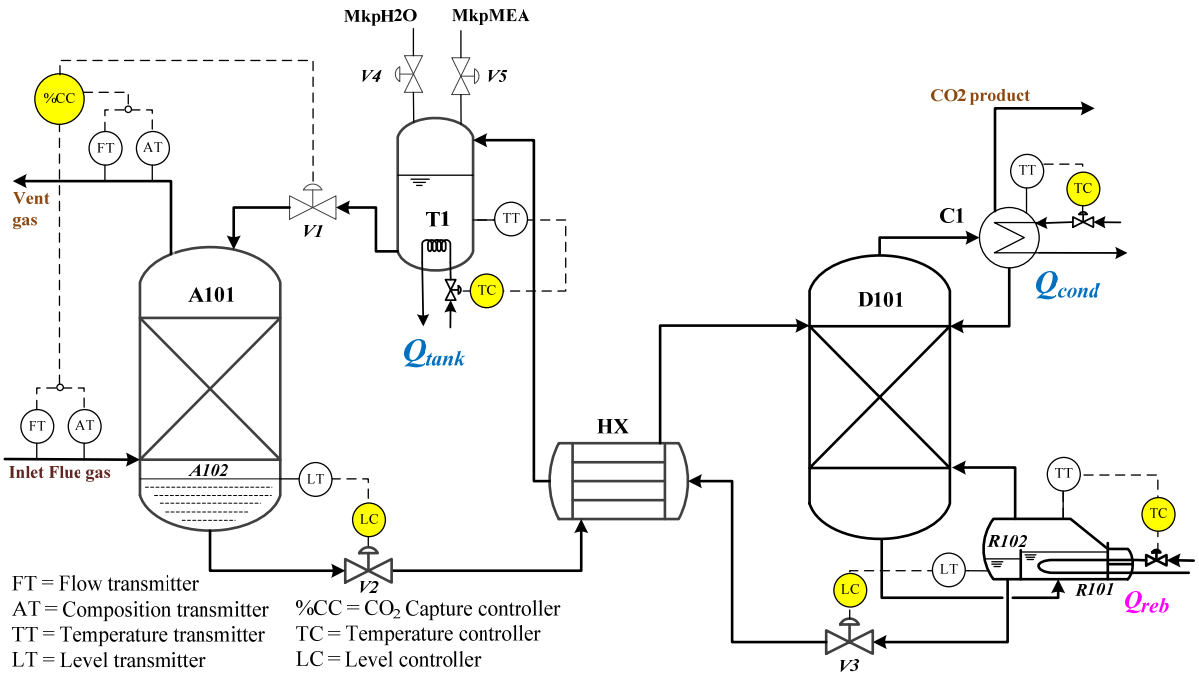

Figure 3.13 Control structure B

45

3.5.6 Control structure C: Heuristic-based approach

This control structure aims at maintaining T_{reb} under tight control. According to control structure C shown in Fig. 3.14, V2 is used to control T_{reb} by adjusting the amount of the liquid flowing to the reboiler. For example, an increase of the flue gas flow rate causes a reduction in %CC and the plant requires higher lean amine flow rate entering the absorber to maintain %CC set point. The increase in the rich amine flow rate may results in a rapid drop of T_{reb}. V2 will slow down the liquid flow rate entering the reboiler to ensure that T_{reb} does not rapidly drop and that the residence time in the reboiler is sufficient to heat the amine solution to the T_{reb} set point. In addition, the control pairing between T_{reb} and V2 in control structure C may result in faster responses than that of T_{reb}-*V1* in control structure A. Another control loop modified from control structure A is that the liquid inventory in A102 is controlled in the direction opposite to flow using V1. The controllers' parameters for control structure C were tuned using IMC for PI controller and manual retuning using the flue gas flow rate as the process disturbance. Table 3.7 shows the tuning parameters for control structure C.

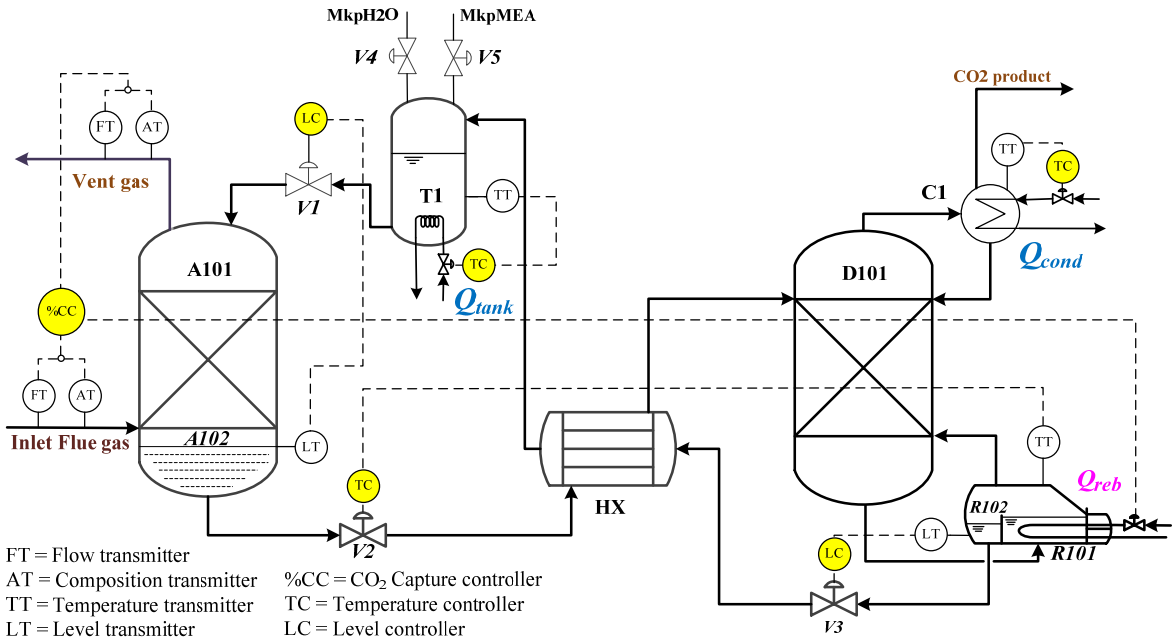

Figure 3.14 Control structure C

Table 3.7 Tuning parameters for control structure C

CV	MV	K_c	τ_I (min)	Set point
L2	V1	0.5	4.00	0.31 m
L3	V3	0.5	1.00	0.32 m
T_{cond}	Q_{cond}	12	1.62	315.4 K
T_{tank}	Q_{tank}	40	4.17	314K
T_{reb}	V2	0.5	8.33	388.5 K
%CC	Q_{reb}	80	4.17	96.3%

3.6 Performance evaluation of the control structures

The control structures proposed in this study for the CO_2 capture process were evaluated under eight scenarios, i.e., changes in the flue gas flow rate and its compositions due to changes in the air flow rate conditions, changes in the percentage CO_2 captured and the purity of the CO_2 in the product stream, the scenario of valve stiction, and imbalance of water and MEA in the system. A summary of the performance evaluation is presented in Table 3.8 and each of these tests is described next.

Table 3.8 Summary of the performance evaluation

No.	Scenario	ISE			Settling times to reach new steady state of %CC		
		Control structure			Control structure		
		A	B	C	A	B	C
1	+10% Flue gas flow rate	1,117.79	198.87	1,095.57	> 10 h	7.45 h	> 10 h
2	+10% Air flow rate	76.47	21.69	73.78	7 h	3 h	7 h
3	-6.3%CC set point	848.16	160.88	833.84	3 h	30 min	3 h
4	+3% CO_2 purity	0.38	0.004	0.41	Slightly affect %CC	Slightly affect %CC	Slightly affect %CC
5.1	V1 stiction (+5% Flue gas)	529.29	*Note1*	657.50	Oscillation (>10h)	*Note1*	Oscillation (>10h) (A102 was dry up.)
5.2	V1 stiction (-2.5%CC)	414.56	*Note1*	252.54	Oscillation (>10h)	*Note1*	22 h (A102 was flood.)
6	Makeup streams	1,144.64	217.04	1,137.15	Insensitive	Insensitive	Insensitive
7	Limited Q_{reb}	996.80	*Note1*	1,036.14	93.7%CC at steady state	*Note1*	94.2%CC at steady state
8	+40% Flue gas	2,689.53	427.34	2,240.22	V2 and V3 saturated	V2 and V3 saturated	V2 and V3 saturated

Note1: Control structure B could not continue and/or attain the %CC set point under the following scenarios: V1 stiction (+5%Flue gas), V1 stiction (-2.5%CC) and limited Q_{reb}.

3.6.1 Flue gas flow rate

This scenario describes the CO_2 capture plant performance in the presence of fluctuations in the flue gas load, which is a common scenario in the operation of power plants, e.g. changes in the flue gas flow rate during plant start-up, shutdown, or during the course of a day. In this study, a step increment of 10% in the flue gas flow rate with respect to its nominal operating point was introduced to the plant at the third hour of operation. As shown in Fig. 3.15, control structure B showed faster disturbance rejection than control structures A and C, and also resumed the %CC to its set point in approximately 5 h. Table 3.8 shows the *Integrated-Squared-Error (ISE)* of the CO_2 removal rate against its set point according to following equation:

$$ISE(\%CC) = \sum_{t=0}^{t_f} \left(\%CC_{SP} - \%CC(t) \right)^2 \tag{3.23}$$

where $\%CC_{SP}$ and $\%CC$ are the set point of CO_2 capture and the CO_2 capture rate at any given time, respectively; and t_f is the final time in which the plant converges to steady-state condition. The lowest ISE (%CC) of control structure B in Table 3.8 indicates that the CO_2 capture rate in control structure B during the disturbance of +10% in the flue gas flow rate possessed the smallest deviation from the %CC set point where control structures C and A had higher deviations, respectively. Also, the control actions performed by control structure B only caused a reduction in the CO_2 capture performance of approximately 1% whereas control structures A and C caused a reduction of almost 3% in CO_2 captured. This result suggests that control scheme A and C may violate the first control objective considered for this process, i.e., operate with a CO_2 removal lower than 90% if the change in the flue gas flow rate is greater than 10%.

Moreover, the three control structures require a similar amount of energy required at the base case operation (4,950 kJ/kg CO_2 captured) and at the final steady state after the introduction of the +10% change in the flue gas flow rate (Fig. 3.16b). As shown in Fig. 3.16c, a small spike in the reboiler temperature was produced by control structure B. This is due to a rapid opening of V1 to increase the lean flow rate once the decrease in %CC was detected, which causes a slight reduction of T_{reb}. However, this offset in T_{reb}'s set point was corrected with the T_{reb}-Q_{reb} control loop by increasing Q_{reb}. In control structure A, due to the increase of the flue gas flow rate which

may result in the reduction of T_{reb}, the reduction in *%CC* was detected; the Q_{reb} controller increased the steam flow rate whereas the lean flow rate was initially reduced to maintain T_{reb} using T_{reb}-*V1* controller. Also, in control structure C, the *%CC*-Q_{reb} controller increased the reboiler heat duty and the T_{reb}-*V2* controller reduced the rich amine flow rate initially to minimise the reduction of T_{reb} due to the increase in the flue gas flow rate. The combined effects of the control actions of controllers T_{reb}-*V1* and *%CC*-Q_{reb} in control structure A, and T_{reb}-*V2* and *%CC*-Q_{reb} in control structure C, resulted in a stable reboiler temperature in control structures A and C, respectively.

Fig. 3.16d shows that the condenser temperature in the three control schemes was tightly controlled and indicates that the CO_2 purity in the product's stream was not significantly affected by this disturbance. As shown in Figures 3.16e and 3.16f, the fractional capacities in the absorber and the stripper slightly increased by 3.5% and 2.8%, respectively. Also, the variability in the liquid levels in A102 and R102 were not significantly affected during changes in this operating condition. This behaviour was generally observed in all scenarios studied in this work.

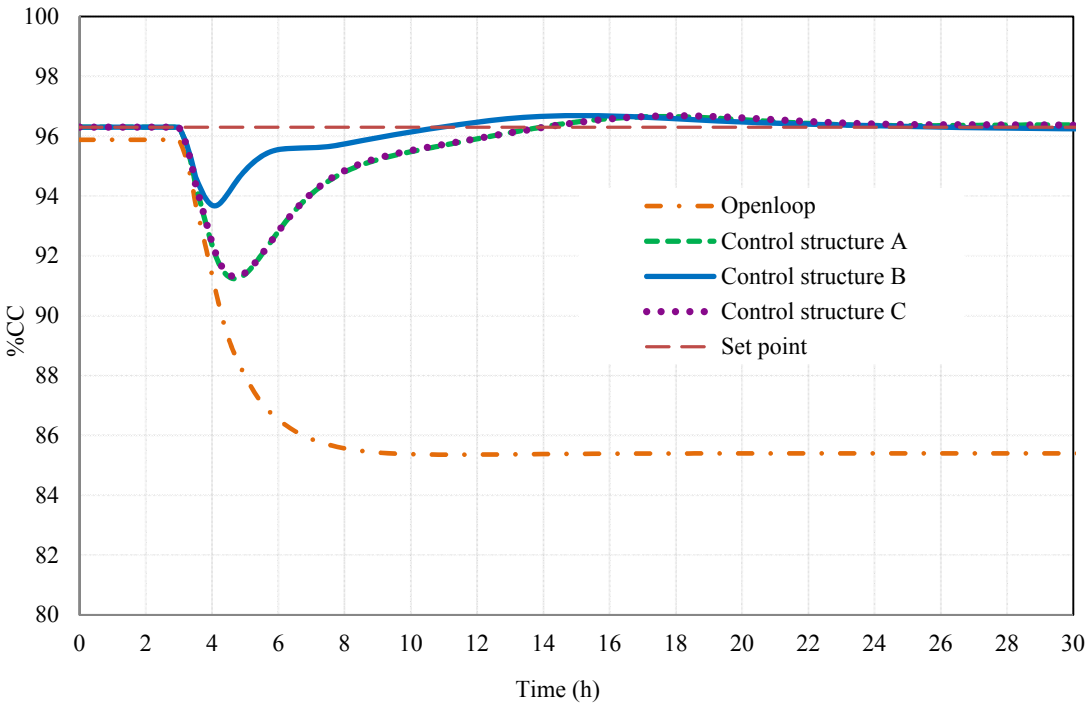

Figure 3.15 Responses of %CC to a +10% change in the flue gas flow rate

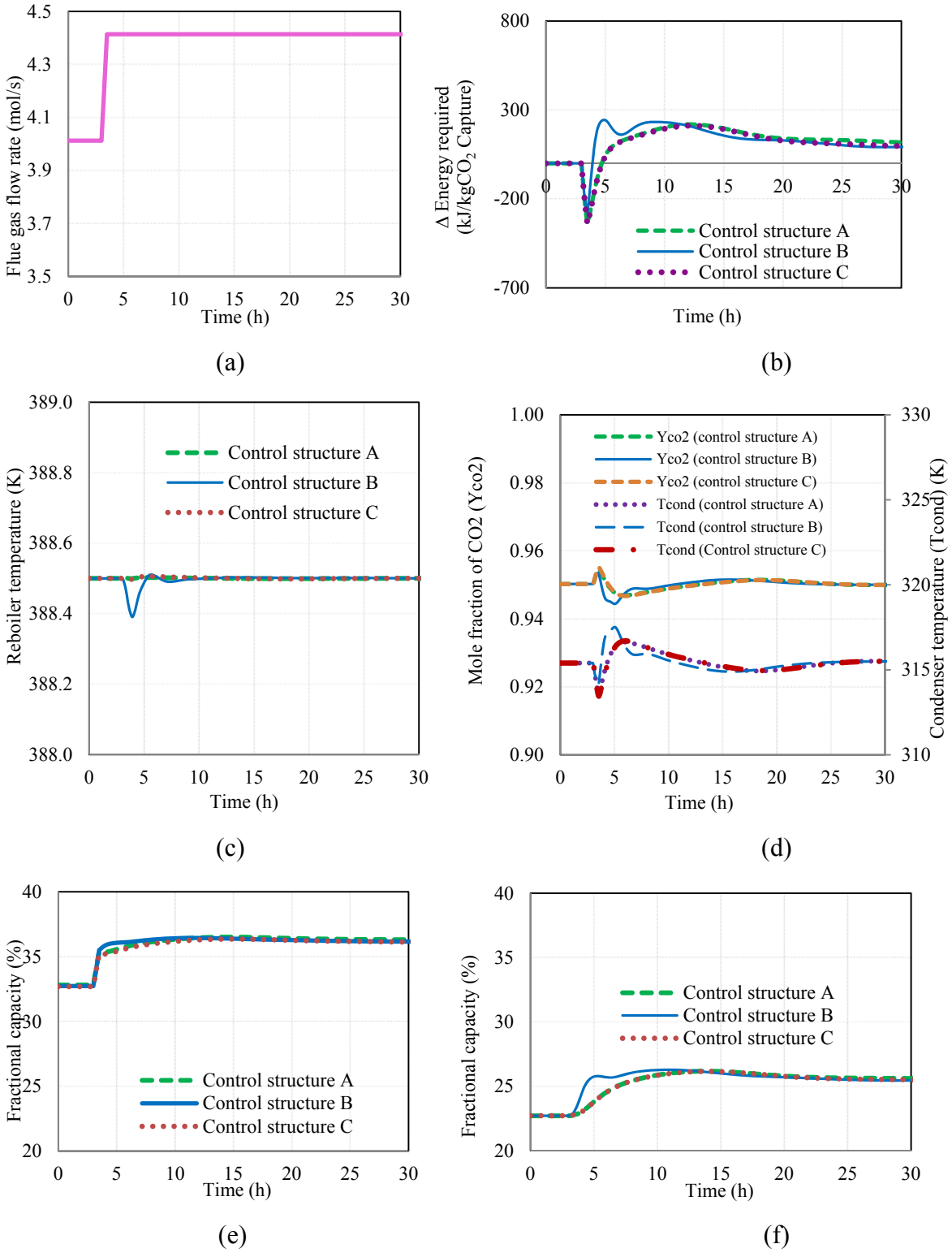

Figure 3.16 Responses of control structures to a +10% change in flue gas flow rate: (a) flue gas flow rate; (b) Δenergy required; (c) T_{reb}; (d) CO_2 purity; (e) fractional capacity in the absorber; and (f) fractional capacity in the stripper

3.6.2 Flue gas composition

The flue gas considered in this work was based on the gas mixture used in a pilot plant (Dugas, 2006). This gas mixture did not content oxygen which explains the absence of this component for the base case condition considered in this study. This scenario aims to represent the case when the air molar flow rate fed into a combustor increases by a certain percentage, causing changes in the flue gas composition and the flue gas flow rate. The hypothetical air flow rate was calculated based on the assumption of the complete combustion of Pittsburgh#8 coal (NETL, 2012); the coal feed rate was assumed as 11.74 g/s so that the flue gas flow rate (4.01 mol/s) and composition remain the same to that used in the base case (see addition description of flue gas flow rate calculation in Appendix B), as reported by Harun et al. (2012). As shown in Table 3.9, a 10% increase in the air molar flow rate changes both the flue gas flow rate and the flue gas composition with respect to its base case condition. Since the free water in the exhaust gas is removed by a scrubber and SO_2 is removed by a desulfurization unit prior to entering the absorber, the mole fraction of water in the flue gas stream is assumed to remain constant at 0.025.

Table 3.9 Flue gas composition and flow rate change due to the variation of the air flow rate

Variable	**Base case**	**+10% Air flow rate**
Air flow rate (mol/s)	4.07	4.481
Flue gas flow rate (mol/s)	4.01	4.426
Mole fraction		
CO_2	0.180	0.164
H_2O	0.025	0.025
N_2	0.795	0.792
O_2	0	0.019

The disturbance in the flue gas flow rate and composition was introduced to the CO_2 capture plant within 30 min of the start of the simulation. As shown in Fig. 3.17b, the flue gas flow rate was increased by approximately 10% and the CO_2 flow rate in the flue gas slightly increased by 0.25%. Fig. 3.17 shows the process response obtained for this scenario. In the open-loop process

response, the percentage of CO_2 captured was reduced by 2.4% from its base case operating condition and required 7 h to reach its new steady condition. Due to the small change in the CO_2 flow rate in the flue gas, for all three control schemes, the percentage of CO_2 absorbed was approximately 1% lower during the transient process prior to resuming to the set point (Fig. 3.17a). Nonetheless, control structure B showed a faster set point recovery of %CC than control structures A and C. Although the performance of control structure C was somewhat similar to that of control structure A and was slower than control structure B, the energy required by control structure C was less than that required by the other control schemes (Fig. 3.17c). Moreover, the change in the flue gas composition had less impact on the condenser temperature since T_{cond} was directly manipulated by the cooling medium flow rate. As a result, only a small variability was observed in the composition of CO_2 in the product stream.

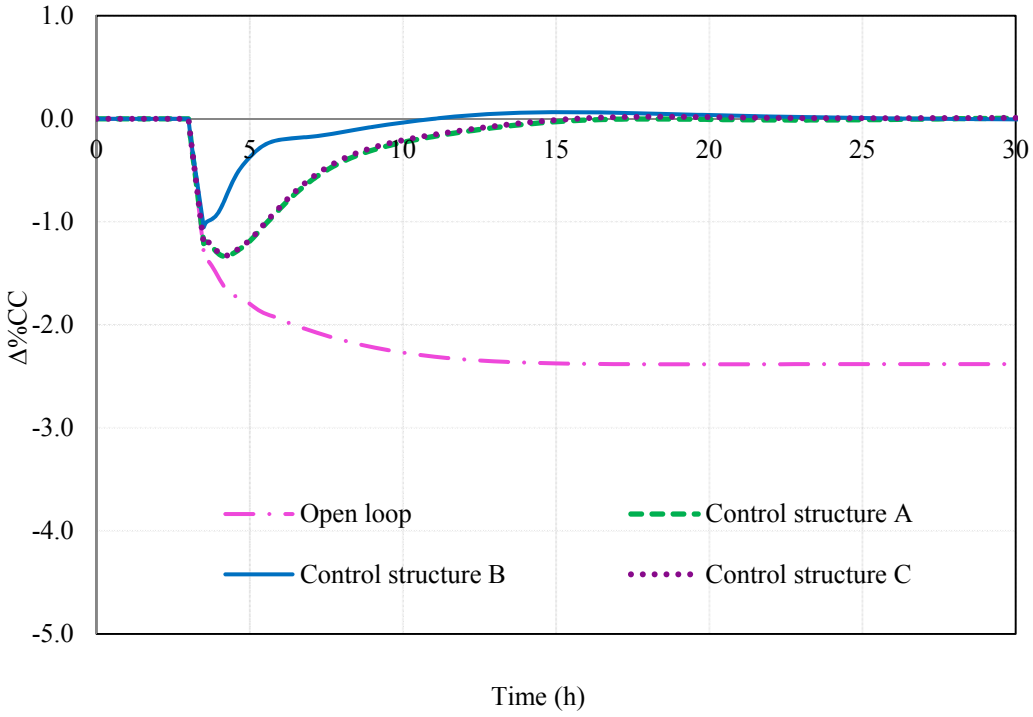

(a)

52

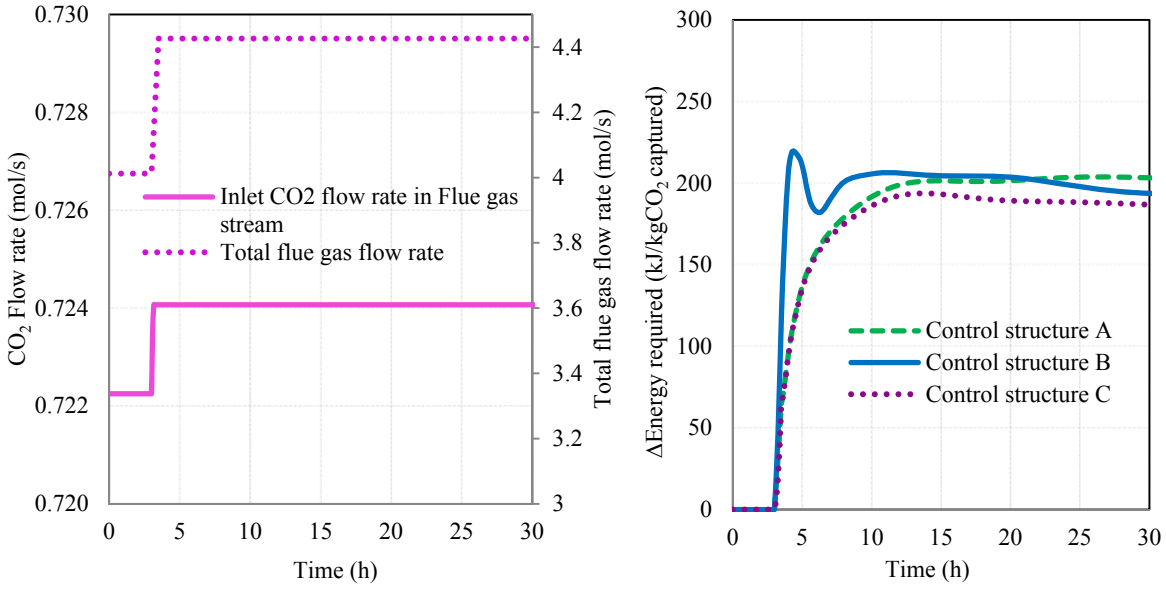

(b) (c)

Figure 3.17 Responses of control structures to a +10% air flow rate: (a) Δ %CC; (b) CO_2 flow rate and total flue gas flow rate; and (c) Δenergy required

53

3.6.3 Change in the CO_2 removal rate

This scenario represents an increase in power demands. The reboiler heat duty, which is the major energy consumption unit in the CO_2 scrubbing plant, has to be significantly reduced to ensure that the amount of steam is sufficient to meet the electricity demands (assuming that the steam supplied to the reboiler comes from the steam cycle). This effect results in a reduction in the amount of CO_2 that can be captured during peaks demand. To test this scenario, a reduction in the CO_2 removal's set point from 96.3% to 90% was considered. This change was achieved using a ramp change in the reboiler heat duty that lasted for 2 h. As shown in Fig. 3.18a, control structures A and C required approximately 3 h to attain the new %CC set point. Although the reboiler heat duty had been reduced with respect to the change in %CC set point (see Fig. 3.18b), a sluggish response of the CO_2 removal rate in control structures A and C was observed. This is because the recycled lean amine stream with low contents of CO_2 concentration was still flowing into the absorber; therefore, the actual %CC did not rapidly respond to changes in Q_{reb}. Once the CO_2 concentration in the lean MEA solution increased due to insufficient Q_{reb}, the actual %CC gradually decreased accordingly. On the other hand, control scheme B was able to perform faster

at set point tracking than control structures A and C, i.e., the action of Q_{reb} in control structure B was faster than that in control structure A. However, a small spike in Q_{reb}, observed in control structure B, indicated that the steam flow rate, which can be potentially supplied from the steam cycle, may change rapidly and therefore affect the stability and performance of the power generation plant. Nevertheless, it may be minimized by applying a small step change of %CC set point. As shown in Figures 3.18e and 3.18f, the three-step change of 2% of CO_2 captured rate every 2 h illustrated the smoothest set point tracking of Q_{reb} and %CC.

As shown in Fig. 3.18a, the control actions performed by the %CC-V1 control loop enabled the valve V1 to reach the new operating valve stem position by the time the CO_2 capture set point reached 90%. This reduction in the lean amine flow rate may result in an increase in T_{reb}; however, the T_{reb} –Q_{reb} control loop rapidly decreased the reboiler heat duty to track the T_{reb} set point as shown in Fig. 3.18b. Although control schemes A and C were able to reach their set points without any major oscillations, the time needed from those control schemes to achieve the set point was slightly over 3 h. Therefore, control structure B shows faster set point tracking performance than that observed for control schemes A and C.

The ratio of the change in the reboiler heat duty to the percentage of CO_2 removal was 1:1.16. This represents an improvement in the operation of this plant since in the dynamic open-loop study performed by Harun et al. (2012), they reported a ratio of 1:1.4 for this same scenario. In addition, this ratio agrees with the result of the closed-loop simulation reported by Lawal et al. (2010).As shown in Fig. 3.18d, the condenser temperature was slightly affected by the reduction in %CC. During the transient period, the decrease of %CC set point and Q_{reb} caused a decrease in T_{cond} and the vapour flow rate entering the condenser resulting in an increase in the CO_2 purity in the product stream. At the new steady state, the set point of T_{cond} was recovered by reducing Q_{cond} from its initial base-case value.

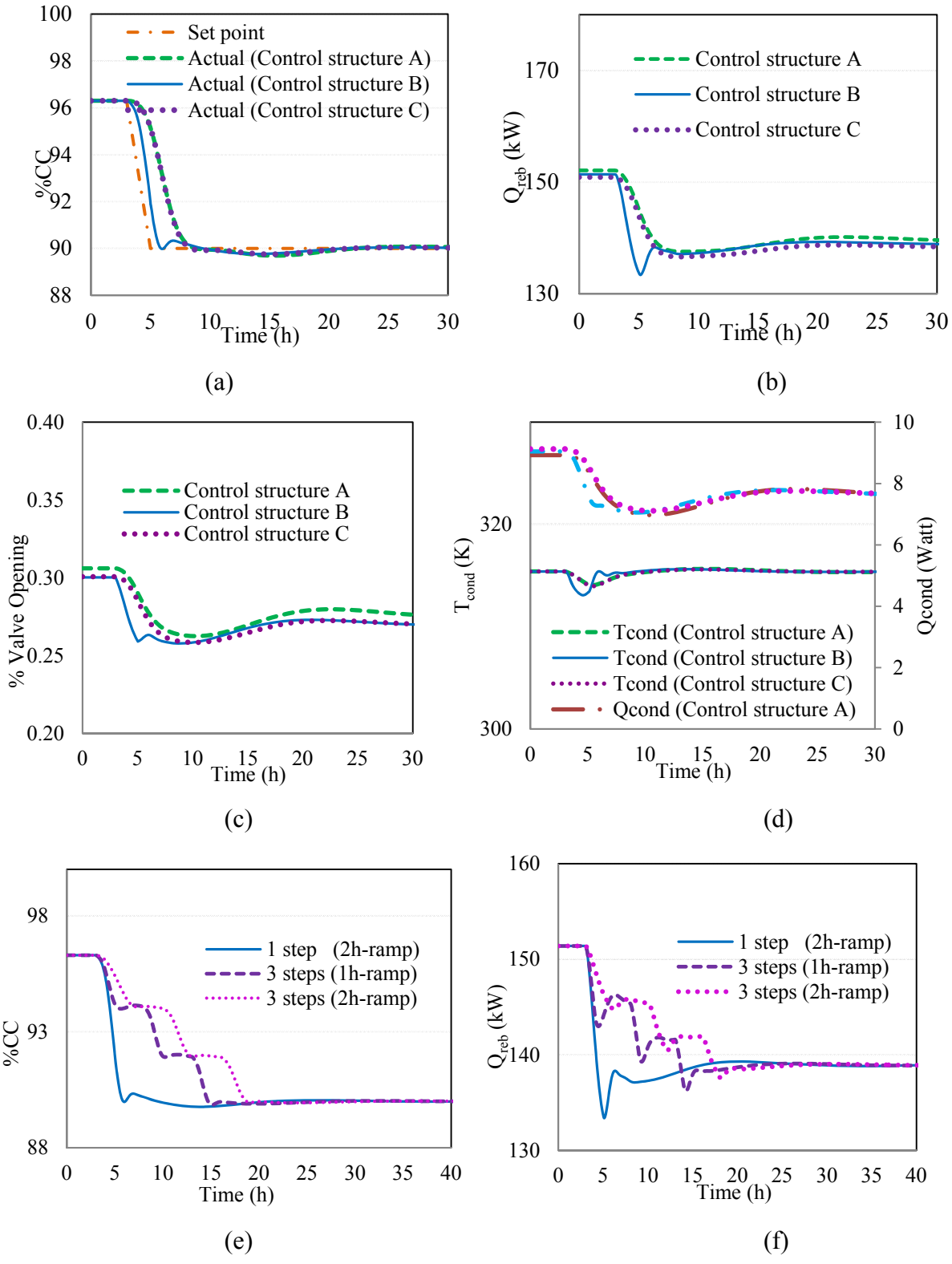

Figure 3.18 Responses of control structures to change in CO_2 removal set point: (a) %CC; (b) Q_{reb} (c) V1; (d) T_{cond}; (e) %CC in control structure B using step change in %CC set point; and (f) Q_{reb} in control structure B using step change in %CC set point

3.6.4 Change of CO_2 purity in the product's stream

This scenario aims to investigate the system's closed-loop performance when there is a higher CO_2 purity requirement for the plant. This case can be achieved by increasing the cooling medium flow rate (Q_{cond}) to lower the condenser temperature and therefore increase CO_2 content in the product stream. The ramp change of CO_2 purity from 95% to 98% caused a change in the T_{cond}'s set point from 315.4 K to 300 K following the correlation presented in Eq. (3.17). As shown in Fig. 3.19a, the new condenser's temperature set point (300 K) was achieved in 30 min by all control schemes. The condenser temperature in those control schemes was controlled using Q_{cond}; therefore, their performance was similar. Fig. 3.19b shows that the three control structures provided similar responses for the CO_2 product flow rate. At the constant pressure of the CO_2 product stream, the reduction in these vapour flow rate may affect the operation of the compression train, downstream of the CO_2 capture plant, by moving the operating point toward the surge limit. Nevertheless, the compression train usually handles this scenario using an anti-surge control system (Lin et al., 2012).

However, Fig. 3.19c and Table 8 show that the variation of %CC in control structures A and C was greater than that in control structure B. The reduction in T_{cond} results in a slight decrease in the temperature gradient in the stripper (D101) and T_{reb}. In control structure A, since the recovery of T_{reb} set point was achieved by adjusting V1, the process disturbance (change in T_{cond} set point) was propagated to the recycled lean amine stream and resulted in the reduction of %CC in the transient period prior to the resumption of the %CC set point. The propagation of the process disturbance was also found in control structure C. The initial reduction of T_{reb} caused that V2 was slightly closed to slow down the rich amine flow rate flowing to the reboiler, which increased the liquid level in A102. The V1 valve then gradually closed to maintain the liquid level in A102. The action of V1 caused a reduction of the lean amine flow rate and resulted in the variation of the CO_2 capture rate during the transient process. Regarding control structure B, the variation of T_{reb} due to the change in T_{cond} was transmitted to Q_{reb} and did not affect the absorption process. As a result, %CC was remained unchanged during the change in T_{cond}'s set point. This results indicate that control structure B is better able to handle the change in the

operating condition by rejecting the process variation to the process utility (Q_{reb}) instead of propagating it through the entire plant.

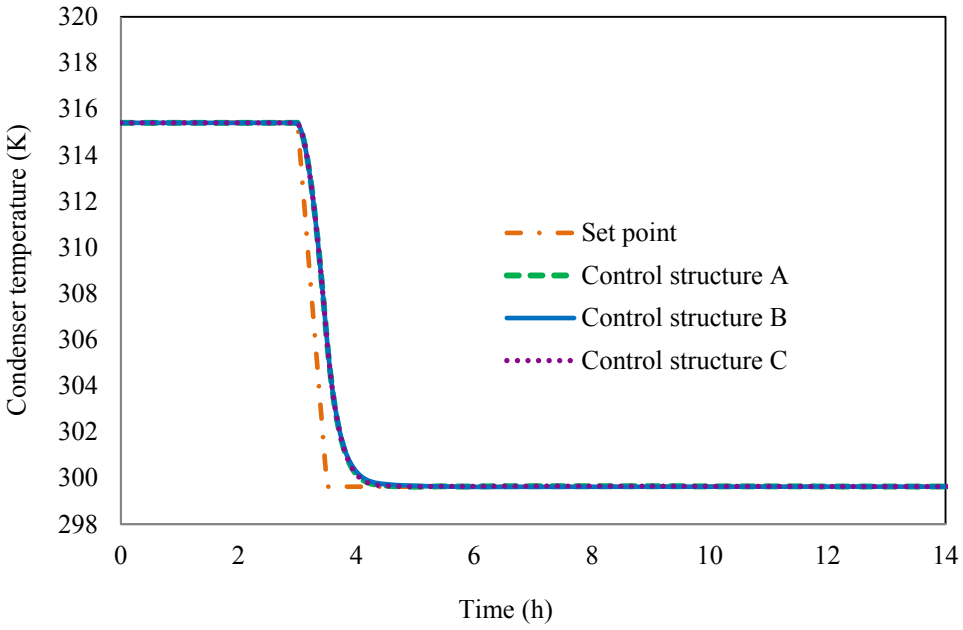

(a)

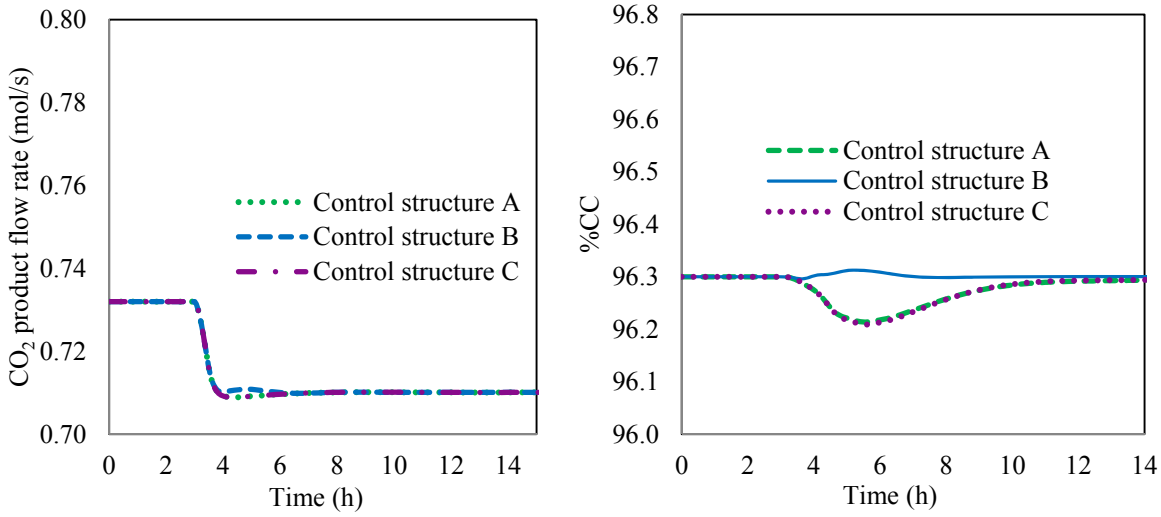

(b) (c)

Figure 3.19 Responses of control structures to the change in CO_2 purity in the product stream: (a) T_{cond}; (b) CO_2 product flow rate; and (c) %CC

3.6.5 Valve stiction of V1

This condition aims to study the effect of V1 stiction on the CO_2 capture performance (%CC) during the disturbance in the flue gas flow rate and the change in %CC set point. This scenario represents the lack of maintenance or an actuator failure causing a valve stiction. That is, the valve stem position of V1 was assumed to remain constant at its base case point during the test whereas the other controllers were functioning normally. A disturbance of 5% increase in the flue gas rate for a period of 30 min was introduced to the plant in the presence of V1 stiction. Fig. 3.20a shows a comparison in the %CC response due to the +5% change in the flue gas flow rate. For control structure A, the stiction of V1 caused oscillations in the CO_2 removal (%CC) that are dampened after a relatively long period of time (>40 h); however, the oscillations ultimately converged to the designated %CC set point. The same behaviour was observed when the set point of CO_2 capture was changed by 2.5% using a ramp. As shown in Fig. 3.20b, the magnitude of the oscillations was approximately ±2%CC at beginning of the test but the system eventually reached its new set point.

For control structure C, oscillations were also observed in the CO_2 capture rate in the presence of V1 stiction and the disturbance in the flue gas flow rate. Although the CO_2 removal rate converged to the %CC set point, the loss of L2-V1 control loop caused a drop in the liquid level in A102 (Fig.3.20c). This effect may result in an insufficient residence time of the rich amine solution in A102. For the scenario of the set point tracking under the condition of V1 stiction, control structure C was able to achieve the new %CC set point without large oscillations as those observed in control structure A's response; however, the liquid level in A102 significantly increased due to the action of *%CC*-Q_{reb} and T_{reb}-*V2* control loops (Fig. 3.20d). The reduction of Q_{reb} (Fig. 3.20f) to attain the new %CC set point reduced the reboiler temperature. The V2 valve thus slightly closed to reduce the rich MEA flow rate so that T_{reb} was maintained at its set point with the new Q_{reb} at the final steady state. Therefore, the accumulation of the rich amine solution in A102 increased due to the action of V2 and the absence of the *L2-V1* controller. In case that the absorber sump tank is not large enough to accommodate enough liquid, this effect may cause column flooding. On the other hand, control structure B could not attain the %CC set point after the disturbance in the flue gas flow rate (Fig. 3.20a) because its %CC set point is controlled

using V1 which was stuck in this case study. Moreover, the test of the set point tracking of %CC was not applicable to control structure B in the condition of the V1 stiction since V1 could not move to obtain the new %CC set point. These results show that control structure B is able to achieve the desired CO_2 capture performance only if V1 is functioning properly.

Even though the performance of the disturbance rejection in control structure C was comparable to control structure A, and showed smoother response in terms of set point tracking than other control schemes under this scenario, control structure C's response also showed that the V1 stiction may cause A102 dried up or flooded in the plant. Moreover, Figures 3.20a and 3.20b show that control schemes A and C were able to reach the CO_2 removal set point, however in an oscillatory fashion. As shown in Figures 3.20e and 3.20f, these oscillations were due to the large fluctuations in the reboiler's heat duty, which is the manipulated variable used to control the CO_2 removal in control schemes A and C. On the other hand, the system's response with control scheme B shows that this control structure avoids large oscillations in CO_2 removal and the reboiler's heat duty, as shown in Figures 3.20a and 3.20e. This more stable operation of the plant is desirable even though the control scheme failed to reach the CO_2 removal target, i.e., there is an offset in the CO_2 removal target.

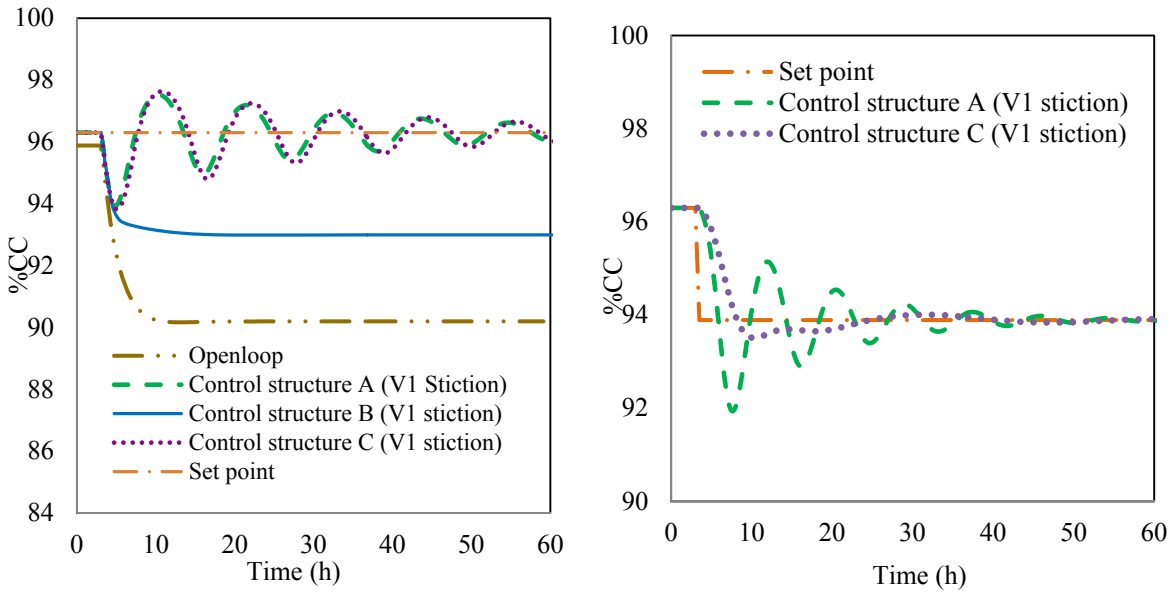

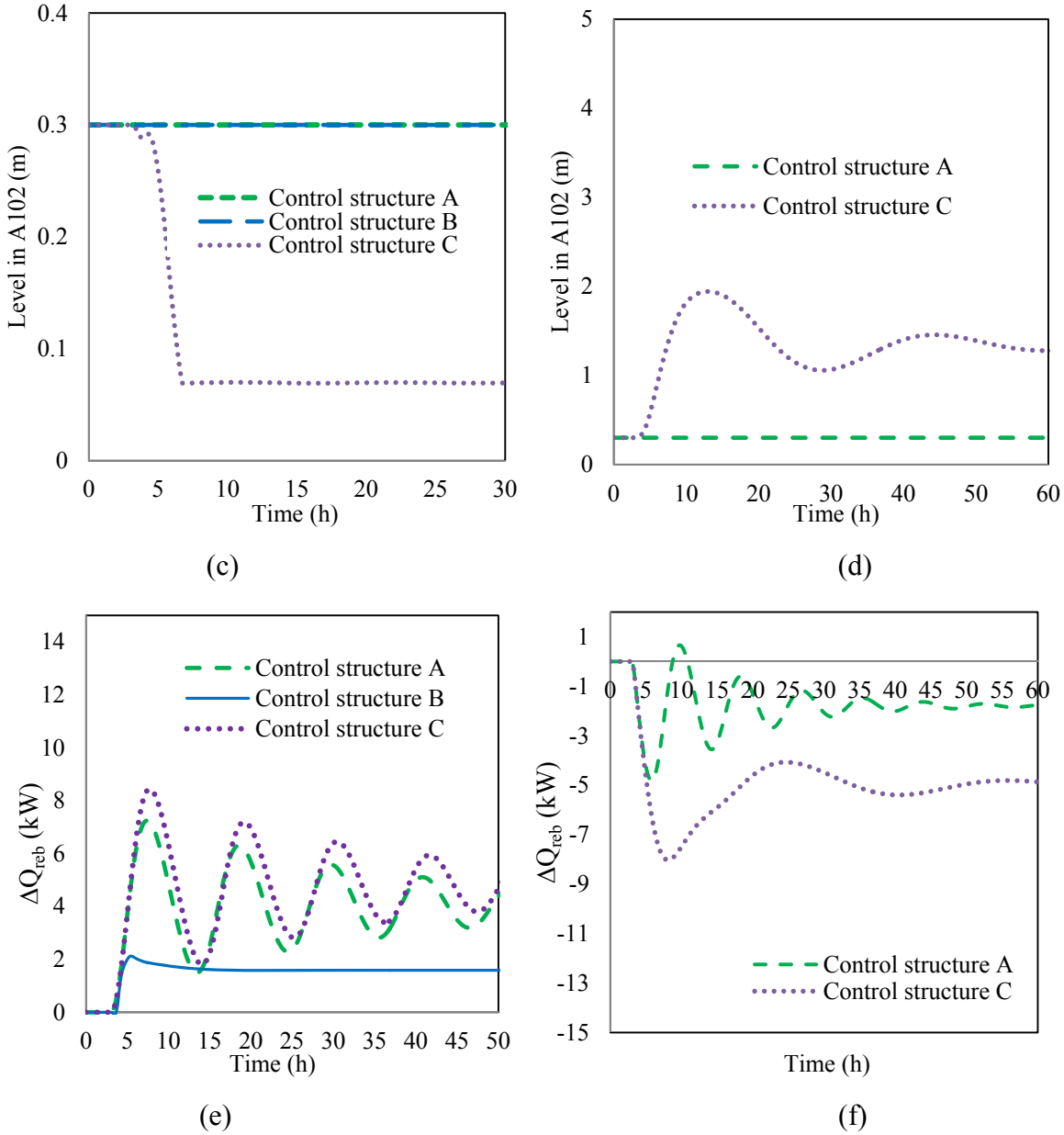

Figure 3.20 Responses of control structures with V1 valve stiction: (a) %CC during a +5% change in the flue gas flow rate; (b) %CC during a -2.5% change in %CC set point; (c) L2 during a +5% change in the flue gas flow rate; (d) L2 during a -2.5% change in %CC set point; (e) ΔQ_{reb} during a +5% change in the flue gas flow rate; and (f) ΔQ_{reb} during a -2.5% change in %CC set point

3.6.6 Constant make up flow rate of water and MEA

This scenario considers the case where, during the presence of the disturbance, the two makeup valves, V4 and V5, are not used to adjust the makeup flow rates of water and MEA because of the lack of information available to a laboratory technician resulting in an imbalance of water and MEA in system. This scenario can be simulated by applying a disturbance of +10% in the flue gas flow rate while keeping the makeup flow rate of both water and MEA constant and equal to their base case values (makeup flow rate of water and MEA at the base case condition are 0.16 mol/s and 0.0002 mol/s, respectively). The present test assumed that makeup streams were resumed to track the need of water and MEA in the CO_2 capture plant after 9 h of operations.

As shown in Fig. 3.21a, the loss of makeup streams did not upset the plant operation for all control schemes. The CO_2 capture performance in the presence of the makeup valve stiction did not deviate significantly from that with the normal operation. Nevertheless, the imbalance material in process indicated an increase in MEA concentration, as shown in Fig. 3.21b, mainly due to water evaporation. The circulation of high MEA concentration in the amine solution leads to an asset integrity problem. Since the scenario of the constant makeup flow rates does not directly impact the plant's operability, the problem may be concealed until an inspection personnel find that the process pipelines are internally corroded. Regardless of the control structure, this result emphasizes the importance of a routine schedule of the sorbent properties analysis.

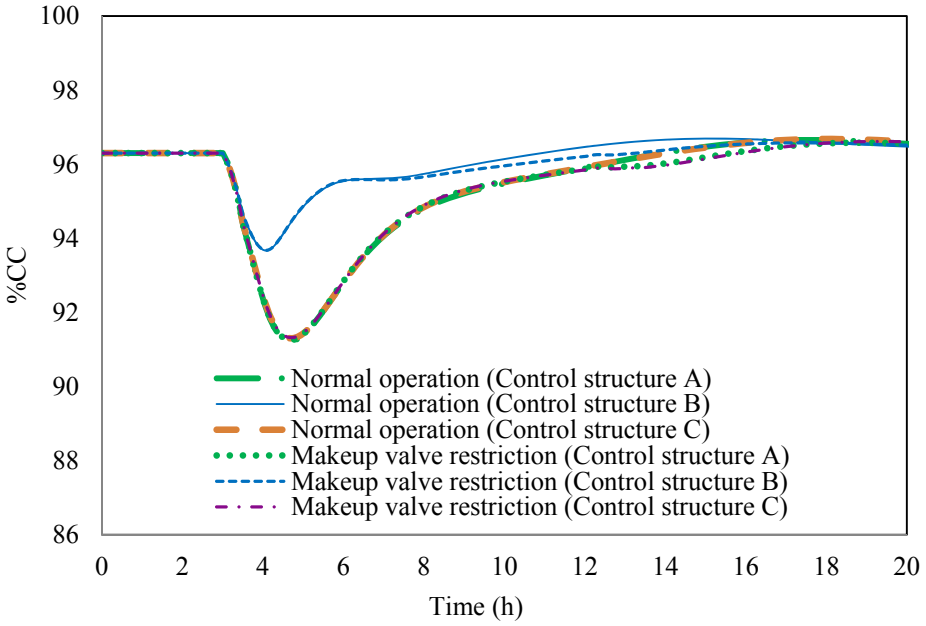

(a)

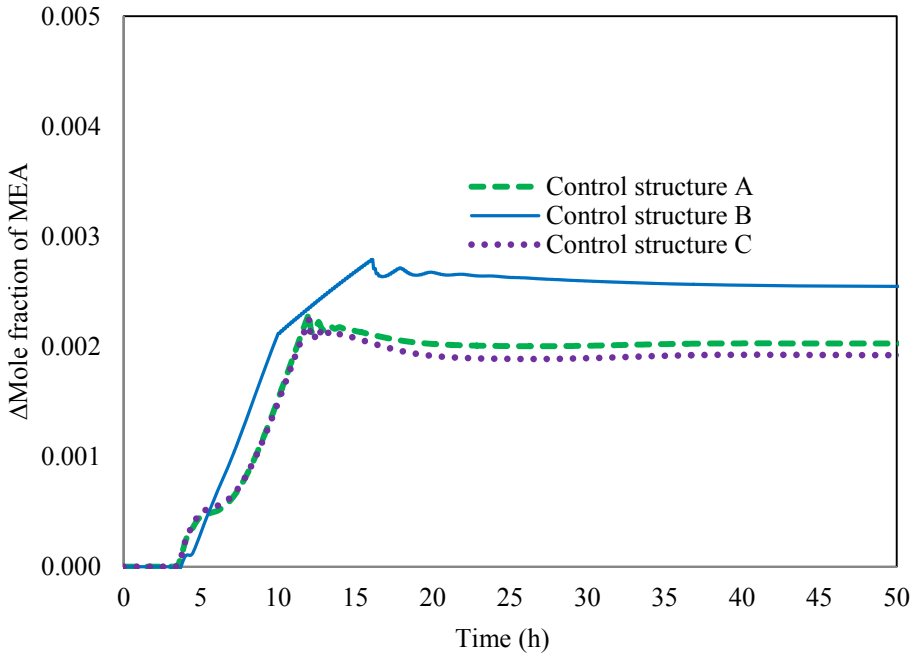

(b)

Figure 3.21 Responses of control structures during constant makeup flow rates: (a) %CC and (b) Δmole fraction of MEA in the lean solution entering the absorber

3.6.7 Limited reboiler heat duty

The maximum reboiler heat duty may be fixed *a priori* to ensure that the amount of steam in the steam cycle is sufficient to generate the minimum electricity required from the power grid. This scenario aims to determine the response of each control scheme once the reboiler heat duty reaches this limiting constraint. In this scenario, it was assumed that the maximum reboiler heat duty was 195 kW, which was 1.3 times the base case value (150 kW). Also, +5% incremental step changes in the flue gas flow rate were introduced to the plant until the flue gas flow rate reached 25% increase in total. Fig. 3.22 shows that control structures A and C were able to continue the operation even though Q_{reb} approached its maximum constraint limit at t = 121 h and t = 137 h, respectively. However, when the flue gas flow rate was 25% above its base case value and Q_{reb} was constant at its maximum value, the %CC set point was not reached: the actual %CC maintained by control structure A was 93.7% whereas that of control structure C was 94.2%. This was because the reboiler heat duty required by control structure C was less than that required by control structure A to achieve the same level of CO_2 captured (Fig. 3.23a). On the other hand, the simulation of the plant with control structure B was stopped when the flue gas flow rate was 20% above its base case value and T_{reb} was not controlled by Q_{reb} (at t=127 h). T_{reb} suddenly dropped when Q_{reb} was constant at its upper limit (Fig. 3.23b). As shown in Fig. 3.23c, the reduction in T_{reb} caused an increase in the lean loading; to counter-act this effect, the V1 valve rapidly opened to maintain the %CC around its set point. Opening V1 is meant to increase the MEA flow rate entering the absorber so that it can capture more of the CO_2 from the flue gas stream and thereby increasing the %CC. However, in this scenario, the lean MEA stream eventually becomes rich in CO_2 because of the low temperature in the reboiler unit. This leads to a reduction in the ability of the MEA solution to capture CO_2 in the absorber. Since T_{reb} keeps decreasing, due to the maximum Q_{reb} constraint, the valve V1 will eventually become saturated at the fully-open position and will cause the %CC to continuously drop until it approaches zero, as shown in Fig. 3.22.

Despite the maximum Q_{reb} reached, the plant with either control structure A or C were able to operate and still attain both process control objectives; even though they were not able to achieve the desired %CC set point. However, at each incremental step change in the flue gas flow rate,

control structure C required less Q_{reb} than control structure A. Also, control structure C was able to maintain a higher CO_2 capture rate than that observed for control structure A when Q_{reb} was at its upper bound. Regarding control structure B, T_{reb} is expected to continuously decrease in a real plant; consequently, a significant reduction in %CC, lower than that of control structures A and C, would also be expected.

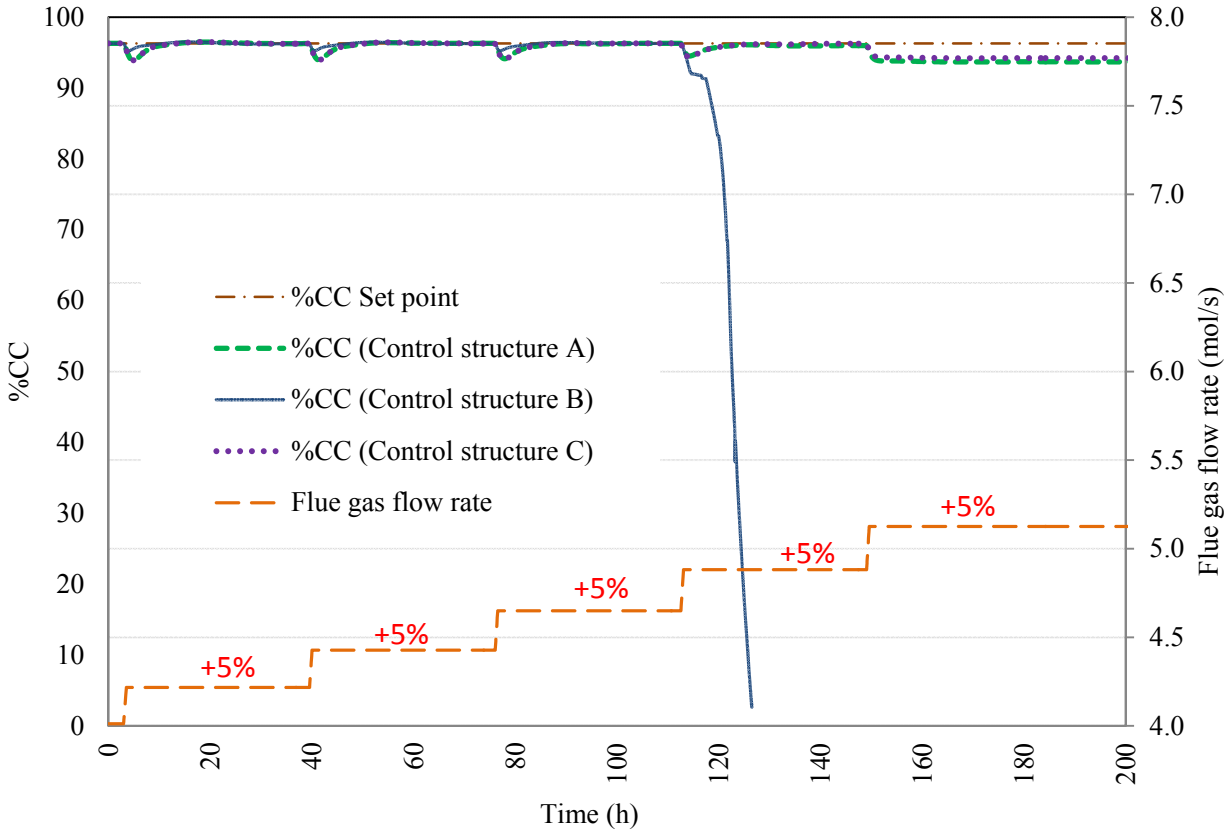

Figure 3.22 %CC Responses of control structures when Q_{reb} is constrained

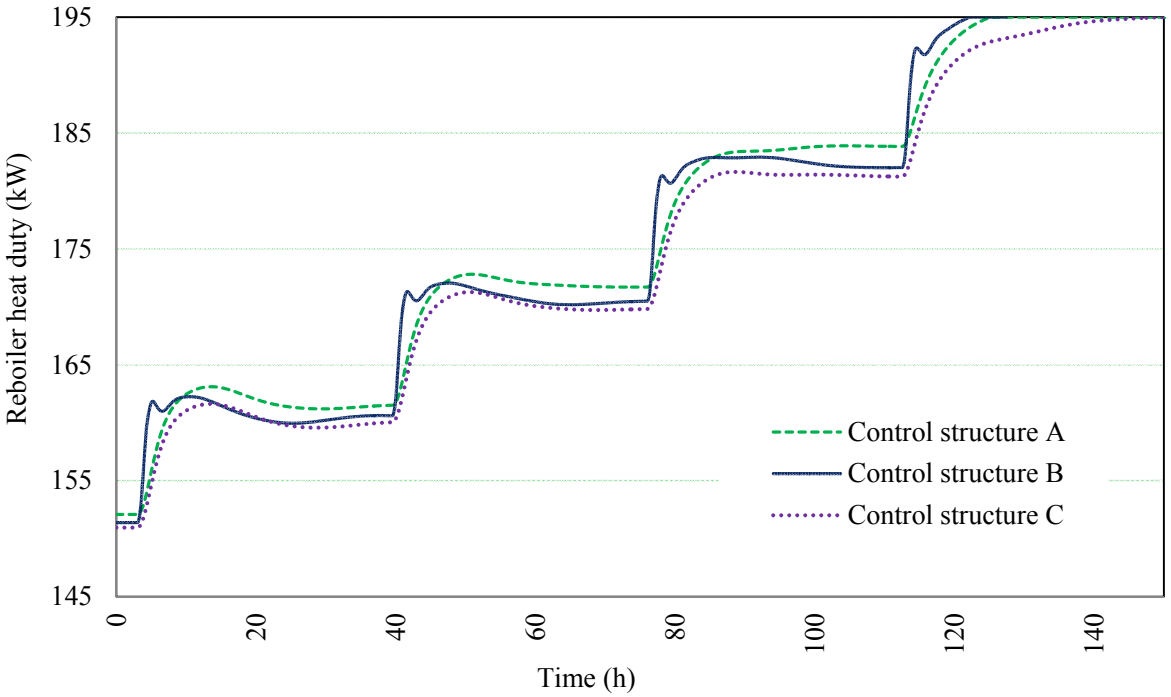

(a)

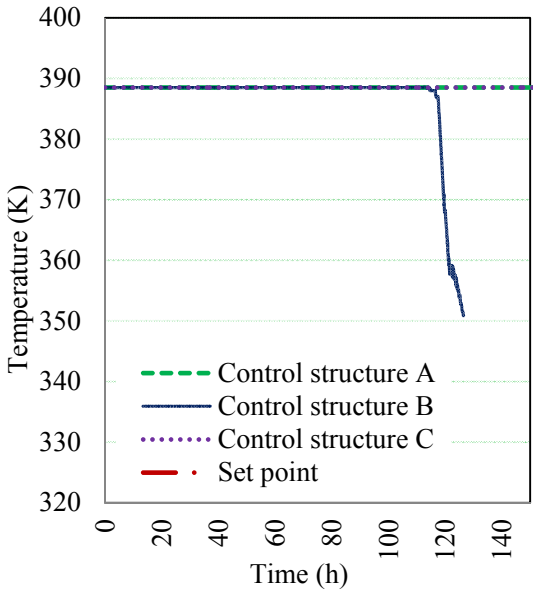

(b)

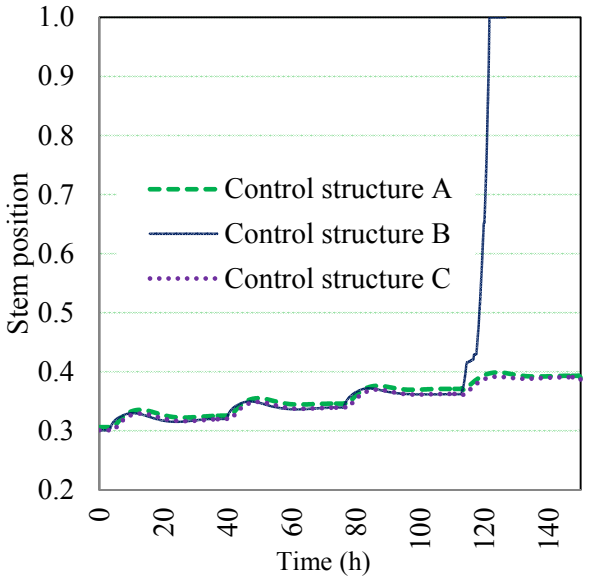

(c)

Figure 3.23 Responses of control structures when Q_{reb} is constrained: (a) Q_{reb}; (b) T_{reb}; and (c) V1

3.6.8 Step-wise increments in the flue gas flow rate

This test aims to determine the response of each control scheme when a large disturbance in the flue gas flow rate is introduced to the plant. Note that the constraint on the reboiler heat duty was not included in this scenario. This scenario was conducted by introducing eight incremental step changes of +5% in the flue gas to the plant, and each step change was introduced every 36 h until the increase in the flue gas flow rate was 1.4 times the base case value.

Due to the large disturbance in the flue gas flow rate, the fractional capacity should be considered to ensure that the operation of the packed columns was within the design range, i.e., 30% to 80% of flooding. Figures 3.24b and 3.24c show the significant change in the fractional capacity in both the absorber (approximately 20%) and the stripper (about 30%) while using the three control schemes considered in this study. As shown in those figures, the % of flooding at the final steady state was still within the acceptable range for both units, i.e., the packed columns never flooded in the presence of these large changes in the flue gas flow rate.

99

As shown in Fig. 3.24a, control structure B was able to attain the CO_2 set point up to the +25% flue gas flow rate; after that point, the settling time required to achieve the same set point was relatively large (> 36 h). On the other hand, control structures A and C resumed the %CC set point slower than control structure B and attained their %CC set point within 36 h up to a +20% increase. When the flue gas flow rate was increased by more than 20%, both control structures also required longer setting times to attain the CO_2 capture set point (> 36 h). When the large disturbance in the flue gas stream was introduced to the plant, the prompt response of the lean amine flow rate entering the absorber became more important to maintain the set point of %CC. For example, due to the controller of %CC-V1 in control structure B, the lean amine flow rate was promptly adjusted when the change in the flue gas flow rate occurred and had the direct effect on the wetted area enhancement in the packed column. In contrast, the sluggish response of *%CC-*Q_{reb} in control structures A and C caused the plant to take longer to attain the CO_2 removal set point when the load disturbance was greater than a +20% increase.

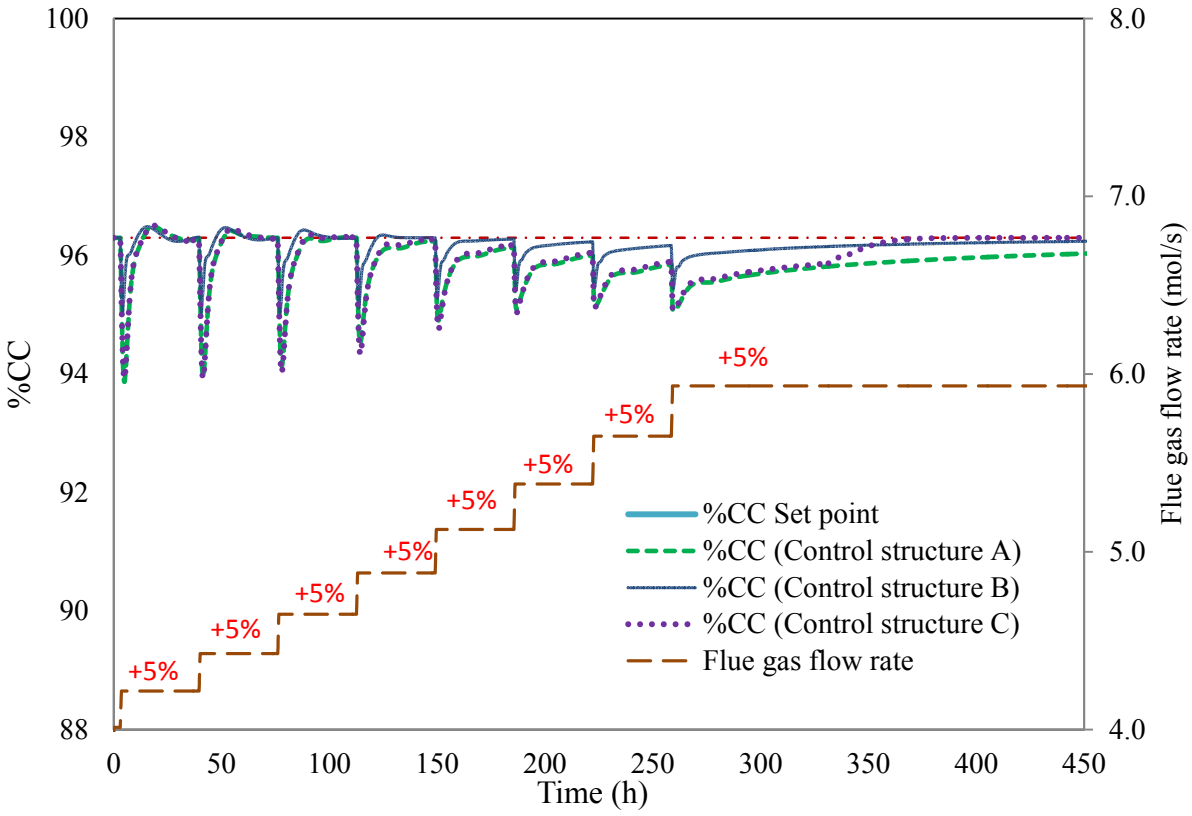

(a)

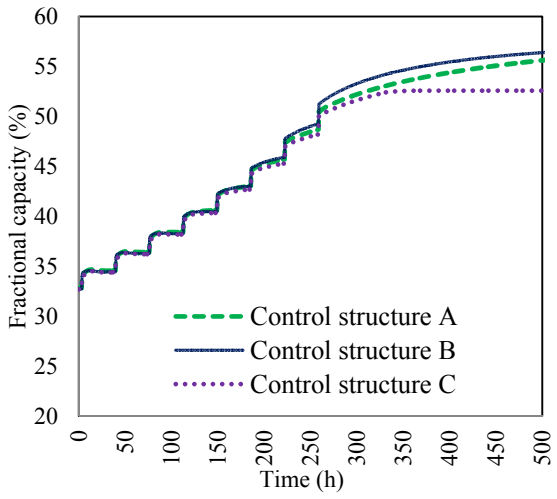

(b)

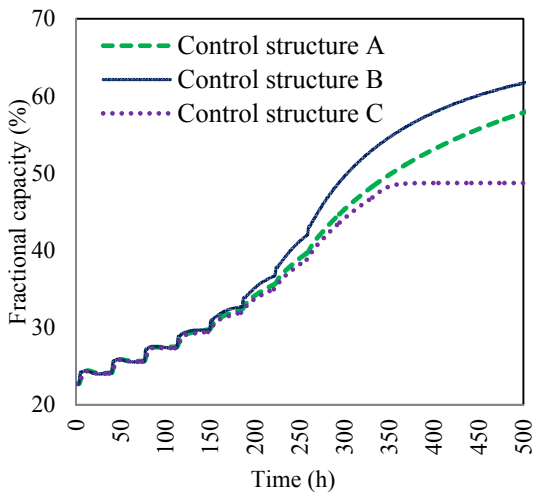

(c)

Figure 3.24 Responses of control structures to large disturbances: (a) %CC; (b) Fractional capacity in the absorber; and (c) Fractional capacity in the stripper

At the disturbance of +40% in the flue gas flow rate, it was observed that in all control schemes that V3 and V2 were saturated, respectively. Fig. 3.25b shows that the V3 valve in control structure B was the first valve that reached its saturation limit due to the quick response of %CC-V1 controller to handle the change in the flue gas flow rate. The high lean MEA flow rate controlled by V1 resulted in large amounts of the rich amine solution accumulated in A102; therefore, the V2 valve need to be opened to maintain the liquid level in A102 until this valve became fully open (Fig. 3.25a). The saturation of V3 and V2 valves also occurred in control structures A and C; however, their valve saturation was slower than that observed for control structure B.

Fig. 3.24a shows that control structures A and B required longer settling times to reach the %CC set point after the loss of those two liquid level controllers, *L2-V2* and *L3-V3*. In addition, A102 and R102 tanks may flood and cause the plant to eventually shutdown (Fig. 3.25c and 3.25d). That is, the liquid inventory control loop is important for the plant to achieve the desired set point faster during transient changes in the operating conditions. On the other hand, control structure C required about 30 h, after V2 reached its saturation limit, to attain the CO_2 capture set point. Due to the absence of the T_{reb}-*V2* controller, the rich MEA flow rate entering the regenerator to maintain the T_{reb} set point approached a constant value. As shown in Fig. 3.25e, the reboiler temperature increased due to the increase in Q_{reb} to attain the %CC set point, and the increase of T_{reb} resulted in the reduction of the lean loading. Although control structure C was able to attain the %CC set point faster than the other control schemes in the presence of large disturbances in the flue gas flow rate, the loss of the T_{reb} controller may cause the overheating of the MEA solution, causing consequently, and sorbent degradation.

In terms of the energy consumption, Fig. 3.25f indicates that the energy required by control structure A was the highest when the disturbance was less than a +20% increase in the flue gas flow rate. For the same region, the energy required by control structures B and C was somewhat similar; however, control structure B showed faster response than control structure C (Fig. 3.24a). For disturbances greater than a +20% increase in the flue gas flow rate, control structure B required the highest energy to capture CO_2 because high lean amine flow rate is needed to maintain the CO_2 capture rate and high Q_{reb} was then required to heat large amounts of MEA

solution in the reboiler. Even though control structures A and C showed similar disturbance rejection performance, the energy required in control structure C was less than that observed for the other control schemes. Furthermore, the variation of the CO_2 purity in the product stream due to the large disturbances in the flue gas flow rate was insignificant since the condenser temperature, which is as a function of the CO_2 content, was tightly controlled using the condenser heat duty.

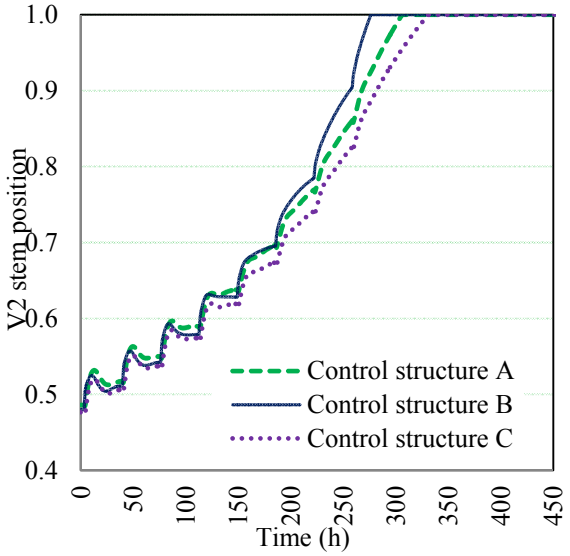

(a)

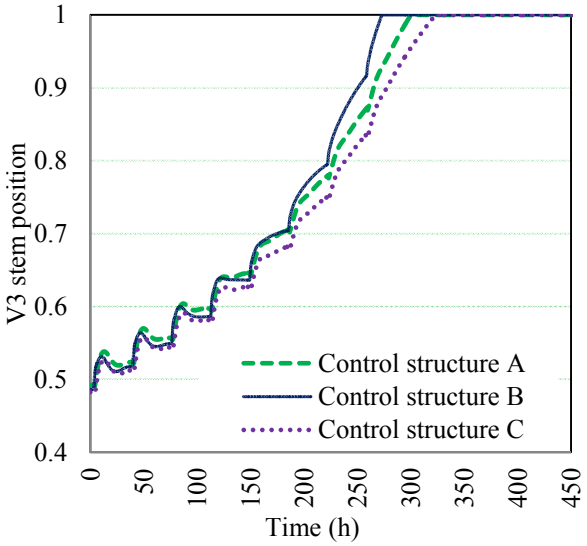

(b)

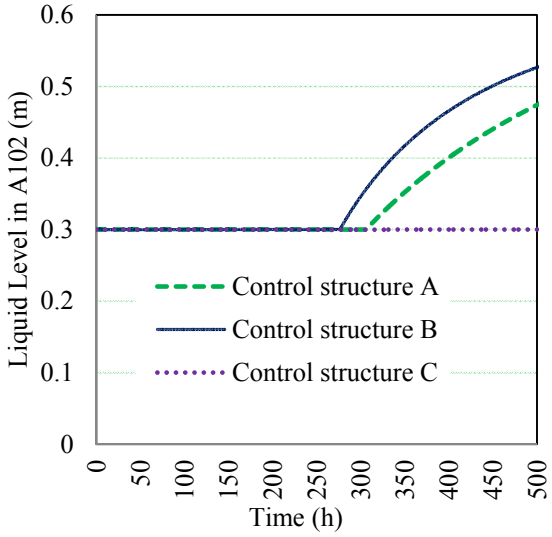

(c)

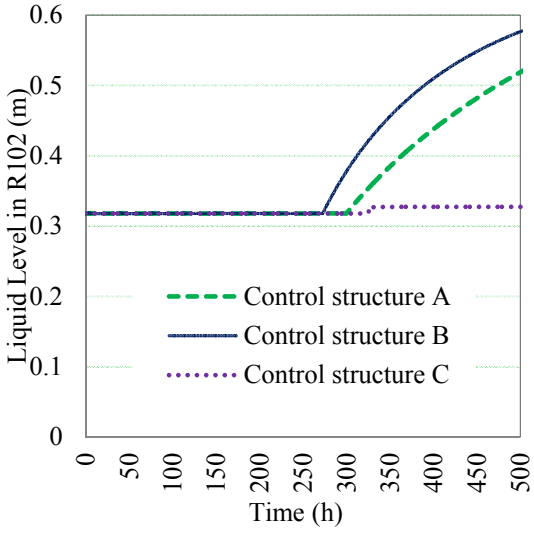

(d)

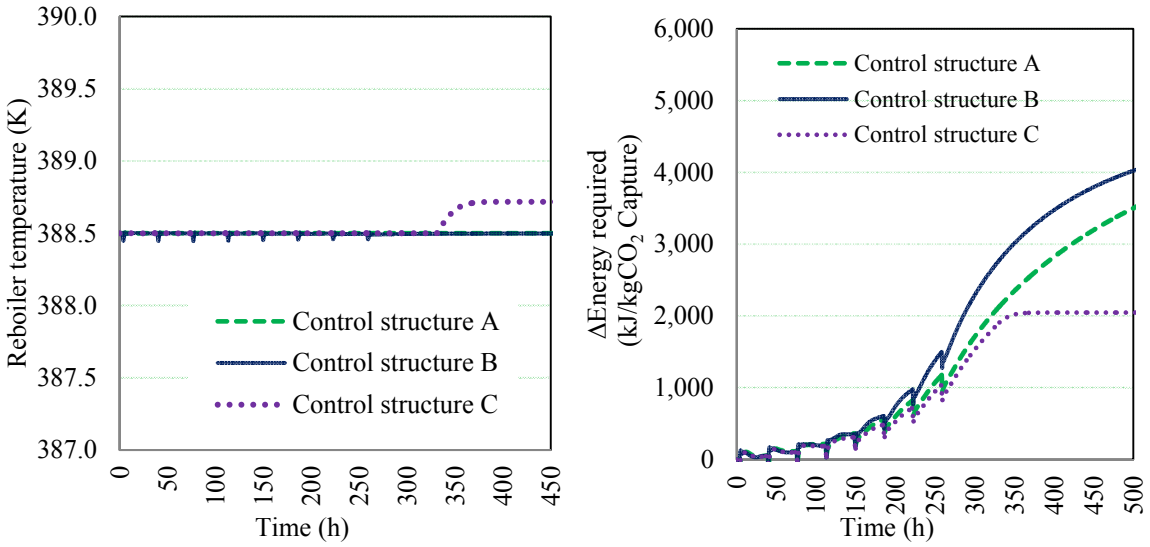

Figure 3.25 Responses of control structures to the large disturbance: (a) V2; (b) V3; (c) Liquid level in A102 (L2); (d) Liquid level in A102 (L2); (e) T_{reb}; and (f) ΔEnergy required

70

3.7 Chapter summary

3.7.1. This chapter presented a mechanistic dynamic model of a post-combustion CO_2 capture pilot plant using MEA as a sorbent. The model proposed in this study represents an improvement over the mechanistic model initially proposed by Harun et al. (2012) by including several process units not considered in the previous work, i.e. the condenser, the absorber sump tank, and the reboiler surge tank. The process units introduced in the model proposed here are essential to design realistic control schemes that can maintain smooth operation of the plant in the presence of changes in the set points or disturbances. Sensitivity analyses were conducted to determine the most suitable controlled and manipulated variables for this process.

3.7.2. Three process control schemes were proposed for the pilot plant of CO_2 capture process. Control structure A was developed using the traditional-RGA analysis approach whereas

the heuristic approach was used to design control structures B and C. These control schemes were evaluated using different scenarios namely changes in the CO_2 capture set points, changes in the operating conditions of the flue gas stream and stiction of the outlet valve of the buffer tank (V1). The proposed control structures were able to achieve the control objectives considered for this process (90 %CC and 95 mol% CO_2 purity).

3.7.3. Control structure B, pairing %CC with V1 and T_{reb} with Q_{reb}, resulted in faster responses to reject disturbances and track the changes in set points than the other control structures. Nevertheless, that control scheme may fail if the reboiler temperature is not in a closed-loop or an error arises in that control loop, e.g., stiction of V1 and/or the saturation of Q_{reb}. The absence of tight control on the reboiler temperature can lead to process variability because V1 will increase the lean solution flow rate if a decrease in %CC is detected while the reboiler heat duty is constant. Although the performance of control structure C, based on the heuristic approach, was somewhat similar to control structure A, control structure C's ISE(%CC) and energy required (ΔEnergy required) was less than that needed for control structure A. The reason that control structures B and C have better performance than control structure A may be due to the assumption of the RGA analysis, i.e., it does not take into account the process dynamics. Furthermore, it is important to note that the regular analysis of process sorbent and valve maintenance are unavoidable to ensure the material balance of water and MEA in process fluid and to prevent an asset integrity problem regardless of which control structure is used.

Chapter 4
Industrial-Scale CO_2 Capture Plant Modelling

Description of the model development for an industrial-scale CO_2 capture plant (for 750 MW supercritical coal-fired power plant) based on the pilot plant model is presented in this chapter. In addition, the purposed control system is implemented to this commercial-scale plant, and the results of its performance evaluation are discussed. The structure of this chapter is organized as follows: Section 4.1 describes the step-by-step method proposed in this study to scale up the process units and describes the mechanistic model development for the CO_2 absorption plant. In addition, the description of the proposed control structure for the commercial-scale CO_2 capture plant is presented in Section 4.1. Section 4.2 presents an analysis on the effect of process equipment design on the plant's energy consumption, and the plant's performance under several scenarios, including a study on the dynamic behaviour of this plant under process scheduling. The commercial-scale CO_2 capture plant's capacity and performance obtained while using the proposed mechanistic plant model are summarized at the end of this article.

4.1 Scale-up procedure and model development

The large-scale CO_2 capture plant dynamic model proposed in this chapter is based on the mechanistic pilot-scale CO_2 capture plant that was proposed in Chapter 3. Based on the insights gained from that model, this chapter presents the dynamic modelling of a commercial-scale MEA absorption processes for CO_2 capture and proposes a process control system that can reject disturbances and switch between different operating conditions in a smoothly fashion.

The scale-up of the CO_2 capture plant aims to determine the major equipment's dimensions that can accommodate the flue gas flow rate normally produced from a coal-fired power plant. An MEA solution with a concentration of 10 mol% (Harun et al., 2012) is used as the absorbent, whereas the operating conditions considered in this commercial-scale plant, i.e. reboiler temperature, lean amine temperature, and CO_2 concentration in the CO_2 product stream, were similar to that of the pilot plant presented in Chapter 3.

The steps proposed for scale-up of the CO_2 capture plant using MEA absorption and the mechanistic model development are as follows:

1) Specification of process objectives
2) Specification of input data, i.e. flue gas flow rate and its composition
3) Estimation of process units' dimensions
4) Integration of all process equipment and implementation of the proposed control scheme.

The process flow sheet of the industrial-scale CO_2 capture plant proposed in this study is presented in Fig. 4.1, whereas each step of the scale-up procedure is discussed next in detail.

4.1.1 Specification of process design objectives

In this study, the industrial-scale CO_2 capture plant was designed to remove CO_2 from flue gas produced from a 750 MW supercritical coal-fired power plant with two specific process design goals:

(i) Maintain the percentage of CO_2 capture rate (%CC) at 87% or more.
(ii) Obtain a CO_2 product stream with a CO_2 concentration of 95% or more.

The CO_2 capture specification of 87% considered in this study is based on an economic study of a commercial-scale CO_2 capture plant presented by Rao and Rubin (2006). In order to meet the second process design objective, a condenser, that can maintain a CO_2 concentration at 95% or above, needs to be designed.

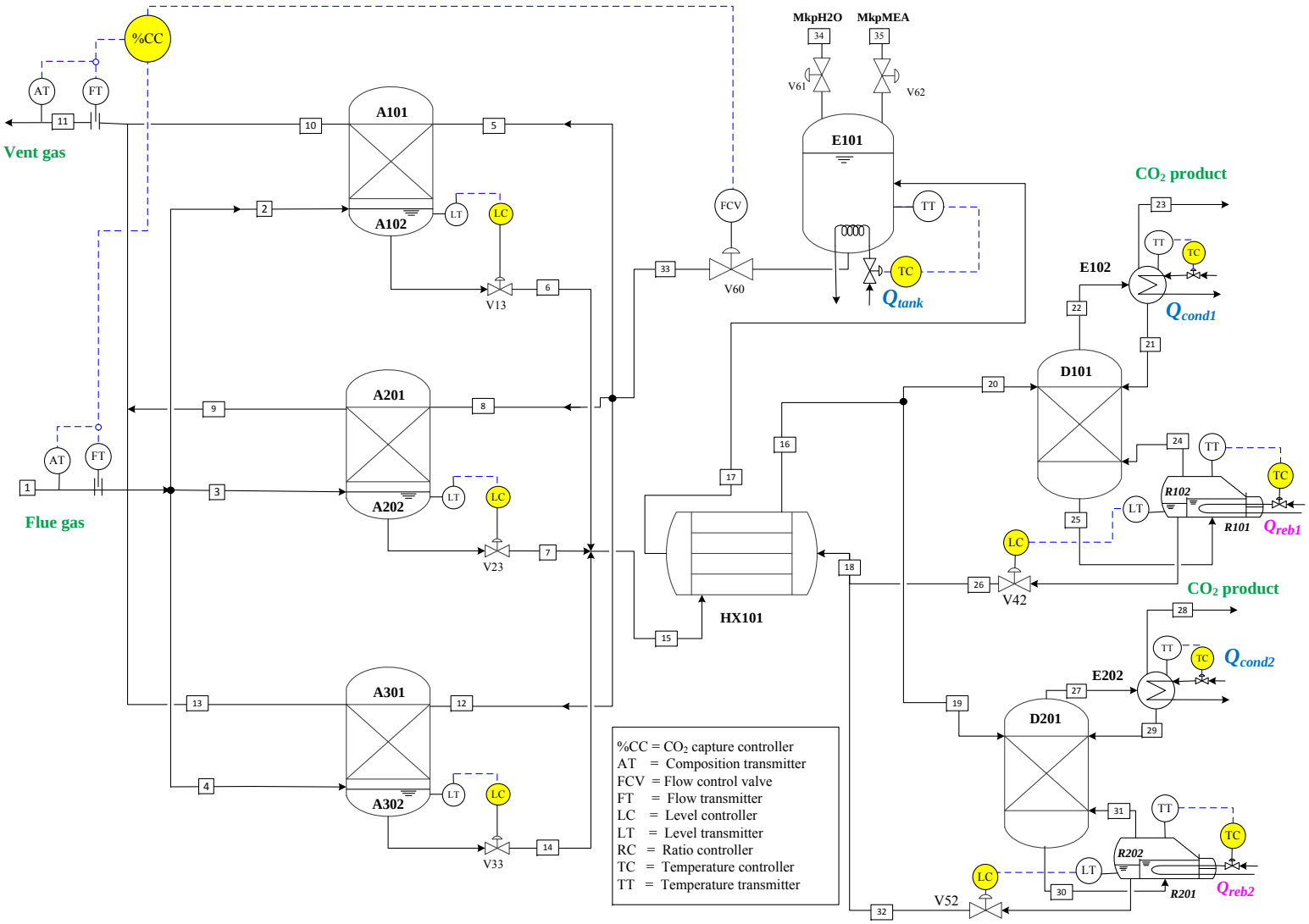

Figure 4.1 Flowsheet of the commercial CO_2 capture plant

4.1.2 Specification of input information

At the base case condition, a typical 750 MW power plant was assumed to generate the electrical power of 650 MW which is approximately 85% of the maximum power plant capacity. That is, the produced flue gas flow rate and composition were determined based on the base case condition and a supercritical power plant's efficiency (HHV basis) of 40% (Dowel and Shah, 2013; Beer, 2009; IEA, 2012). The flow rate of Pittsburgh#8 bituminous coal (NETL, 2012) fed into a furnace was estimated using the following equation (Dowell and Shah, 2013):

$$Q_e = \eta_{comb} m_{coal} HHV \tag{4.1}$$

where Q_e (MW) is the electrical energy; η_{comb} (%) is the overall plant efficiency; m_{coal} (kg/s) is the mass flow rate of coal; HHV (kJ/kg) is the high heating value. As a result, a coal flow rate of 52 kg/s (6.2 kmol/s) was required. The estimation of the total flue gas flow rate and compositions entering an industrial-scale CO_2 capture plant was based on the following assumptions:

i) The excessive air flow rate (10% higher than that required for complete combustion) was fed into a combustor to ensure a complete combustion.
ii) Particulate matter, sulphur dioxide (SO_2) and nitrogen oxide (NO_x) in the flue gas stream leaving the furnace have been removed prior to entering the CO_2 capture plant since those compounds may negatively affect the efficiency in the absorption process; a SO_2 content of 10 ppm or higher in the flue gas may lead to the formation of stable salts due to the reaction of SO_2 with MEA (Wang et al. 2011).

Based on the above, the flue gas flow rate entering the CO_2 capture plant (20 kmol/s) and its composition are presented in Table 4.1.

Table 4.1 Flue gas flow rate and its composition at the base case condition (650 MW)

Variable	Value
Flue gas flow rate (kmol/s)	20
Mole fraction	
CO_2	0.163
H_2O	0.025
N_2	0.793
O_2	0.019

4.1.3 Estimation of process units' dimensions

4.1.3.1 Packed columns

This section aims to determine the dimensions of the absorber and stripper required to meet the process objectives mentioned in Section 4.1.1. Consequently, the original packed column models (Harun et al. 2012) were modified in accordance with the packed column dimensions obtained from the scale-up calculation. The size of the packed columns, including packed bed height, column internal diameter, and the number of the packing columns, was determined based on available commercial columns and features, i.e. this study assumed that the maximum column diameter available in the market is 12 m (Chapel et al., 1999; Reddy et al., 2003; and Ramezan and Skone, 2007). The design approach for the packed columns in this study is as follows:

i) Specification of the process unit objectives
ii) Input process information
iii) Select the packed column's internal feature
iv) Determine liquid and gas flow rates required for the absorption and desorption, respectively
v) Specify the column diameter (D_c)
vi) Determine the packed bed height (Z_c)

The description of each step is presented next.

i) The design objective of the absorber is to capture 87% of the CO_2 included in the flue gas stream using the lean amine stream, which contains 10 mol% of MEA. The goal of the stripper is to regenerate the absorbent by reducing the CO_2 concentration in the rich amine solvent,

resulting in attaining a lean loading in the recycled lean amine stream in the range of 0.25 to 0.3 moles of CO_2/ moles of MEA (Alie et al., 2005; Abu-Zahra et al., 2007). Note that, for safety reason, the flue gas molar flow rate used to size the packed columns (absorber and stripper) was 15% higher than the normal operating condition, i.e. the total flue gas flow rate produced from the power plant was 20 kmol/s at the base case condition while the design flue gas flow rate used to design the packed columns was assumed to be 23 kmol/s.

ii) Process information was used for the preliminary calculation including the physical properties of the MEA solution, i.e. density and kinematic viscosity, and operating conditions, i.e. design temperature and pressure. This information was obtained from the pilot plant model previously developed and presented in Chapter 3.

iii) In this study, the internal feature of the packed columns was the same used in the packed columns in the pilot plant, i.e., random packing; however, instead of 40 mm random packing, the packing size of 50 mm diameter, with the packing factor (F_p) of 59 m^{-1} (18 ft^{-1}) (Kister, 1992), was filled into the large-scale packed columns to prevent high pressure drops in those columns which might result in a flooding problem in packed columns.

iv) In this step, the lean amine flow rate required to remove 87% of CO_2 in the flue gas stream entering the absorber needs to be estimated. This calculation was performed assuming constant gas and liquid flow rates throughout an absorber column and the outlet amine stream containing the rich loading of 0.5 (Harun et al., 2012). As for the stripper, the steam flow rate (gas phase) entering the bottom of the stripper was estimated based on the design objective to produce a lean loading in the lean MEA stream leaving the reboiler of 0.3. These calculations showed that this commercial-scale CO_2 capture plant required a lean amine flow rate and a steam flow rate of approximately130 kmol/s and 12 kmol/s, respectively.

v) The required diameter of the packed column mainly depends on two factors:

(1) The ratio of the gas flow rate to the liquid flow rate entering the column.
(2) The design flooding point, which is described by the hydraulic packing parameters, i.e. percentage of flood (*%flood*), flow parameter (*FP*) and capacity parameter (*CP*).

In order to determine *%flood*, the total pressure drop on each packed column was computed as follows (McCabe et al., 2005):

$$\Delta P_{flood,tot} = 0.115 F_p^{0.7} \tag{4.2}$$

where $\Delta P_{flood,tot}$ (inH_2O/ ft of packing) is the total pressure drop in the packed column in which the column flooding occurs due to high gas flow rate, and F_p (ft^{-1}) is the packing factor. The packed column using 50 mm random packing may be flooded at a pressure drop of 0.7 kPa/m of packing (0.87 inH_2O/ ft of packing). According to the Generalized Pressure Drop Correlation (GPDC) chart for random packing given in Kister et al. (2007), experimental data is available at 0.5 and 1.0 inH_2O/ft; however, to avoid an inaccuracy due to interpolation, the estimation of the flooding point in this study used a pressure drop at the flooding point of 0.5 inH_2O/ft. The mathematical correlation of the flow parameter (*FP*) and the capacity parameter (*CP*) at the pressure drop at flood of 0.5 inH_2O/ft, which has been determined using data from Kister et al. (2007), is shown in Fig. 4.2; fitting equation as follows:

$$CP = -0.235 \ln(FP) + 0.6728 \tag{4.3}$$

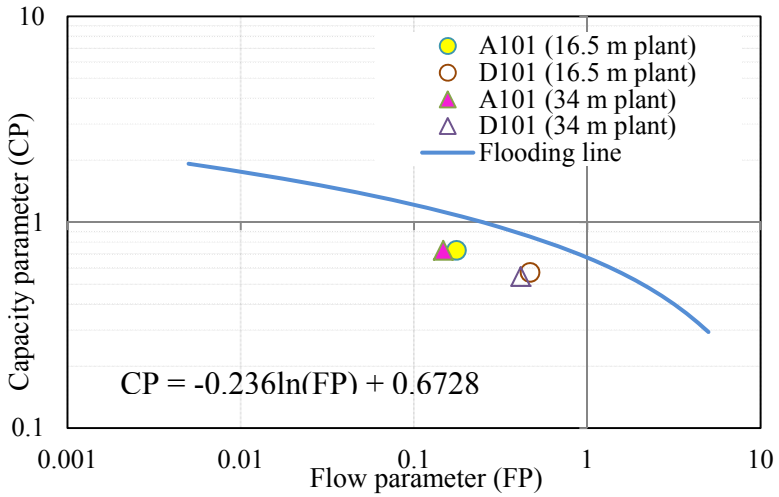

Figure 4.2 Hydraulic packed column for the pressure drop at flooding point of 0.5 inH_2O/ft

The flow parameter (FP) mainly depends on the ratio between the gas flow rate and the liquid flow rate entering a packed column (McCabe et al., 2005), i.e.

$$FP = \frac{G_m}{L_m}\sqrt{\frac{\rho_g}{\rho_l}} \tag{4.4}$$

where G_m (kg/m^{2}s) and L_m (kg/m^{2}s) are mass velocities of gas and liquid streams entering a packed column, whereas ρ_g (kg/kmol) and ρ_l (kg/kmol) are densities of gas and liquid in those streams, respectively. Using Fig.4.2 and the FP value, the capacity parameter (CP) was then determined. Next, the flooding velocity (C_s) in both the absorber and stripper were computed using the following expression (McCabe et al., 2005):

$$C_s = \frac{CP}{F_p^{0.5}\upsilon^{0.05}} \tag{4.5}$$

where υ (centistoke) is the kinematic viscosity of the liquid stream and C_s (ft/s) is the flooding velocity. A percentage of flood of 70% was assumed in both packed columns (Kister,1992); therefore, the operating flooding velocity ($C_{s,oprt}$) was determined by multiplying 0.7 to the flooding velocity (C_s). Furthermore, the operating superficial velocity (u_o) of the gas stream, i.e.

the flue gas stream entering an absorber and the steam flowing into a stripper, was estimated as follows (McCabe et al., 2005):

$$u_o = \frac{C_{s,oprt}}{\sqrt{\frac{\rho_g}{\rho_l - \rho_g}}} \tag{4.6}$$

As a result, the required diameter of a packed column designed to operate at 70% flooding velocity was estimated as follows (McCabe et al., 2005):

$$D_c = \sqrt{\frac{4F_{G,m}}{\pi u_o \rho_g}} \tag{4.7}$$

where $F_{G,m}$ (kg/s) is the mass flow rate of the gas stream whereas D_c (m) is the diameter of the packed column. As shown in Fig. 4.3, a CO_2 capture plant from a 750 MW coal-fired power plant required three absorbers with 11.8 m diameter each and two strippers with diameter of 10.4 m. These calculations were based on the assumption that the maximum column's diameter for a commercial absorption or stripper tower is 12 m.

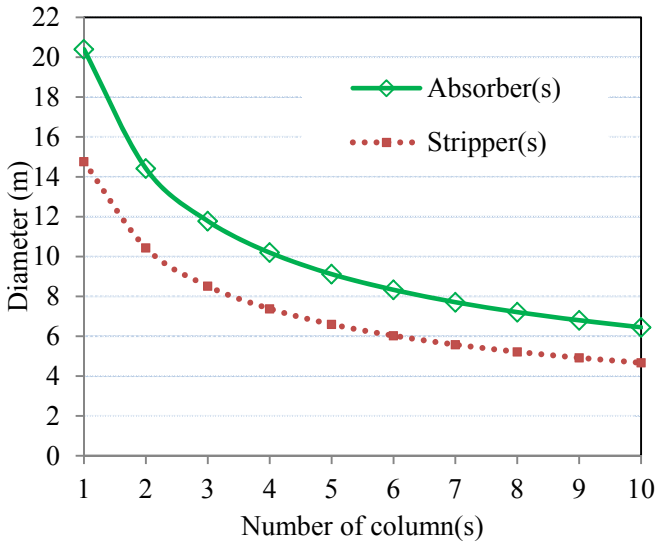

Figure 4.3 Relationship of the number of packed columns and packed columns' diameters

vi) As shown in Eq. 4.8, the packed bed height (Z_c) is a function of the overall mass transfer coefficient and components in gas and liquid streams (McCabe et al., 2005), i.e.

$$Z_c = \frac{G_m}{K_G a \cdot P} \int_{y_1}^{y_2} \frac{1}{y - y_e} dy = H_{OG} N_{OG} \tag{4.8}$$

where y_1 and y_2 are the mole fraction of solute in the inlet and outlet gas streams (See Fig.4.4), respectively; y is the mole fraction of solute in gas phase at any point in the column whereas y_e is the equilibrium mole fraction of solute; $K_G a$ (1/h) is the overall volumetric mass transfer coefficient for the gas phase; N_{OG} is the number of overall transfer units based on the gas phase whereas H_{OG} (m) is the height of the transfer unit.

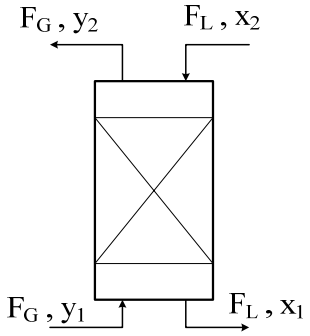

Figure 4.4 Packed column flowsheet

The number of overall transfer units (N_{OG}) is the average driving force in the liquid and vapour phase, i.e., N_{OG} indicates the level of difficulty of the separation. High N_{OG} indicates that a high packed column is required to achieve the designated concentration of solute in an outlet gas stream. In this study, the lean amine stream flowing to the absorber was considered as the dilute solution, i.e. CO_2 concentration in the amine solvent is less than 10 wt%. Therefore, the number of overall transfer unit is calculated as follows (Towler and Sinnott, 2008):

$$N_{OG} = \frac{1}{(1-\lambda)} \ln\left((1-\lambda) \frac{y_1}{y_2} + \lambda \right) \tag{4.9}$$

where y_1 and y_2 are the mole fractions of CO_2 in the flue gas and in the vent gas streams (See Fig.4.4), respectively; λ is the ratio of gas to liquid molar flow rates, i.e.,

$$\lambda = \frac{mF_G}{F_L} \tag{4.10}$$

where m is the slope of the equilibrium line between mole fraction of CO_2 in vapour and liquid phases, and F_G (kmol/s) and F_L (kmol/s) are the gas molar flow rate and the liquid molar flow rate entering a packed column (See Fig.4.4). Moreover, the height of the transfer unit (H_{OG}) indicates the packing efficiency and is calculated as follows (McCabe et al., 2005):

$$H_{OG} = H_G + m\frac{F_G}{F_L}H_L \tag{4.11}$$

The film transfer unit height in the gas (H_G) and the liquid (H_L) are computed using Onda's method (Towler and Sinnott, 2008), which was based on experimental data from different types of packing. The expression for H_G and H_L are as follows:

$$H_G = \frac{G_m}{k_G \cdot a_w \cdot P} \tag{4.12}$$

$$H_L = \frac{L_m}{k_L \cdot a_w \cdot C_t} \tag{4.13}$$

where a_w (m^2/m^3) is the interfacial area per unit volume, which is a specific characteristic of packing types and size, P (kPa) is the operating pressure in a packed column, whereas k_G ($kmol/s.m^2kPa$) and k_L (m/s) are the gas film mass transfer coefficient and the liquid film mass transfer coefficient, respectively. C_t ($kmol/m^3$) is the total concentration of liquid which is determined by the ratio of the density of MEA solution to its molecular weight.

In addition, the height equivalent of a theoretical stage (*HETP*) is a useful parameter that specifies the height of the packing column required to provide the same separation as an equilibrium stage. The expression used to estimate the *HETP* is as follows (Towler and Sinnott, 2008):

$$HETP = H_{OG}\frac{\ln \lambda}{\lambda - 1} \tag{4.14}$$

Based on the above, the bed height of each absorber considered in this study was estimated to be 16.5 m and its HETP is 1 m whereas the individual stripper requires a bed height of approximately 5 m with an HETP of 0.85 m. The stripper's bed height obtained from the present analysis might be underestimated for the following reasons: (i) the assumption regarding an instantaneous reaction in the stripper results in high mass transfer rates of CO_2 from the liquid phase to the gas phase, and (ii) the equilibrium condition assumption in the reboiler unit (Harun et al., 2012; Freguia and Rochelle, 2003). Based on the recommended length-diameter (L_c/D_c) ratio for a vertical vessel, L_c/D_c should be in the range of 2 – 5 (InIPED, 2013), where L_c is the total vessel length including packed bed height and the mechanical parts, i.e. demister, liquid redistributor, liquid accumulator. Each stripper's total height was thus assumed to be 27.6 m while its bed height was 16 m. The vessel length required for other mechanical parts was 11.6 m, estimated based on the guidelines provided by Campbell et al. (2004). Therefore, L_c/D_c of the each stripper was 2.6. Likewise, the absorber bed height of 16.5 m and its column length for mechanical parts was 12 m; consequently, L_c/D_c of each absorber was 2.4. Nevertheless, only the bed height was considered in the mechanistic modelling. The dimension of the packed columns is presented in Table 4.2.

4.1.3.2 Other process units

The dimensions of other process units presented in Fig. 4.1, including cross heat exchanger, reboilers, condensers, tanks and valves, were determined based on equations described in Chapter 3. The size of the cross heat exchanger (HX101) was recalculated in order to achieve the design outlet liquid temperatures (rich and lean amine streams (stream 16 and 17 in Fig. 4.1)). Likewise, for the three absorber sump tanks (A102, A202, and A302), their diameters were assumed as 11.8 m which were the same diameter of those absorbers (A101, A201, and A301). Similarly, the reboiler surge tanks' diameter of 10.4 m (R102 and R202) is equal to the strippers' diameters. The liquid levels in the absorber sump tanks and reboiler surge tanks were maintained such that the residence time of liquid in these tanks is in the range of 3 – 5 min (GPSA, 1999). Note that the reboilers and the condensers were modeled based on the thermodynamic

equilibrium relationships (Harun et al. 2012; Harun, 2012), i.e., the outlet flow rates of vapour and liquid streams were determined using the vapour-liquid equilibrium ratio (K_{value}). Therefore, the sizes of these units have no effect on the thermodynamic equilibrium conditions. The dimensions of the process equipment is summarised in Table 4.2.

Table 4.2 Equipment specification and operating condition for a commercial-scale CO_2 capture plant model

Parameter	**Value**
Absorber (A101, A201, A301)	
- Internal diameter (m)	11.8
- Height (m)	16.5
- Packing size (mm)	IMTP#50
- Nominal packing size (m)	0.05
- Specific area (m^2/m^3)	102
- Operating temperature (K)	314 – 329
- Operating pressure (kPa)	101.3 – 104.7
- HETP (m)	1
Stripper (D101, D201)	
- Internal diameter (m)	10.4
- Height (m)	16
- Packing size (mm)	IMTP#50
- Nominal packing size (m)	0.05
- Specific area (m^2/m^3)	102
- Operating temperature (K)	350 – 380
- Operating pressure (kPa)	156.7 – 160
- HETP (m)	0.85
Reboiler (R101, R201)	
- Operating temperature (K)	383 – 393
- Operating pressure (kPa)	160
Condenser (E102, E202)	
- Operating temperature (K)	312 – 315
- Operating pressure (kPa)	159
Cross heat exchanger (HX101)	
- Internal diameter of shell (m)	3.048
- Internal diameter of tube (m)	0.016
- Outer tube diameter of tube (m)	0.019
- Length (m)	6
- Number of tubes (number of pass(es))	14,459 (1)
- Conductive heat transfer coefficient of tube metal (W/m^2)	16
Buffer tank (E101)	
- Internal diameter (m)	12
Absorber sump tank (A102, A202, A301)	
- Internal diameter (m)	11.48
Reboiler surge tank (R101T, R201T)	
- Internal diameter (m)	10.44
Valves	
C_v of V13,V23,V33 (m^2)	0.37
C_v of V42, V52 (m^2)	0.55
C_v of V60 (m^2)	0.93

4.1.4 Integration of all process equipment and implementation of a control scheme

Fig. 4.1 presents the process flowsheet of a commercial-scale CO_2 capture plant equipped with a control system. At the base case condition, the flue gas flow rate of 20 kmol/s, produced from a 750 MW power plant, enters the CO_2 capture plant and is assumed to be equally distributed between the three absorbers (A101, A201 and A301) whereas the lean amine flow rate of 43.6 kmol/s enters each absorber to achieve 87% CO_2 capture. Three rich amine streams are mixed and enter the cross heat exchanger (HX101, in Fig. 4.1) on the tube side to be preheated, by the lean amine streams from the reboilers flowing through the shell side. Then, the hot rich amine stream is equally separated to two streams, flowing to each stripper (D101 and D201 in Fig. 4.1). The amine sorbent regeneration occurs in the strippers due to the instantaneous reaction between CO_2 and MEA at high operating temperature (350 – 380 K). The vapour phase streams, leaving strippers D101 and D201 with a high content of CO_2 (70 – 78 mol%), flow to condensers E102 and E202, respectively. Those condensers are used to increase the CO_2 concentration in the CO_2 product stream (gas phase) to at least 95% by condensing water and MEA using a cooling medium. The liquid phase streams leaving the condensers, which are composed of mainly water (95 mol% H_2O) coming from E102 and E202, are recycled back to the top of strippers D101 and D201, respectively. In order to produce steam (vapour phase) to regenerate the rich amine solution in strippers and reduce the lean loading of the recycled lean amine streams (liquid phase), the liquid streams leaving from the bottom of strippers D101 and D201 are sent to reboilers R101 and R102, respectively. The combined lean amine stream from the two reboilers then flows to the cross heat exchanger (HX101) and mixes with the makeup streams of water and MEA in the buffer tank, E101, prior to being distributed to each absorber. At the base case condition, every absorber operates at 67.5% flood whereas the flooding velocities of the two strippers are 67.1%, as presented in Fig. 4.2. In addition, the total reboiler heat duty required to attain 87%CC at the base case condition is 4.4 GJ/tCO_2.

Furthermore, the process control scheme (see Fig. 4.1) used for the industrial-scale CO_2 capture plant in this study was based upon the control configuration similar to control structure B,

proposed in Chapter 3. That control structure was evaluated based on the pilot plant model and showed good performance of disturbance rejection and set point tracking when compared to other control schemes (control structures A and C). Control structure B was designed using heuristics and is composed of two key control loops:

i) The first control loop is the pairing of the percentage of CO_2 removal (%CC) with the lean amine flow rate entering an absorber. Indeed, the adjustment of the MEA solution flow rate has the direct and fast effect on the %CC change.
ii) The second control loop is the pairing of the reboiler temperature (T_{reb}) and the reboiler heat duty (Q_{reb}). The $T_{reb} - Q_{reb}$ controller aims at maintaining the reboiler temperature since T_{reb} indirectly affects the CO_2 concentration in the recycled lean amine stream entering the absorption process.

The rest of the control loops follows the Relative gain array (RGA) recommendations. Since the process flow sheets of the pilot plant, presented in Chapter 3, and this commercial-scale CO_2 capture plants are somewhat similar, the basic principle of control structure B was applied to the industrial-scale plant model, presented in this chapter.

Based on the above, a decentralized multi-loop control scheme composed of 11 Proportional-Integral (PI) controllers, shown in Fig. 4.1 and Table 4.3, was used to control this industrial-scale CO_2 capture plant. The liquid levels in the absorber sump tanks (A102, A202, and A302) and the reboiler surge tanks (R102 and R202) are controlled using the corresponding tanks' outlet valves. The temperature in the reboilers R101 and R201 are controlled using the reboiler heat duties Q_{reb1} and Q_{reb2}, respectively. Likewise, the condenser heat duties in Q_{cond1} and Q_{cond2} are used to maintain the condenser temperatures (T_{cond1} *and* T_{cond2}) at 310 K which corresponds to 96.3 mol% CO_2 in the CO_2 product streams (streams 23 and 28 in Fig. 4.1). Using a coolant represented by the buffer tank heat duty (Q_{tank}), the temperature of the lean amine stream leaving E101 (stream 33 in Fig. 4.1) was maintained at 314 K, which is the optimum temperature to enhance the exothermic reaction in absorbers (Moser et al., 2009). Moreover, Proportional-

Integral (PI) controllers were used for each control loop considered in the present control strategy. The tuning parameters (Table 4.3) for each controller, i.e., controller gain (K_c) and integral time constant (τ_I),were initially tuned using Internal Model Control (IMC) (Seborg et al., 2011) and manually retuned, aiming to obtain fast and smooth process responses to changes in the operating conditions.

As shown in Fig. 4.1, the overall CO_2 capture rate (%CC) is measured using the CO_2 composition transmitters (AT) and flow transmitters (FT) located at the inlet flue gas stream (stream 1) and at the vent gas stream (stream 11), and %CC is maintained at 87%CC using V60 to manipulate the total lean amine flow rate entering the absorbers. Although the individual control of %CC in each absorber can be practically used in the real plant by controlling the lean amine flow rate entering each absorber, the individual %CC control could not be implemented in the present model due to the limitation in the number of degrees of freedom. The following equation describes the total material balance of the lean amine flow rates leaving E101 (stream 33) and entering each absorber (streams 5, 8, and 12):

$$F_{out,E101} = F_{L,A101} + F_{L,A201} + F_{L,A301} \tag{4.15}$$

where $F_{L,A101}$, $F_{L,A201}$, and $F_{L,A301}$ (kmol/s) are lean amine flow rates entering each absorber, A101, A201 and A301, respectively. The lean amine flow rate leaving E101 ($F_{out,E101}$, kmol/s) is computed based on the liquid level in E101 and the V60 stem position. Therefore, there are only another two variables (out of 3) in Eq. (4.15) to be specified. For example, if $F_{L,A101}$ and $F_{L,A201}$ were specified aiming to maintain 87%CC in A101 and A201, the remaining lean amine flow rate flowing from E101 would enter A301. That is, during transient changes in the plant's operating conditions, the lean amine flow rate entering A301 ($F_{L,A301}$) might become a disturbance and affect the %CC in A301. Instead of controlling %CC on each absorber, the overall %CC control was thus measured and used to determine the plant's performance.

Table 4.3 Set points and tuning parameters

NO.	CV	MV	Set point	K_c	τ_I (min)
1	Liquid level in A102 (L13)	Outlet valve stem position of A102 (V13)	2.5 m	25	1.7
2	Liquid level in A202 (L23)	Outlet valve stem position of A202 (V23)			
3	Liquid level in A302 (L33)	Outlet valve stem position of A302 (V33)			
4	Liquid level in R102 (L42)	Outlet valve stem position of R102 (V42)	4 m	0.5	1.7
5	Liquid level in R202 (L52)	Outlet valve stem position of R202 (V52)			
6	Condenser temperature in E102 (T_{cond1})	Condenser heat duty in E102 (Q_{cond1})	310 K	0.06	1.33
7	Condenser temperature in E202 (T_{cond2})	Condenser heat duty in E202 (Q_{cond2})			
8	Reboiler temperature in R101 (T_{reb1})	Reboiler heat duty in R101 (Q_{reb1})	388.7 K	1.52	2.78
9	Reboiler temperature in R101 (T_{reb2})	Reboiler heat duty in R201 (Q_{reb2})			
10	Lean amine temperature in E101 (T_{tank})	Buffer tank heat duty in E101 (Q_{tank})	314K	1.5	2.73
11	Overall percentage of CO_2 removal (%CC)	Outlet valve stem position of E101(V60)	87%	0.01	100

4.2 Performance evaluation of an industrial-scale CO_2 capture plant

This section presents first the analysis on the effect of the absorber bed height on the plant's energy consumption. The absorber bed height obtained from that analysis was then used to evaluate the plant's performance under four different scenarios. The summary of the plant performance is presented in Table 4.4. Note that an analysis on the stripper bed height was not conducted due to the assumptions made for the stripper and reboiler models, i.e., an instantaneous reaction in strippers due to high operating temperature and an equilibrium condition between liquid and vapour phase in reboilers (see Section 4.1.3).

Table 4.4 Summary of the commercial-scale CO_2 capture plant's performance

NO.	Scenario	Settling time to reach new steady state of %CC	Remark
1	Effect of the absorber bed height on the energy consumption	Steady state test	A 34 m absorber bed height offers the minimum energy required.
2.1	+10% Flue gas flow rate	6 h	Insignificant oscillation
2.2	Maximum flue gas flow rate	6 h	Maximum flue gas flow rate is 24.3 kmol/s
3	+5% CC set point	2 h	Insignificant oscillation
4	Sinusoidal change in the flue gas composition	2 h	The disturbance frequency affected the variation in the controlled variables' amplitudes and frequencies.
5.1	Sinusoidal change in the flue gas flow rate	Actual %CC varied around 86% – 88 %	–
5.2	Sinusoidal change in the flue gas flow rate and %CC change	Actual %CC varied around 86 % – 90 %	Avoid a poor wetting condition in the strippers during low power demand.

4.2.1 Effect of the absorber bed height on the energy consumption

A key design parameter that affects the entire CO_2 capture process is the absorber bed height. This is because large bed heights promote CO_2 mass transfer from the gas to the liquid phase due to the enhancement of the wetted contact area of packing and contact time, which will therefore

affect the recycled lean amine flow rate, the liquid temperature profile in the absorbers and the plant's energy consumption. Accordingly, this study varied the absorber bed height from 15 m to 38 m to assess the effect of this design parameter on the plant's key process variables, i.e., the energy consumption in the reboiler unit may be changed due to the change in the absorber bed height whereas the same flue gas flow rate (20 kmol/s) is steadily introduced to the CO_2 capture plant. In this analysis, the tuning parameters and the controlled variables were kept at their corresponding set points (Table 4.3), e.g., the CO_2 capture rate was maintained at 87%, and the dimensions of the other process units considered in the commercial-scale plant's flowsheet remained constant at their nominal values (see Table 4.2).

Fig. 4.5a shows that the energy required by the CO_2 capture plant decreases exponentially when the absorber bed height is increased; thus, an absorber bed height of 34 m offers the minimum energy required (4.1 GJ/tCO_2). Due to the reboiler temperature controllers T_{reb1}-Q_{reb1} and T_{reb2}-Q_{reb2} for R101 and R201, respectively, the reboilers' temperature were maintained at 388.7 K, and the lean loading of the recycled amine stream (stream 18) was indirectly controlled at approximately 0.3 moles of CO_2/ moles of MEA. On the other hand, the rich loading in the outlet liquid stream (stream 15), flowing from the bottom of the absorbers, increased when the absorber bed height increased (Fig. 4.5b), due to the influence of large contact times between the gas and the liquid phases on each absorber. Fig. 4.5c shows that the required lean amine flow rate circulating in the CO_2 capture plant decreased when the absorber bed height increased. Consequently, the heat requirements in the buffer tank (Q_{tank})decreased due to this effect. A similar behaviour was also observed for the condenser heat duties (Q_{cond1} and Q_{cond2}).

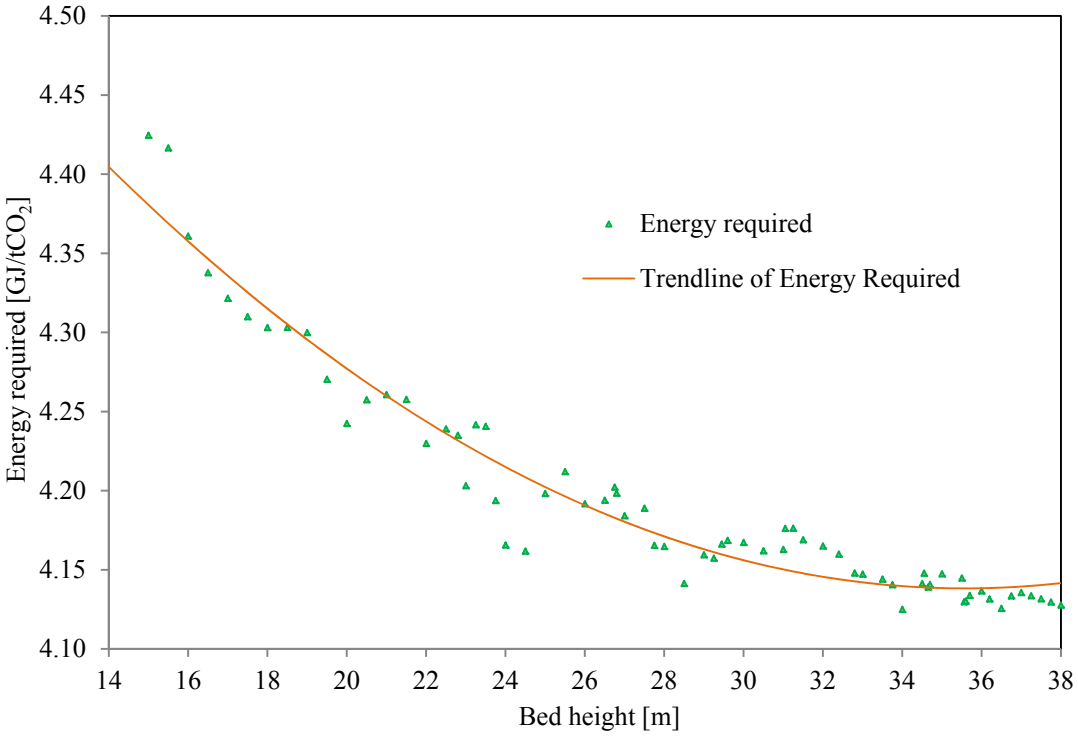

(a)

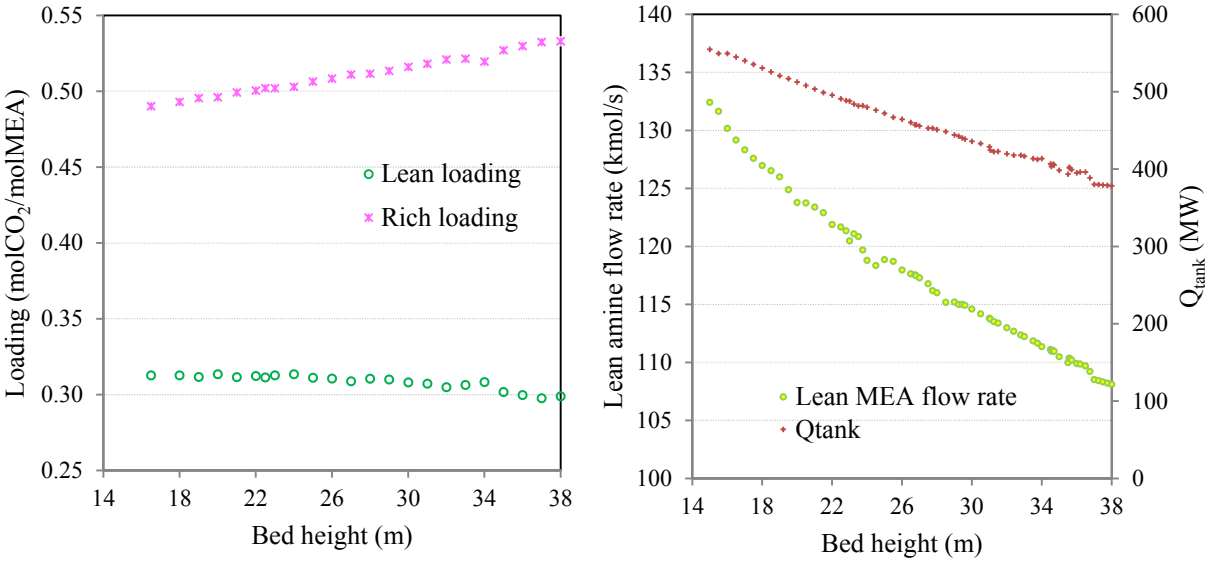

(b) (c)

Figure 4.5 Effect of the absorber bed height:

(a) Energy required; (b) CO_2 loading; and (c) Lean amine flow rate and Q_{tank}

Fig.4.6 presents the liquid temperature profiles obtained for the different absorber bed heights considered in this study. As shown in that Figure, the location of the high chemical reaction rate of CO_2 and MEA due to the exothermic reaction varies according to the absorber bed height: the temperature bulge moves toward the top of the column when the absorber bed height is increased. This behaviour occurs because large bed height reduces the *L/G* ratio (the ratio of liquid to gas flow rates entering a packed column), which influences the chemical reaction occurring at the top of the absorber. Also, the liquid phase flowing towards the bottom of the absorber is cooled down by the flue gas stream which usually has a lower temperature; therefore, the outlet temperature of the rich amine stream leaving a 34 m-height column (318 K) is lower than that of a 16.5 m-height absorber (325 K), which has a liquid temperature bulge at the middle of the absorber. Moreover, the rich amine flow rate in the 34 m-absorber bed height plant is 16% less than that in the 16.5 m-absorber bed height; therefore, the reboiler heat duty required by a 34 m-absorber bed height is lower when compared to that required by a 16 m-absorber bed height. Furthermore, the flooding points on each absorber and stripper in the 34 m-absorber bed height are reduced by 3% to 8% from those in the original design bed height (16.5 m), i.e., the flooding point on each 34 m-height absorber and the stripper (with 16 m height) are 65% and 62% flood, respectively (see Fig. 4.2).

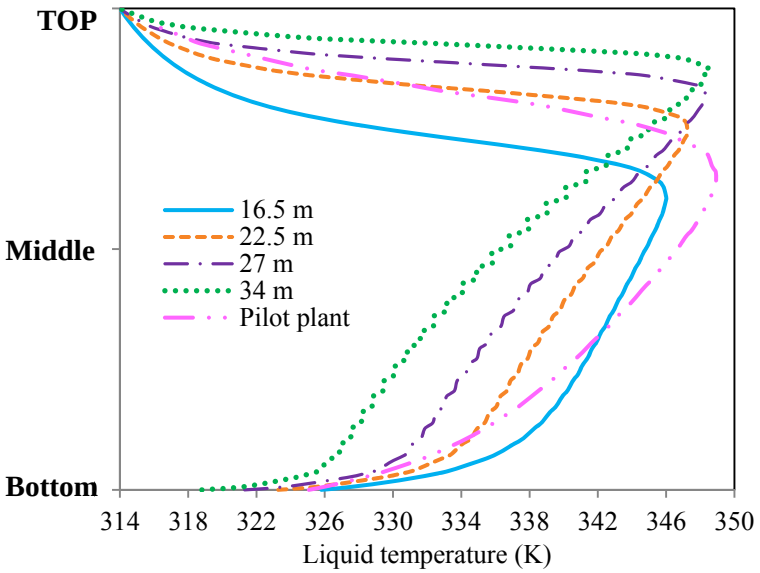

Figure 4.6 Liquid temperature profiles in different absorber bed heights at 87%CC

Based on the previous sensitivity analysis, it is clear that having a large absorber bed height will reduce the plant's energy requirements. Therefore, the absorber bed height was changed from 16.5 m, which was the initial design height, to 34 m, which offers the minimum energy consumption in the CO_2 capture plant.

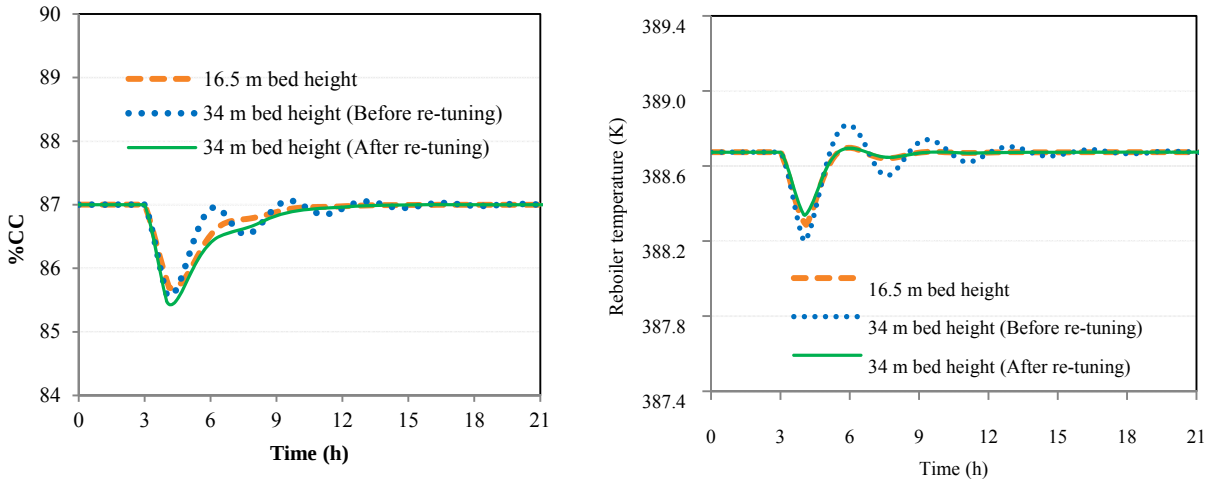

(a) (b)

Figure 4.7 Comparison of process responses of 3 different plants (the 16.5 m and 34 m absorber bed height plant using the same tuning parameters (Table 4.3) and the 34 m absorber bed height plant with retuned tuning parameters) to a +5% change in flue gas flow rate: (a) %CC; and (b) T_{reb1}

Since the absorbers' dimension was changed, the current tuning parameters (see Table 4.3) might not provide satisfied performance. To check this, the disturbance in the total flue gas flow rate of + 5% was introduced to 16.5 m and 34 m absorber bed height plants, which have the same control parameters as presented in Table 4.3. Figures 4.7a and 4.7b illustrate that the responses of %CC and the reboiler temperature from the 16.5 m absorber bed height plant are smooth whereas those of the 34 m absorber bed height plant present oscillating signals which are not desired from a process control point of view. This oscillating behaviour can be avoided by improving the controller tuning. The control parameters for the 34 m-absorber bed height CO_2 captured plant were thus manually retuned in order to obtain prompt and smooth process

responses. Figure 4.7a and 4.7b also show that after re-tuning control parameters, the process responses of 34 m absorber bed height plant are smoother and present insignificant oscillation. The tuning parameters for the 34 m-absorber bed height CO_2 captured plant are presented in Table 4.5. Also, the comparison of the key variables between the design conditions of 16.5 m and 34 m absorber bed height plants is shown in Table 4.6.

Table 4.5 Set points and tuning parameters for 34 m-absorber bed height plant

NO.	CV	MV	Set point	K_c	τ_I (min)
1	L13	V13	2.5 m	25	1.7
2	L23	V23			
3	L33	V33			
4	L42	V42	4 m	0.5	1.7
5	L52	V52			
6	T_{cond1}	Q_{cond1}	310 K	0.06	1.33
7	T_{cond2}	Q_{cond2}			
8	T_{reb1}	Q_{reb1}	388.7 K	1.6	2.78
9	T_{reb2}	Q_{reb2}			
10	T_{tank}	Q_{tank}	314K	1.5	2.73
11	%CC	V60	87%	0.006	82

Table 4.6 Comparison of key variables for different absorber bed heights

Variable	Unit	Design Specification	Normal operating condition		
			16.5 m absorber	34 m absorber	% difference
%CC	%	87%	87%	87%	0.0%
CO_2 purity	%	96.3%	96.3%	96.3%	0.0%
Flue gas flow rate	kmol/s	23	20	20	0.0%
Lean MEA flow rate	kmol/s	130	130.7	110	-15.8%
L/G ratio [a]	molLiquid/molGas	6.13	6.5	5.5	-15.9%
Lean loading [a]	molCO_2/molMEA	0.3	0.313	0.32	-0.7%
Rich loading [a]	molCO_2/molMEA	0.5	0.486	0.52	6.7%
%flood in an absorber	%	70%	67.5%	65%	-3.7%
%flood in a stripper	%	70%	67.1%	62%	-7.6%
Energy required	GJ/tCO_2 captured	-	4.4	4.1	-7.2%
Manipulated variables					
Q_{reb} per a reboiler	MW_{th}	-	274.7	256.3	-6.7%
Q_{tank}	MW_{th}	-	549.7	407.6	-25.9%
Q_{cond} per a condenser	MW_{th}	-	23.3	17.8	-23.6%
V13,23,33	%	50%	54%	45%	-17.0%
V42,52	%	50%	44%	37%	-16.5%
V60	%	50%	36%	30%	-15.7%

[a] entering an absorber

4.2.2 Ramp change in flue gas flow rate

The performance of the commercial-scale CO_2 capture plant in closed-loop was evaluated assuming sustained changes in flue gas flow rate, which is the key external disturbance that affects this process. Hence, the present analysis considered a 10% ramp increase in the flue gas flow rate with respect to the base case condition, which was introduced to the plant at the third hour of the operation over a period of 1 h. Fig. 4.8a shows that %CC decreased to 84.3% prior to returning to its set point at 87% after 6 h of operation. As shown in Fig. 4.8b, the plant required more reboiler energy per tonne of CO_2 capture when the flue gas flow rate entering the plant increased. Moreover, the fractional capacities in the packed columns slightly changed; however, they were in the acceptable region (30 % – 80 % flood (Tontiwachwuthikul, 1990)). As shown in Fig. 4.8c, the increase in *%flood* in the absorbers and strippers due to a + 10% increase in the

flue gas flow rate were approximately 6.8% and 7.2%, respectively. Note that the *%flood* in A101 represents the *%flood* in other absorbers since the absorbers' mechanical design and operating conditions in all three absorbers are identical. Also, the *%floods* in the two strippers are represented by the *%flood* in D101. Furthermore, the variability in the CO_2 concentration in the product streams leaving from E102 and E202 was relatively small due to the tight control of the condenser temperature. A similar behaviour was observed for the tanks' liquid levels.

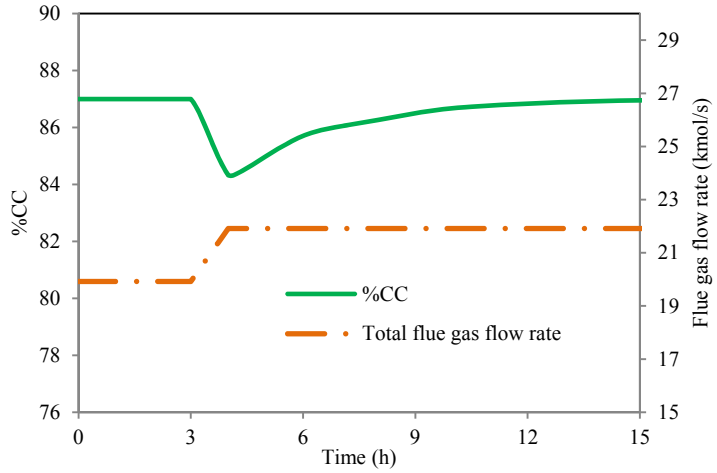

(a)

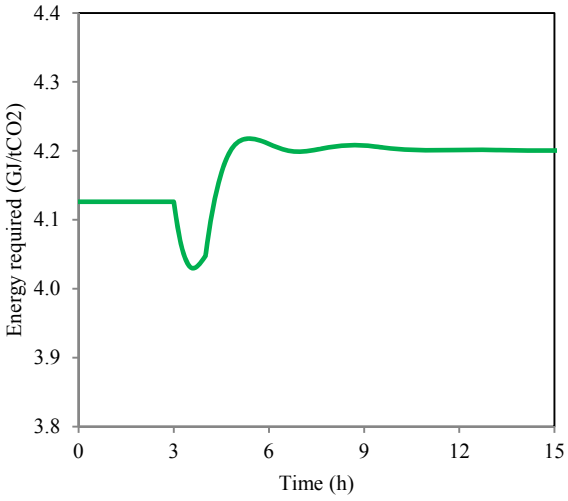

(b)

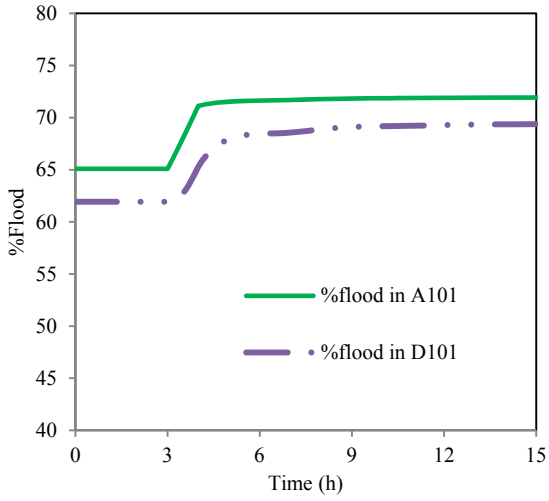

(c)

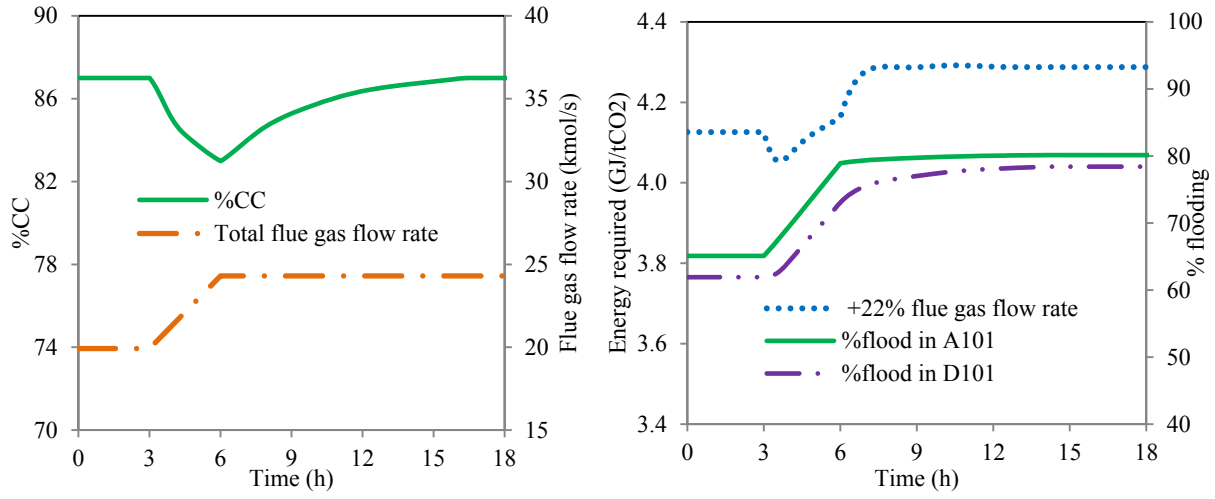

Figure 4.8 Process responses to ramp changes in the flue gas flow rate: (a)%CC and flue gas flow rates responses to +10% flue gas flow rates; (b) energy required responses to +10% flue gas flow rates; (c) %flood in absorber and stripper responses to +10% flue gas flow rates; (d) %CC and flue gas flow rates responses to +22% flue gas flow rates; and (e) %floods and energy required responses to +22% flue gas flow rates

In the present analysis, the estimation of the maximum capacity of this plant was conducted by keeping the increase in the total flue gas flow rate until any of the process units reach an operational constraint, e.g., maximum or minimum *%flood* in a packed column, fully-open or fully-closed valve stem positions. This study showed that, when the flue gas flow rate reached 24.3 kmol/s (22% higher than that at the base case condition), the percentage of flood in the absorbers (A101, A201 and A301) reached 80% (Fig. 4.8e), which was the maximum *%flood* allowed in the packed columns; the two strippers operated at 78%flood (Fig. 4.8e) at that same flue gas flow rate level. At this operating condition, the plant required approximately 4.3 GJ/tCO_2, which is about 4% more than what was needed for the base case condition.

Note that the design *%flood* for those packed columns (three absorbers and two strippers) is 70% (see Sec. 4.1.3), and the design flue gas flow rate is 15% above the base case flow rate. In this test, the maximum allowable %flood in the packed column was set at 80%; therefore, the maximum flue gas flow rate which can be handled by this commercial-scale plant is higher than the design flue gas flow rate (23 mol/s).

4.2.3 Change in CO_2 capture rate set point

The plant's ability to switch between different CO_2 capture levels (*%CC*) was also studied here. For example, in the case where the heat duty required by the reboilers (Q_{reb1} and Q_{reb2}) were coming from the steam extraction, a power plant operator may consider decreasing the extract steam rate from the steam cycle in order to generate more electrical power during peak hours, which may result in a reduction in the %CC set point from the normal operating point. On the other hand, when the power demand is low, e.g., in the night time and/or during long weekend, an increase in %CC set point may be considered to compensate for the amount of CO_2 removal missed during the peak hours. The present set point tracking analysis was conducted by increasing 5% the CO_2 capture set point using a ramp change over a period of 1 h. As shown in Fig. 4.9a, the plant was able to reach the new %CC set point of 92% within 2 h; the energy required to achieve such change increased by 2% when the CO_2 capture rate was increased by 5% (Fig. 4.9b).

The effect of changes in the CO_2 removal rates on the fractional capacity in the packed columns is presented in Fig. 4.9c. For +5%CC set point change, the circulating MEA flow rate in the plant increased, by partially opening V60, to enhance the wetted area in absorbers. This action caused an increase in the liquid flow rate entering each reboiler; consequently, higher vapour flow rate produced by the reboilers was recycled back to the bottom of each stripper. As a result, the fractional capacity in the strippers increased by 5%. On the other hand, the variation in fractional capacities in the absorbers was insignificant as only the molar liquid flow rate was changed whilst the flue gas flow rate remained constant. That is, the variability in the gas flow rate dominates the hydraulic conditions in the packed column. Furthermore, the variation in the

liquid temperature bulge in the absorber at different CO_2 removal rates is illustrated in Fig. 4.9d. The temperature bulge on each absorber moved downward the bottom of the column as the *L/G* ratio in an absorber increased when a high CO_2 capture rate is required.

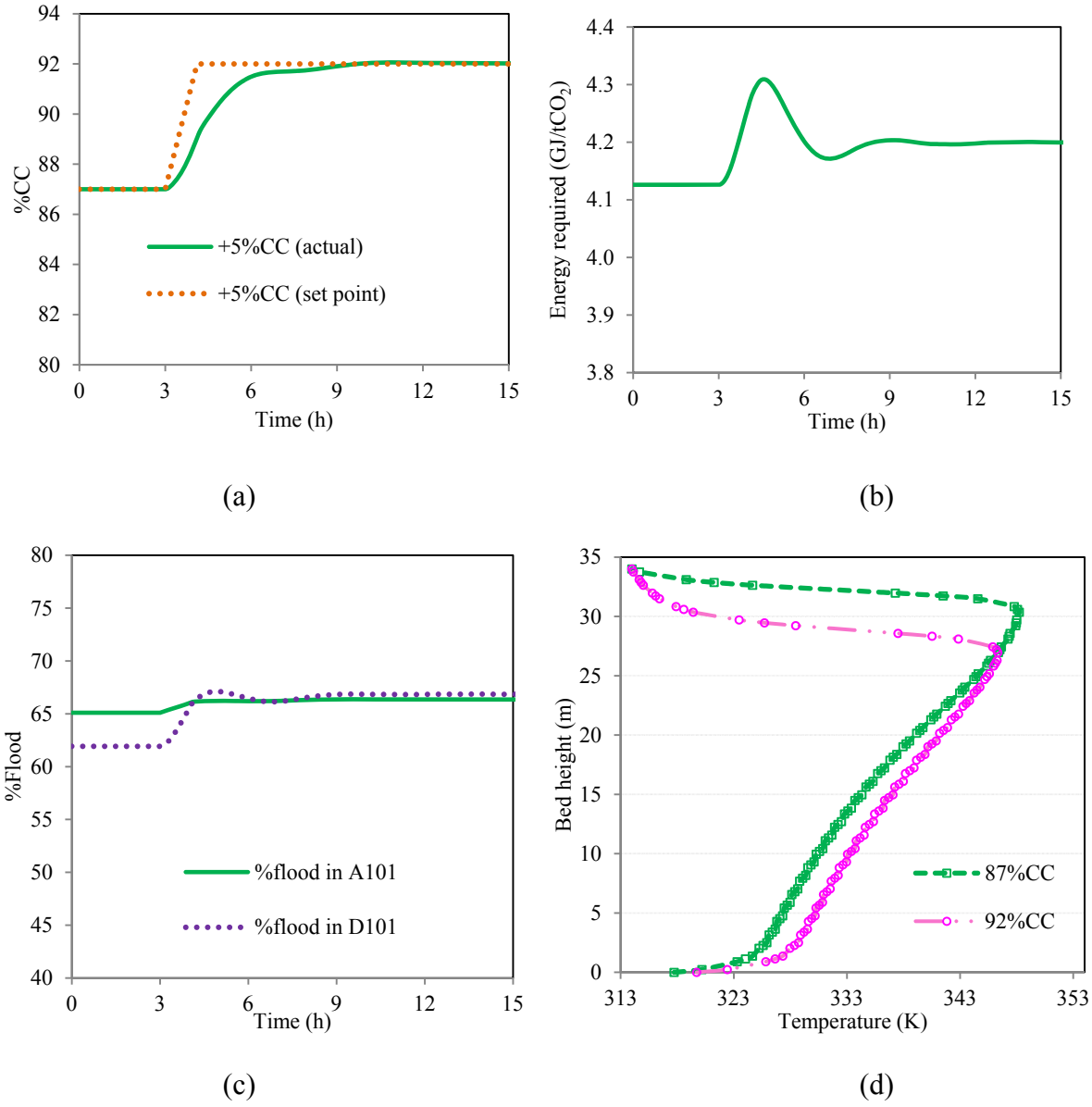

(a) (b)

(c) (d)

Figure 4.9 Process responses to changes in ±5% CO_2 capture's set points: (a)%CC; (b) Energy required; (c) %flood; and (d) liquid temperature bulge in absorber

4.2.4 Change in flue gas composition

Although the same type of coal is often used to feed the furnace, its composition may slightly change from batch to batch thus causing variations in the flue gas composition. In this study, the Pittsburgh#8 bituminous coal was considered. This type of coal produces a flue gas with a 16.3 mol% CO_2 composition (after the flue gas desulfurization (FGD)). To evaluate the ability of the industrial-scale CO_2 capture plant to handle changes in the flue gas composition, a sinusoidal change in the CO_2 flow rate in the flue gas stream, at different amplitudes and frequencies, was introduced to the plant; therefore, the total flue gas flow rate varied, accordingly. As shown in Fig. 4.10a, the plant had been steadily operated for 2 h prior to the introduction of the sinusoidal disturbance in the CO_2 flow rate, which was varied in the range of ±2.5% of the normal CO_2 flow rate (3.24 kmol/s) with a varying frequency between 0.5-1 cycle/h. From times 4 to 10 h, the %CC varied in the range of ±0.5%CC from the %CC set point (87%) as shown in Fig. 4.10a. After that time, the variation in %CC was approximately 0.8% though the amplitude of the sinusoidal change in the disturbance was still at ±2.5%. A similar behaviour was also observed in the energy required and the total lean amine flow rate leaving the buffer tank (E101), as shown in Fig. 4.10b. Particularly, the variation in %flood in the strippers (D101 and D201) increased from ±0.1% to ±0.5% when the frequency of the disturbance changed from 1 to 0.5 cycle/h (see Fig. 4.10c). After the CO_2 flow rate in the flue gas returned to its nominal value, the CO_2 capture plant with the proposed control system required about 2 h to converge to the steady state condition.

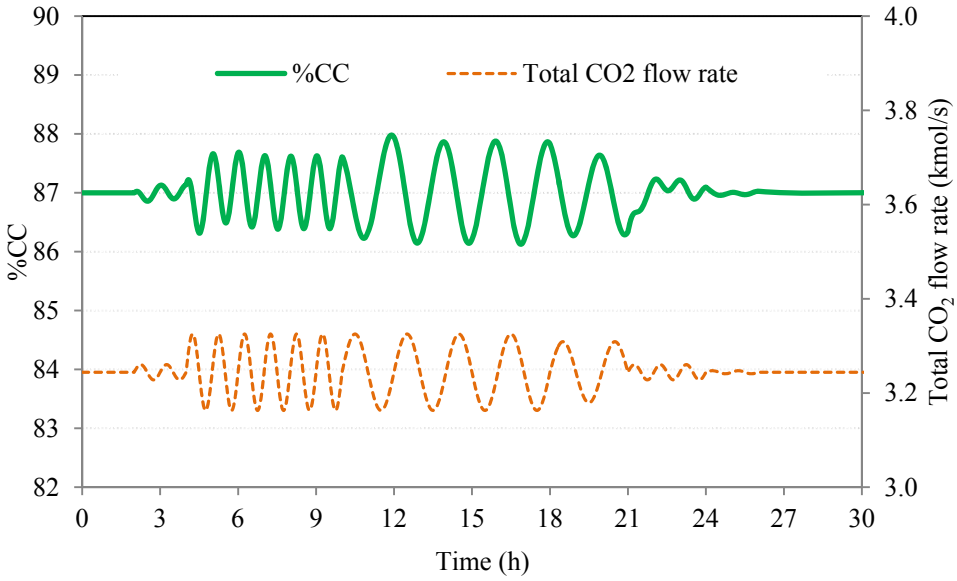
%CC
Total CO2 flow rate
%CC
Total CO_2 flow rate (kmol/s)
Time (h)
90
89
88
87
86
85
84
83
82
4.0
3.8
3.6
3.4
3.2
3.0
0
3
6
9
12
15
18
21
24
27
30

(a)

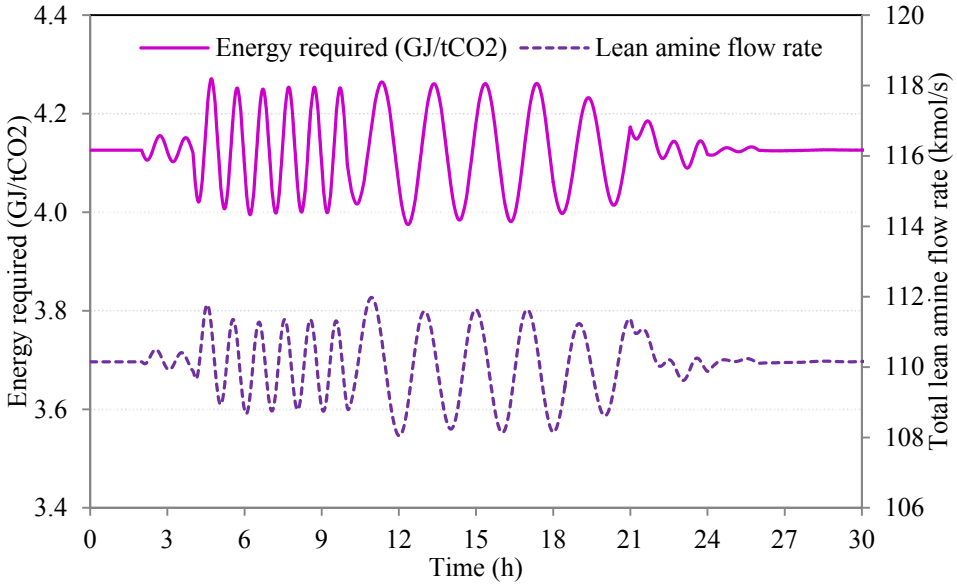
Energy required (GJ/tCO2)
Lean amine flow rate
Energy required (GJ/tCO2)
Total lean amine flow rate (kmol/s)
Time (h)
4.4
4.2
4.0
3.8
3.6
3.4
120
118
116
114
112
110
108
106
0
3
6
9
12
15
18
21
24
27
30

(b)

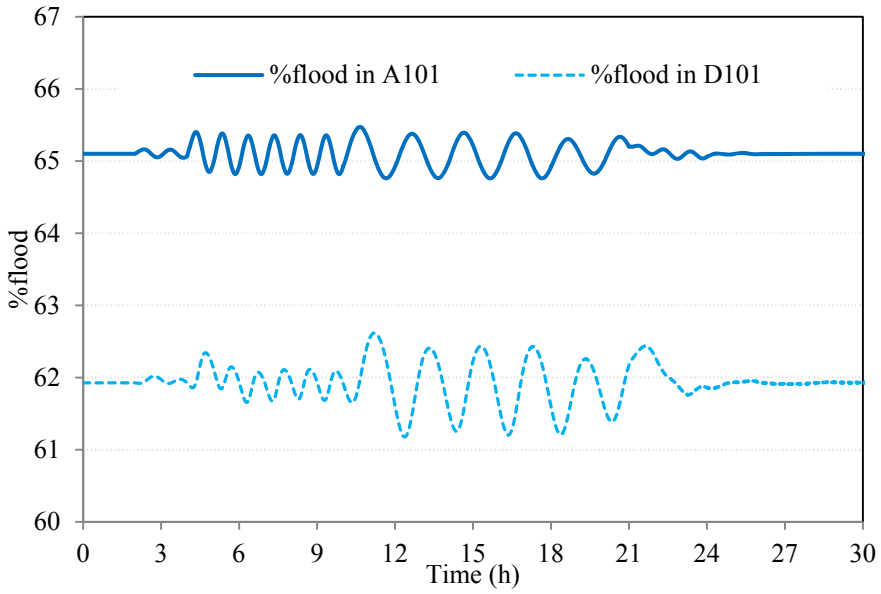

(c)

Figure 4.10 Process responses to sinusoidal change in flue gas composition: (a)%CC and mole fraction of CO_2 in the flue gas stream; (b) energy required and lean amine flow rate; and (c) %flood

4.2.5 Process scheduling

The variation of the electricity demand over the course of a day depends on human activities. The increase in the power required starts in the morning due to the beginning of daily activities; whereas these activities decrease in the evening, thus resulting in reduced electricity demand. This pattern was studied in this scenario using a sinusoidal change in the flue gas flow rate, which varied between ±5% with respect to the base case operating condition, as shown in Fig. 4.11a. Moreover, the MEA scrubbing plant may be not able to operate with a constant (desired) CO_2 capture rate due to varying changes in electricity demands, especially during peak electricity demands or upsets in a power plant. In those cases, a plant operator may choose to increase the CO_2 capture rate during periods of low electricity demands to compensate for a loss of the CO_2 removal during the (high-peak) day time. That is, an operator may be able to follow a schedule

for the CO_2 capture plant based on the typical day-to-day conditions that occur in a coal-fired power plant. Therefore, the aim of this section is to analyze the plant's behaviour due to a preliminary schedule of the CO_2 capture plant. In this case, a sinusoidal change in the flue gas flow rate was assumed to represent the day-to-day behaviour of a CO_2 capture plant whereas scheduled changes in the %CC's set points were induced in the plant based on the high and low electricity demands, represented here by a high and low variation of the flue gas flow rate entering into the plant. In order to analyze the effect of the %CC set point change on the process responses during the sinusoidal changes in the flue gas flow rate, two scenarios were considered in the present analysis:

- Scenario A: sinusoidal change in the flue gas flow rate of ±5% with respect to the base case condition and constant %CC's set point at 87%;
- Scenario B: the same disturbance in the flue gas flow rate considered in Scenario A but with varied %CC's set point scheduled based on the disturbance's dynamic behaviour. For example, the %CC set point was maintained at 87% during the day time (high flue gas flow rate), and then it was gradually ramped up to 89% in the period of 4 h in the afternoon. The %CC's set point was then kept at 89% during the night time (low flue gas flow rate). The %CC's set point was started to ramp down to 87% when the flue gas flow rate tended to increase in the morning. This scheduled changes in %CC's set point were repeated throughout the test for Scenario B.

Fig. 4.11a shows that the actual %CC in Scenario A varied between 86% and 88%. For Scenario B, the %CC changed in the range of 86 % to 90 %; moreover, the response of the actual %CC showed smooth transitions during the set point change in %CC, i.e. during 2:00 – 6:00 and 14:00 – 18:00 in day 2. Fig. 4.11b shows the variation in total Q_{reb} required and total CO_2 capture rate due to process scheduling. The total amount of CO_2 captured and the total reboiler heat duty required in a period of 48 h in Scenario B were higher than that in Scenario A by 1.1 % (5,400 kmol) and 1.4%, respectively. The variation in CO_2 capture rate is directly proportional to the change in the overall reboiler heat duty; as a result, the average energy required for this plant remained at approximately 4.1 GJ/tCO_2.

Fig. 4.11c shows that the changes in the *%flood* in absorbers in both scenarios were somewhat similar due to similar *L/G* ratios. Nevertheless, the increase in the %CC set point during low electricity demand periods required high MEA flow rate circulating in the plant and consequently caused an increase in the steam flow rate flowing to the strippers. That is, the *%flood* in the strippers in Scenario B slightly increased (~2%), compared to Scenario A. The latter may be used to minimise the fluctuation of the hydraulic condition in the packed column, i.e., a plant operator can prevent poor wetting, which may probably occur in the stripper during low demands.

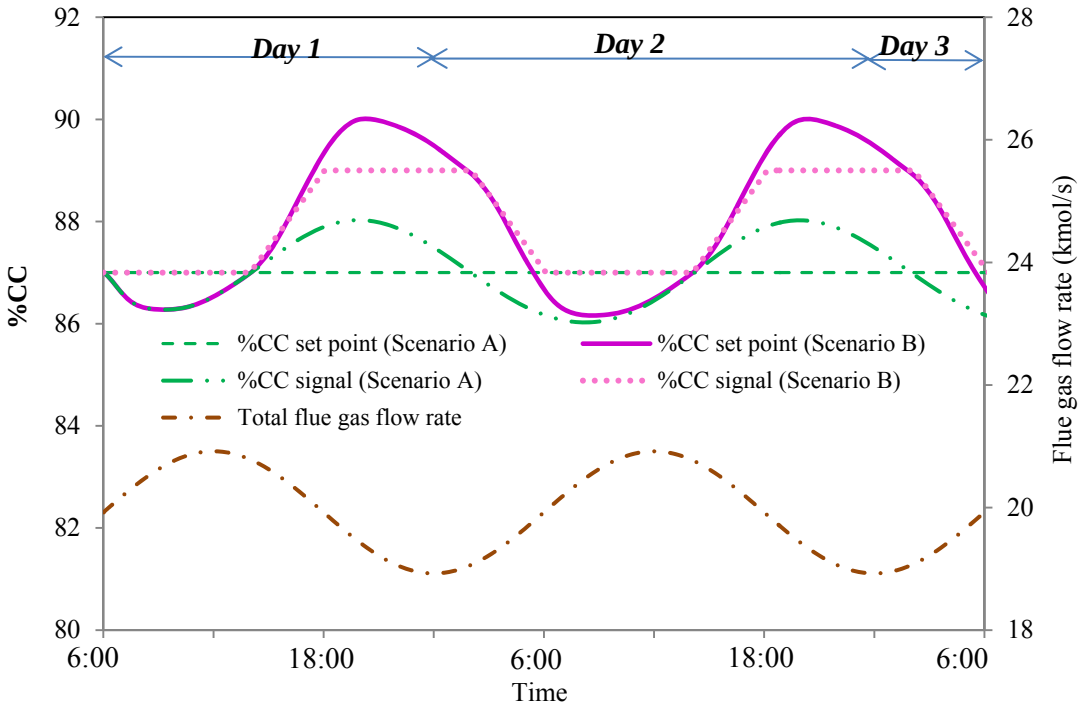

(a)

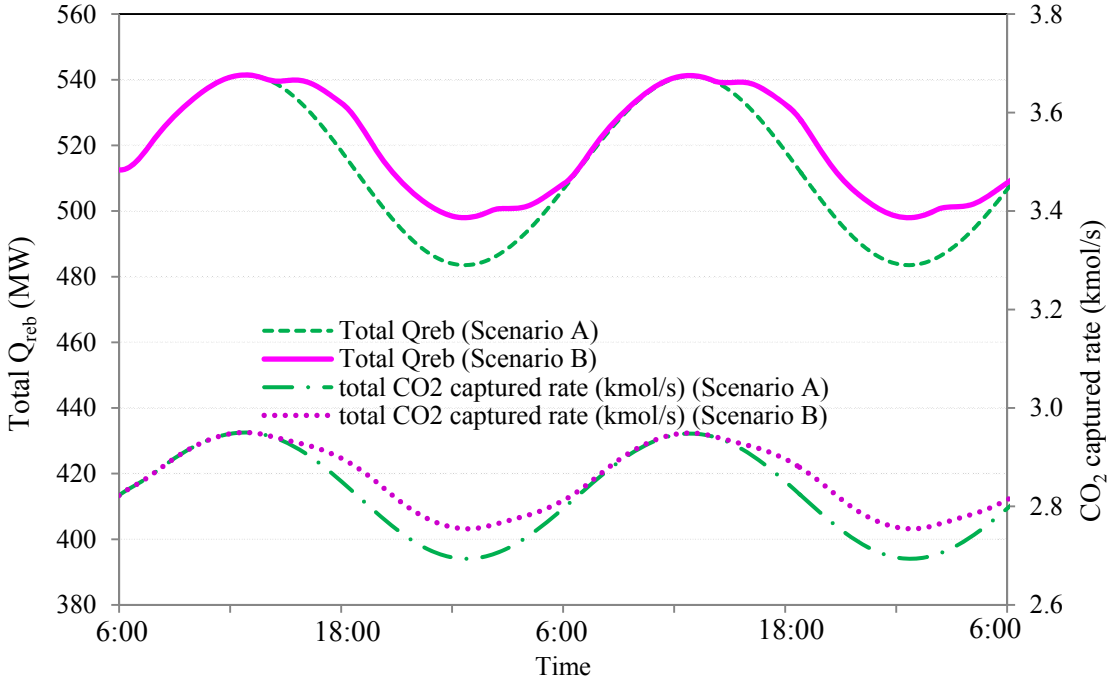

(b)

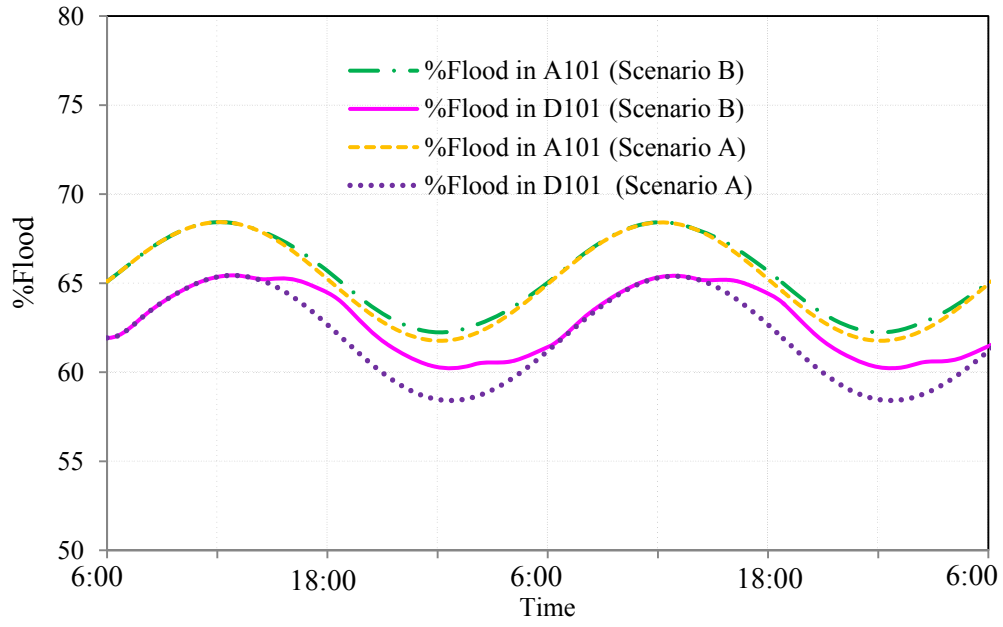

(c)

Figure 4.11 Process responses to sinusoidal changes in flue gas flow rate and %CC set point: (a) %CC and the flue gas flow rate; (b) energy required and %difference; and (c) %flood

4.3 Chapter summary

4.3.1. A scale-up procedure for a commercial-scale MEA absorption processes for CO_2 capture from 750 MW coal-fired power plants was presented. The equipment sizing was based on the following design objectives: CO_2 capture rate of 87% and CO_2 concentration in the CO_2 product stream of 95% or above, which results in a CO_2 removal of approximately 10,000 tCO_2/d. Given a flue gas flow rate from 650 MW power generations at the base case condition and the limitations of the manufacturing of column towers, three absorbers and two strippers are required for the commercial-scale CO_2 capture process. A decentralized control scheme based on PI controllers was implemented to maintain the dynamic operability of this process in the presence of disturbances or changes in the process operating conditions.

4.3.2. The plant's performance was evaluated in terms of both the equipment design and the process dynamic response. The results showed that an absorber bed height of 34 m provides minimum energy requirement which is 4.1 GJ/tCO_2 at the base case operating condition. The resulting plant's design can accommodate a maximum flue gas flow rate of 24.3 kmol/s, which is approximately 22% higher that the base case flue gas flow rate condition. Also, the preliminary study on the process scheduling shows that the adjustment of %CC corresponding to power demand may avoid a poor wetting condition in the strippers during low power demand periods. According to the responses of the key process variables, this industrial-scale CO_2 scrubbing plant, with the proposed control scheme and their corresponding PI controllers' tuning parameters, showed smooth transition and small oscillating behaviour.

Chapter 5
Conclusions and Recommendations

5.1 Conclusions

5.1.1 Pilot plant modelling and process controllability analysis

i) The model of the pilot plant for CO_2 removal proposed in this study is an improvement from the mechanistic model initially proposed by Harun et al. (2012). The initial process flowsheet proposed contained the absorber, stripper, cross heat exchanger, reboiler. In order to represent realistic conditions, several process units and process streams have been added in this work, i.e., condenser, absorber sump tank, reboiler surge tank, control valves, and makeup streams.

ii) The design of the process control schemes has been systematically described. This work proposed three decentralised control structures based on the insights gained from sensitivity analysis, on six manipulated variables and six potential controlled variables. The first control structure (control structure A) was designed using traditional-RGA analysis whereas the other two control schemes (control structures B and C) were developed using a heuristic approach. Basic PI controllers were implemented in every control loops in the proposed control schemes and the controller parameters were tuned using IMC and manual tuning methods.

iii) The performance of those control structures was evaluated using eight scenarios, i.e. changes in flue gas flow rates and its composition, change in condenser temperature set point, limited reboiler heat duty, and valve stiction. The evaluation results revealed that, under the condition where the reboiler temperature is to be controlled, control structure B (heuristic-based approach) shows prompter responses to disturbance rejection and set point tracking, when compared to control structure A and C. Control structure C's performance was similar to control structure A; however, control structure C resulted in

lower energy requirement and possessed less ISE than that of control scheme A. The control structure A showed sluggish responses since the RGA analysis does not consider the process dynamics.

iv) Several highlights obtained from the performance evaluation results are presented in this work, as follows:

- The energy required by this pilot plant is 4.95 GJ/tCO_2 to achieve 96.3% CO_2 removal and CO_2 purity of at least 95%.
- This pilot plant can accommodate a flue gas flow rate up to 40% above the based case condition; otherwise, it may be shut down due to liquid overflow.
- An asset integrity problem due to internal corrosion can be avoided by regular analysis of MEA solution properties, regardless of which control scheme is used.

v) This pilot plant model and proposed control structures were used as a guideline for the industrial-scale CO_2 capture plant modelling.

5.1.2 Industrial-scale CO_2 capture plant modelling and plant's performance evaluation

i) The description of a scale-up methodology for an industrial-scale CO_2 capture plant for a 750 MW supercritical coal-fired power plant was presented in this work. This commercial-scale CO_2 capture plant consists of three absorbers (11.8 m diameter, 34 m bed height) and two strippers (10.4 m diameter, 16 m bed height) to achieve 87% CO_2 captured rate and 95% CO_2 purity. At the base case condition, this plant requires a thermal energy of 4.1 GJ to capture 1 tCO_2.

ii) A proposed control structure for the commercial-scale CO_2 capture plant is somewhat similar to control scheme B, obtained from the process controllability analysis for the pilot plant model. This control scheme consists of 11 PI control loops and tuning parameters for each control loop are provided.

iii) Four scenarios were used to evaluated the performance of this plant, i.e. change in CO_2 capture set point, sinusoidal change in CO_2 flow rate in flue gas stream, and implementation of process scheduling. The evaluation results show that this industrial-scale plant using the proposed control scheme displayed smooth process responses with insignificant oscillating signals to given changes in operating condition. Moreover, the preliminary study on process scheduling indicates that poor wetting in strippers during low demand may be avoided.

5.2 Recommendations

5.2.1 Reduction in energy consumption

One of key challenges for an industrial-scale CO_2 capture is the energy required for solvent regeneration. Several alternatives aiming at reducing the energy consumption have been researched. Research studies on those alternatives can be extended from this study, i.e. instead of traditional MEA solution, blended-amine solution (Aroonwilas and Veawab, 2004) can be used as the solvent to absorb CO_2 from flue gas stream. Moreover, the reduction in energy consumption can be achieved by the improvement of an absorber by including intercooler to enhance the exothermic reaction in an absorption process. As a result, the same amount of MEA solution can absorb more CO_2 from the flue gas stream, thus resulting in the decrease in the reboiler heat duty required for an absorbent regeneration. Likewise, the replacement of internal packing in packed columns increases the absorption performance, due to an increase in the contact area between gas and liquid phases, and also decreases the circulating solvent flow rate, resulting in a reduction in the energy required.

5.2.2 Controllability study

This work proposes a decentralised PI control structure for the pilot plant and the industrial-scale CO_2 capture plant. According to the evaluation results, after the introduction of changes in operating condition, these plants were able to recover

controlled variables' set points; however, it took about 4 – 7 h to do so. Therefore, the improvement of switchability (ability to change from one to another operating condition with proper fashion) can be conducted to reduce plant' settling time to reach a new steady state. In addition, a centralised control structure can be designed for the CO_2 capture plant. The evaluation results of a centralised control structure can be then compared to that of a plant using a decentralised control structure, to determine a promising control strategy for post-combustion CO_2 capture plant. Furthermore, a study on process scheduling can be proposed to minimise an impact of energy required by a CO_2 capture plant to electrical generation during peak load. The flexibility of plant operation may be also considered in the process scheduling study, i.e., a plant operator may consider to shut down an absorber in which the flooding velocity is less than 30% due to poor wetting condition during low electrical demand.

5.2.3 Integration of post – combustion CO_2 capture, power plant's steam cycle, and CO_2 compression train

A dynamic model of the steam cycle in a power plant and CO_2 compression train can be developed and integrated to the CO_2 removal plant using MEA solution proposed in this work. That integrated model will provide insights regarding the dynamic response of entire processes, i.e., the impact of energy needed, for solvent regeneration, on electricity generation; the effect of change in CO_2 product flow rate on a CO_2 compression train and downstream product properties; and the effect of change in electricity demand over a 24 h period on CO_2 removal plant and CO_2 compression train. Furthermore, a study on process optimisation can be pursued to determine a promising process flowsheet and an optimum operating point.

Bibliography

Abu-Zahra, M.R.M., Niederer, J.P.M., Feron, P.H.M. (2007) CO_2 capture from power plants Part II A parametric study of the economical performance based on mono-ethanolamine. *International Journal of Greenhouse Gas Control*. 1(2), 135 – 142.

Alie, C., Backham, L., Croiset, E., Douglas, P.L. (2005) Simulation of CO_2 capture using MEA scrubbing: a flowsheet decomposition method. *Energy Conversion and Management*. 46(3), 475 – 487.

Aroonwilas, A. and Tontiwachwuthikul, P. (2000) Mechanistic model for prediction of structured packing mass transfer performance in CO_2 absorption with chemical reactions. *Chemical Engineering Science*. 55(18), 3651 – 3663.

Aroonwilas A, Tontiwachwuthikul P, Chakma A. (2001) Effects of operating and design parameters on CO_2 absorption in columns with structured packings. *Separation and Purification Technology*. 24(3), 403 – 411.

Aroonwilas, A. and Veawab, A. (2004) Characterization and comparison of the CO_2 absorption performance into single and blended alkanolamines in a packed column. *Industrial & Engineering Chemistry Research*. 43(9), 2228-2237.

Aroonwilas, A. and Veawab, A. (2007) Integration of CO_2 capture unit using single- and blended-amines into supercritical coal-fired power plants: Implications for emission and energy management. *International Journal of Greenhouse Gas Control*. 1(2), 143 – 150.

Bedelbayev, A., Greer, T., and Lie, B. (2008) Model based control of absorption tower for CO_2 capturing. *Proceeding for the 49th Scandinavian Conference*. Norway.

Beer, J.M. Higher Efficiency Power Generation Reduces Emissions. National Coal Council Issue Paper, 2009. [2013-09-15], http://mitei.mit.edu/system/files/beer-emissions.pdf

Brimblecombe, P. *Air composition and chemistry*, 2nd Ed. Cambridge environmental chemistry series 6, Cambridge University Press 1986, New York USA

Bristol, E.H. (1966) On a new measure of interactions for multivariable process control. *IEEE Trans. Auto.Control.* 11, 133 – 134.

Buckley, P.S. *Techniques of process control*. Wiley:New York; 1964.

Chapel, D.G., Mariz, C.L., Ernest, J. (1999) Recovery of CO_2 from flue gases: commercial trends. *Proceedings of the Canadian Society of Chemical Engineers Annual Meeting*. 1999 October 4 – 6; Saskatchewan, Canada.

Chi, S., Rochelle, G.T. (2002) Oxidative Degradation of Monoethanolamine. *Industrial & Engineering Chemistry Research*. 41(17), 4178 – 4186.

Chien, I.L. and Fruehauf, P.S. (1990) Consider IMC tuning to improve controller performance. *Chemical Engineering Progress*. 86(10), 33 – 41.

Dooley, J.J., Davidson, C.L., and Dahowski, R.T. An assessment of the commercial availability of carbon dioxide capture and storage technologies as of June 2009 [2013-05-1], http://www.pnl.gov/main/publications/external/technical_reports/PNNL-18520.pdf

Dowell, N.M. and Shah, N. (2013) Identification of the cost-optimal degree of CO_2 capture: An optimisation study using dynamic process models. *International Journal of Greenhouse Gas Control*. 13, 44 – 58.

Dugas, E.R. Pilot plant study of carbon dioxide capture by aqueous monoethanolamine. M.S.E.

Thesis, University of Texas at Austin; 2006.

Edward, J.E., *Design and rating shell and tube heat exchangers*. P&I Design Ltd: Teesside, UK; 2008.

EU ETS. The EU Emissions Trading System (EU ETS), 2013. [2013-09-15], http://ec.europa.eu/clima/publications/docs/factsheet_ets_2013_en.pdf

Freguia, S. and Rochelle, G.T. (2003) Modeling of CO_2 capture by aqueous monoethanolamine. *AIChE Jounal*. 49(7), 1676 – 1686.

Garcia, C.E. and Morari, M. (1982) Internal model control: A unifying review and some new results. *Industrial and Engineering Chemistry Process Design and Development*. 21(2), 308 – 323.

gPROMS ModelBuilder 3.5.3. Process Systems Enterprise, London, UK.2012

gPROMS Process Model Library (PML) Documentation. Flow transportation. Release 3.5 London, UK. 2012

GPSA Engineering Data Book. 11th Ed. (Electronic) Volume I and II,1999.

Harun, N., Nittaya, T., Douglas, P.L., Croiset, E., Ricardez-Sandoval, L.A. (2012) Dynamic simulation of MEA absorption process for CO_2 capture from power plants. *International Journal of Greenhouse Gas Control*. 10, 295 – 309.

Harun N. Dynamic simulation of MEA absorption process for CO_2 capture from power plant. PhD Thesis, University of Waterloo; 2012.

Hovd, M. and Skogestad, S. (1994) Sequential design of decentralized controllers. *Automatica*. 30(10), 1601 – 1607.

Idem, R., Wilson, M., Tontiwachwuthikul, P., Chakma, A., Veawab, A., Aroonwilas, A., Gelowitz, D. (2006) Pilot Plant Studies of the CO_2 Capture Performance of Aqueous MEA and Mixed MEA/MDEA Solvents at the University of Regina CO_2 Capture Technology development plant and the boundary dam CO2 capture demonstration plant. *Industrial & engineering chemistry research*. 45(8), 2414 – 2420.

IEA. Technology roadmap: High-efficiency, low-emissions, coal-fired power generation. [2013-09-15], http://www.iea.org/publications/freepublications/publication/name,32869,en.html

Incropera, F.P. and Dewitt, D.P. *Fundamentals of heat and mass transfer*. 5th ed. Wiley:USA; 2002.

InIPED. BN-EG-UE109 Guide for Vessel Sizing, [2013-09-15], http://www.red-bag.com/jcms/engineering-guides/337-bn-eg-ue109-guide-for-vessel-sizing.html

Inwood, S. Program on technology innovation: Integrated generation technology options, 2011. [2013-09-15],http://integrating-renewables.org/wp-content/uploads/LINK-E-CCUG-000000000001022782.pdf

IPCC. An Assessment of the Intergovernmental Panel on Climate Change (IPCC) Climate change 2007: Synthesis report. [2013-09-15]. http://www.ipcc.ch/pdf/assessment-report/ar4/syr/ar4_syr.pdf

Kern, D.Q. *Process heat transfer*. McGraw-Hill:Singapore; 1965

Kister, H.Z. *Distillation design*. McGraw-Hill: New York; 1992.

Kister, H.Z., Scherffius, J., Afshar, K. and Abkar, E. (2007) Realistically predict capacity and pressure drop for packed columns. *AIChE*. 28 – 38.

Knudsen, J.N.J, Vilhelmsen, P., and Biede, O. (2007) First year operation experience with a 1t/h CO_2 absorption pilot plant at Esbjerg coal-fired power plant. *Proceedings of European Congress of Chemical Engineering (ECCE-6)*, Copenhagen, Denmark.

Kohl AL, Nielsen RB. *Gas purification*. 5th ed. Houston, Tex.: Gulf Pub.;1997.

Kvamsdal, H.M., Hetland, J., Haugen, G., Svendsen, H.F., Major, F., Karstad, V., and Tjellander, G. (2010,) Maintaining a neutral water balance in a 450 Mwe NGCC-CCS power system with post-combustion carbon dioxide capture aimed of offshore operation. *International journal of greenhouse gas control*. 4(4), 613 – 622.

Lawal, A., Wang, M., Stephenson, P., Koumpouras, G., and Yeung, H. (2010) Dynamic modelling and analysis of post-combustion CO_2 chemical absorption process for coal-fired power plants. *Fuel*. 89(10), 2791–2801.

Lawal, A., Wang, M., Stephenson, P., Obi, O. (2012) Demonstrating full-scale post-combustion CO_2 capture for coal-fired power plants through dynamic modelling and simulation. *Fuel.* 101, 115-128.

Lin, Y., Wong, D.S., Jang, S. (2012) Control strategies for flexible operation of power plant with CO_2 capture plant. *AICHE Journal*. 58(9), 2697 – 2704.

Larsson, T. and Skogestad, S. (2000) Plantwide control – A review and a new design procedure. *Modeling, Identification and Control*. 21(4), 209-240.

Luyben, M.L., Tyreus, B., Luyben, W.L. (1997) Plantwide control design procedure. *AIChE Journal*. 43(12), 3161 – 3174.

McAvoy, T.J. and Ye, N. (1994). Base control for the Tennessee Eastman Problem. *Computers and chemical engineering*. 18(5), 383 – 413.

McCabe, W.L., Smith, J.C., and Harriott, P. *Unit operations of chemical engineering*. 7th ed. Singapore:McGrawHill; 2005.

Mitsubishi Heavy Industries (MHI). (2009) Determining the technologies and system components for commercially viable CCS, IEA GHG – What have we learned from large-scale CCS projects?. *Presentation of the eighth annual conference on Carbon Capture and Sequestration*. Pittsburgh, USA.

Moser, P., Schmidt, S., Sieder, G., Garcia, H., and Ciattaglia, I. (2009) Enabling post combustion capture optimization – the pilot plant project at Niederaussem. *Energy Procedia*. 1(1), 807 – 814.

NETL. Quality guidelines for energy system studies: Detailed coal specifications [Internet]. 2012. [2013-09-15], http://www.netl.doe.gov/energy-nalyses/pubs/QGESS_DetailCoalSpecs_Rev4_20130510.pdf

Nittaya, T., Douglas, P.L., Croiset, E., Ricardez-Sandoval, L.A. (2014) Dynamic modelling and control of MEA absorption process for CO2 capture from power plants. *Fuel Journal.* 15, 672 – 691.

Panahi, M. and Skogestad, S. (2011) Economically efficient operation of CO_2 capturing process part I: Self-optimizing procedure for selecting the best controlled variables. *Chemical engineering and processing*. 50(3), 247 – 253.

Panahi, M. and Skogestad, S. (2012) Economically efficient operation of CO_2 capturing process part II: control layer. *Chemical engineering and processing*. 52, 112 – 124.

Posch, S. and Haider, M. (2010) Dynamic modelling of CO_2 absorption from coal-fired power plants into an aqueous monoethanolamine solution, *Chemical Engineering Research and*

Design. Doi:10.1016/j.cherd.2012.09.016.
Price, R.M. and Georgakis, C. (1993) Plantwide regulatory control design procedure using a tiered framework. *Industrial & Engineering Chemistry Research*. 32(11), 2693-2705.
Price, R.M., Lyman, P.R., and Georgakis, C. (1994) Throughput manipulation in plantwide control structure. *Industrial & Engineering Chemistry Research*. 33, 1197-1207.
Rao, A.B. and Rubin, E.S. (2002) A technical, economic, and environmental assessment of amine-based CO_2 capture technology for power plant greenhouse gas control. *Environ. Sci. Technol*. 36, 4467 – 4475.
Rao, A.B. and Rubin, E.S. (2006) Identifying cost-effective CO_2 control levels for amine-based CO_2 capture systems. *Industrial & engineering chemistry research*. 45(8), 2421 – 2429.
Ramezan, M. and Skone, T.J. (2007) Carbon dioxide capture from existing coal-fired power plants. *National Energy Technology Laboratory*; DOE/NETL-401/110907.
Reddy, S., Scherffius, J., and Freguia, S. (1999) Fluor's Econamine FG Plus SM Technology: An enhanced amine-based CO_2 capture process. *Proceeding for the 2nd National Conference on Carbon Sequestration National Energy Technology Laboratory/ Department of Energy*. Virginia, USA.
Robinson, P.J. and Luyben, W.L. (2010) Integrated gasification combined cycle dynamic model: H_2S absorption/Stripping, water-gas shift reactors, and CO_2 absorption/stripping. *Industrial & Engineering Chemistry Research*. 49(10), 4766–4781.
Sanpasertparnich, T., Idem, R., Bolea, I., deMontigny D, and Tontiwachwuthikul P. (2010) Integration of post-combustion capture and storage into a pulverized coal-fired power plant. *International Journal of Greenhouse Gas Control*. 4(3), 499 – 510.
Schach, M.O., Schneider, R., Schramm, H., and Repke, J. (2010) Techno-economic analysis of post combustion processes for the capture of carbon dioxide from power plant flue gas *Industrial & Engineering Chemistry Research*. 49(5), 2363–2370.
Schach, M.O., Schneider, R., Schramm, H., and Repke, J. (2011) Control structure design for CO_2 absorption processes for large operating range. *Proceedings of the 1st post combustion capture conference*; Abu Dhabi, UAE.
Seborg, D.E., Edgar, T.F., Mellichamp, D.A., and Doyle, F.J. *Process Dynamics and Control*, 3rd ed. New York:Wiley; 2011.
Singh, D., Croiset, E., Douglas, P.L., and Douglas, M.A. (2003) Techno-economic study of CO_2 capture from an existing coal-fired power plant: MEA scrubbing vs. O_2/CO_2 recycle combustion. *Energy Conversion and Management*. 44(19), 3073 – 3091.
Skogestad, S. and Postlethwaite, I. *Multivariable feedback control: Analysis and design*, 2nd ed. Toronto: Wiley; 2001.
Steeneveldt. R., Berger, B., and Torp, (2006) T.A. CO_2 capture and storage closing the knowing- doing gap. *Chemical Engineering Research and Design*. 84(A9), 739 – 763
Thomas, P.J. Simulation of industrial processes for control engineers. *Elsevier Science & Technology Book*, 1999.
Tontiwachwuthikul, P. New pilot plant technique for designing gas absorbers with chemical reactions. PhD Thesis, University of British Columbia; 1990.
Towler, G. and Sinnott, R. *Chemical engineering design: Principles, practice and economics of plant and process design*. London: Elsevier; 2008.

Wang, M., Lawal, A., Stephenson, P., Sidders, J. and Ramshaw, C. (2011) Post-combustion CO_2 capture with chemical absorption: A state-of-the-art review. *Chemical engineering research and design*. 89(9), 1609 – 1624.

Ziaii, S., Rochelle, G.T., and Edgar, T.F. (2009) Dynamic modelling to minimize energy use for CO_2 capture in power plants by aqueous monoethanolamine. *Industrial & Engineering Chemistry Research*. 48(13), 6105-6111.

Appendix A

Principles of Process Control and Design of Process Control System

A.1 Design of process control structure and controllability analysis

The plantwide control design procedure has been studied and proposed by many works. For example, Buckley (1964) described the alternatives of material balance control loops: direction of flow and direction opposite to flow; the tiered design framework focusing on the inventory and production rate control was proposed by Price and Georgakis (1994); and Larsson and Skogestad (2000) demonstrated the top-down analysis and bottom-up design for the plantwide control design. However, the general procedure to design control structures for chemical processes is not available in the open literature. Nevertheless, the design of a basic control scheme for a given process (see Fig. A.1) is traditionally obtained from the following steps:

1) Specification of the process control objectives is based on the process operating requirement and constraints, i.e. the percentage of CO_2 removal and the CO_2 concentration in the CO_2 product streams.
2) Selection of manipulated and controlled variables is based on the selection guideline (Seborg et al., 2011), i.e., a potential controlled variable is sensitive to and/or rapidly affects the change in a manipulated variable.
3) Sensitivity analysis determines the potential controlled variables' responses to changes in the manipulated variables in the given ranges.
4) Relative gain array (RGA) analysis (Bristol, 1966) is preliminarily approach to pair the controlled variables and the manipulated variables in multiple-input, multiple-output (MIMO) processes.
5) The control structure designed using RGA analysis is evaluated using multiple scenarios to determine its ability of disturbance rejection and set point tracking.
6) Insight of the process dynamic, obtained from the sensitivity analysis and the performance evaluation in Step 5, may be used to design other control schemes aiming to improve the process controllability which is called *heuristic approach*, i.e. plant with the

heuristic-based control scheme may be able to return its set point faster than the RGA-based control structure.

7) The heuristic-based control structure is to be tested using the same scenarios as Step 5 for the performance evaluation.

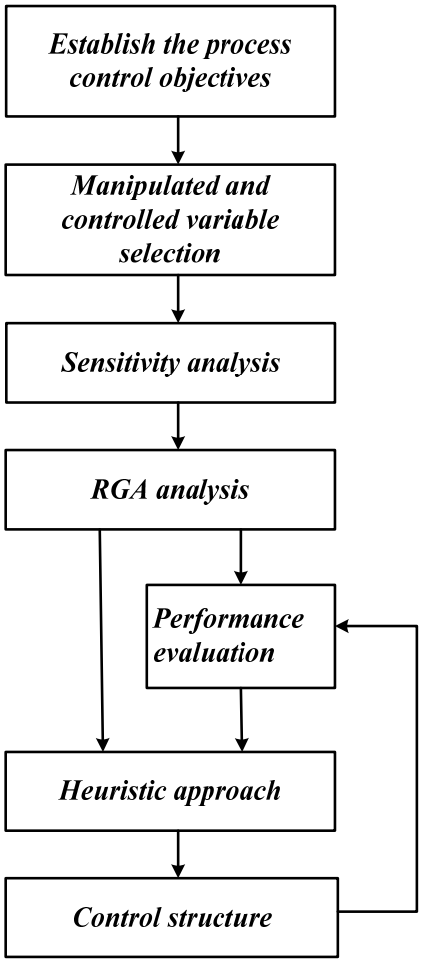

Figure A.1 Controllability analysis

A.2 Selection of control configurations and controller types

The control configuration is the arrangement of controllers implemented in a process plant, and an individual controller connects three components: final process element, measurement devices, and controlled variable set point. The control configuration depends on the control objective of particular plants. In the case that the interaction among control loops in a plant is insignificant, the *decentralized control configuration* is sufficient to maintain the controlled variables at their set points. Moreover, a plant may require the high accuracy and the optimisation of the operation, the *centralized control configuration* may be considered since it provides the optimal set point of a controlled variable using internal model calculation (Larsson and Skogestad, 2000; Seborg et al., 2011). However, the difficulty of dynamic model development for the centralized control configuration may be challenged to a modelling study.

That is, the decentralised control configuration is widely implemented in the industrial control system. The control system with the decentralised control configuration is consisted of multiple of independent feedback control loops and those manipulated variables which have been already used to control the given controlled variables should not be used to control other controlled variables (Skogestad and Postlethwaite, 2001). For the simplicity of the design of the process control in this study, the decentralised control system was implemented in both the pilot plant and the industrial-scale CO_2 absorption plant.

A.3 Selection of controller modes

Three basic control modes are proportional (P) controller, integral (I) controller, and derivative (D) controller. Proportional-integrate (PI) controller was implemented in every control loops in this work since it offers the elimination of the steady state error (offset) and fast time to reach a steady state condition after a change in the operating condition. The generic equation of PI-controller expresses as following equation:

$$M = \overline{M} + K_c \left(e + \frac{1}{\tau_I} \int e \ \mathrm{dt} \right) \tag{A.1}$$

where $\overline{M}$ denotes a value of manipulated variable at normal steady state, known as *bias*; M is a value of a control output i.e. the valve stem position is to be adjusted to obtain the desired liquid flow rate; e is an error of a set point between a controlled variable (CV_{SP}) and actual values of controlled variable (CV_{ACT}), $e = CV_{SP} - CV_{ACT}$; K_c is denoted as a controller gain. The tuning parameters K_c and τ_I were initially obtained using Internal Model Control (IMC) and then manually tuned to attain faster process responses. The implementation of PI controller into the mechanistic model in gPROMS can be written as following:

$$\begin{aligned} e &= CV_{SP} - CV_{ACT} \\ \frac{d}{dt}\tilde{e} &= \frac{e}{\tau_I} \\ M &= \overline{M} + K_c \left(e + \tilde{e} \right) \end{aligned} \tag{A.2}$$

The control parameters, i.e. $\overline{P}$, K_c, τ_I and CV_{SP} are to be specified. In the case of manipulated variable constraints, the upper and lower bounds of manipulated variables are involved in the mathematic model, i.e. the percentage of valve opening, which has the minimum value and the maximum value at zero and 100%, respectively; therefore, the implementation of valve constraint is to ensure that the computed controller output of the valve stem position should be in this acceptable range. Note that, to simplify the dynamic modelling in this study, the reset windup technique was not included in the PI controller. Furthermore, the proportional-integrate-derivative (PID) controller was not used since the implementation of PI controllers was able to handle different scenarios of changes in the operating condition and produced insignificant oscillating signal. Likewise, the estimation of the PID tuning parameters, especially derivative time constant (τ_D), is complex.

A.4 Tuning of controller parameters and multi-loop controls

The tuning is a method whereby the controller parameters, a controller gain (K_c) and an integral time constant (τ_I), are determined such that the plant's dynamic response to change in the operating condition is fast and smooth. Since the decentralised configuration was implemented in this work, the tuning parameters for a single loop were determined using Internal Model Control (IMC) method (Garcia and Morari, 1982). In addition, the tuning procedure for the multiloop controllers followed the sequential loop tuning method proposed by Hovd and Skogestad (1994) due to its simplicity and straightforwardness. The concept of the sequential loop tuning method is that only single pair is tuning at a time. The general procedure for the parameter tuning using in this work can be described as follows:

1) The sensitivity analysis is conducted to determine the relationship between potential controlled variables (CVs) and manipulated variables (MVs); as a result, the process gains (K_p) and the process time constants (τ_p) are obtained.
2) After the pairs of CVs and MVs are assigned, the tuning parameters, K_p and τ_p, for the first control loop were initially obtained using IMC method for PI controller, as described by Eq. A.3, and, practically, this first controller is the fastest control loop. For instance, this first controller to be added to a plant model is a level control loop, and the next controllers follow by the flow rate, temperature and composition control loops, respectively.

$$K_c K_p = \frac{\tau_p}{\tau_I} \tag{A.3}$$

3) This first controller, with tuning parameters obtained from IMC method, is implemented to the plant. For a preliminary test, the process disturbance is introduced to the plant, and the characteristic of process responses, i.e. time to reach the steady state, oscillating signal and offset, is observed. These tuning parameters are then manually tuned until fast and smooth process responses are attained.

4) The second controller with the tuning parameters determined by IMC approach is added to the plant model, and the manual tuning is conducted, as the description in Step 3.
5) The tuning parameters for remaining control loops are tuned as same method as Step 3.

A.5 Evaluation of the performance of the plant's control system

The performance of the plant's control system is defined by its dynamic process response to the variation in the operating condition. The control scheme which possesses the good performance is able to achieve the process control objectives and provides the fast and smooth transient fashion to reject disturbance and track controlled variables' set point. Likewise, the oscillation and offset are undesired. Therefore, the analysis of the closed loop system's performance in this study considered multiple scenarios to determine the promising control strategy for the MEA absorption processes for the CO_2 capture. Some of these scenarios have not been considered by previous works, i.e. the effect of the valve stiction on the CO_2 capture performance, the sinusoidal change in the flue gas composition, and the process scheduling of CO_2 removal varied with power demand.

Appendix B

Estimation of Flue Gas Flow Rate and Composition

The total flue gas flow rate is computed from the mass flow rate of coal which is calculated using Eq. 4.1 (Dowell and Shah, 2013) The assumptions made to calculate the flue gas flow rate are:

a) Pittsburgh #8 bituminous coal is a fossil fuel and its composition is shown in Table B.1.

b) Power plant efficiency is 40% (Dowell and Shah, 2013).

$$Q_e = \eta_{comb} m_{coal} HHV \tag{4.1}$$

Table B.1 Ultimate analysis of Pittsburgh#8 coal in dry basis (NETL,2012)

Composition (wt%)						**Heating value (kJ/kg)**	
C	H	O	S	N	Other[a]	HHV	LHV
75.13	5.1	6.39	2.42	1.5	9.46	31,331	30,238

[a] Other compositions are chlorine and ash

The air flow rate (which has the composition of 78.084 vol% N_2, 20.946 vol%O_2 and 0.97 vol% other components (Brimblecombe, 1986) required to produce the complete combustion reaction based on the coal combustion reaction as follows:

$$\begin{aligned} C + O_2 &\rightarrow CO_2 \\ H_2 + \frac{1}{2}O_2 &\rightarrow H_2O \\ S + O_2 &\rightarrow SO_2 \\ O + O &\rightarrow O_2 \end{aligned} \tag{B.1}$$

Assume that the sulfur dioxide (SO_2) in the flue gas stream leaving furnace is completely removed using the flue gas desulfurization (FGD) and the free water in the exhaust gas is removed by the scrubber unit prior to entering the absorber (see Fig.1.3). As a result, the mole fraction of water is 0.025 and no SO_2 is left in the dry flue gas flowing to the CO_2 capture plant. The flue gas molar flow rate and its composition are presented in Table B.2.

Table B.2 Flue gas flow rate and composition at base case conditions

Variable	Pilot plant	Industrial-scale plant
Coal flow rate	11.7 g/s	52 kg/s
Air flow rate required for complete combustion	4.07 mol/s	20.7 kmol/s
Flue gas flow rate leaving furnace	4.33 mol/s	21 kmol/s
Flue gas flow rate entering CO_2 absorber	4.01 mol/s	20 kmol/s
Mole fraction		
- CO_2	0.18	0.163
- H_2O	0.025	0.025
- N_2	0.795	0.792
- O_2	-	0.019

Appendix C

Stream Tables

Table C.1 Base case operating condition for a pilot plant with control structure B (closed-loop)

Stream	Phase	Flow rate (mol/s)	Temperature (K)	Pressure (kPa)	Mole fraction			
					CO_2	H_2O	MEA	N_2
1	Gas	4.01	319.7	103.5	0.180	0.025	-	0.795
2[a]	Liquid	32.0	314	103.5	0.027	0.874	0.099	-
3[a]	Liquid	32.6	328.7	103.5	0.048	0.855	0.097	-
4	Gas	3.4	314.1	101.3	0.007	0.066	6E-5	0.926
5	Liquid	32.6	350.5	160.0	0.048	0.855	0.097	-
6	Liquid	0.2	315.4	159.5	0.041	0.956	0.003	-
7	Liquid	35.3	380.5	160.0	0.030	0.880	0.090	-
8	Gas	3.4	388.5	160.0	0.059	0.939	0.002	-
9	Liquid	31.9	388.5	160.0	0.027	0.874	0.099	-
10	Liquid	31.9	366.5	160.0	0.027	0.874	0.099	-
11	Gas	0.9	351.6	159.5	0.758	0.242	6E-4	-
12	Gas	0.7	315.4	159.5	0.950	0.050	1E-6	-
13	Liquid	0.2	298	103.5	-	1	-	-
14	Liquid	2.1E-4	298	103.5	-	-	1	-

Table C.2 Key variables at the base case condition for a pilot plant (closed-loop)

Variable	Unit	Control structure		
		A	B	C
Energy required	GJ/tCO_2 captured	4.97	4.95	4.93
Lean MEA flow rate (entering absorber)	mol/s	32.3	32	31.8
L/G ratio (in absorber)	molLiquid/molGas	8.1	8.0	7.93
Lean loading (entering absorber)	molCO_2/molMEA	0.28	0.27	0.27
Rich loading (leaving absorber)	molCO_2/molMEA	0.49	0.49	0.49
%flood in an absorber	%	32.8%	32.7%	32.7%
%flood in a stripper	%	22.7%	22.7%	22.7%
Q_{reb}	MW_{th}	152.1	151.4	151.0
Q_{tank}	MW_{th}	159	156.5	155.1
Q_{cond}	MW_{th}	8.9	9.0	9.1
V1	%opening	30%	30.0%	30.1%
V2	%opening	49%	48.0%	47.7%
V3	%opening	49%	48.6%	48.3%

Table C.3 Base case operating condition for an industrial-scale CO_2 capture plant (close-loop) (34 m absorber bed height plant)

Stream	Phase	Flow rate (kmol/s)	Temperature (K)	Pressure (kPa)	Mole fraction				
					CO_2	H_2O	MEA	N_2	O_2
1	Gas	20.0	319.7	104.7	0.163	0.025	-	0.793	0.019
2	Gas	6.7	319.7	104.7	0.163	0.025	-	0.793	0.019
3	Gas	6.7	319.7	104.7	0.163	0.025	-	0.793	0.019
4	Gas	6.7	319.7	104.7	0.163	0.025	-	0.793	0.019
5[a]	Liquid	36.7	314.0	103.5	0.039	0.838	0.123	-	-
6[a]	Liquid	37.4	317.7	104.7	0.063	0.816	0.121	-	-
7[a]	Liquid	37.4	317.7	104.7	0.063	0.816	0.121	-	-
8[a]	Liquid	36.7	314.0	103.5	0.039	0.838	0.123	-	-
9	Gas	5.9	315.7	101.3	0.024	0.067	1E-4	0.887	0.022
10	Gas	5.9	315.7	101.3	0.024	0.067	1E-4	0.887	0.022
11	Gas	17.8	315.7	101.3	0.024	0.067	1E-4	0.887	0.022
12[a]	Liquid	36.7	314.0	103.5	0.039	0.838	0.123	-	-
13	Gas	5.9	315.7	101.3	0.024	0.067	1E-4	0.887	0.022
14[a]	Liquid	37.4	317.7	104.7	0.063	0.816	0.121	-	-
15	Liquid	112.2	317.7	104.7	0.063	0.816	0.121	-	-
16	Liquid	112.2	353.7	104.7	0.063	0.816	0.121	-	-
17	Liquid	109.3	352.3	160.0	0.039	0.837	0.125	-	-
18	Liquid	109.3	388.7	160.0	0.039	0.837	0.124	-	-
19	Liquid	56.1	353.7	104.7	0.063	0.816	0.121	-	-
20	Liquid	56.1	353.7	104.7	0.063	0.816	0.121	-	-
21	Liquid	0.4	310.0	103.5	0.043	0.953	0.004	-	-
22	Gas	1.8	352.4	103.5	0.776	0.022	8E-4	-	-
23	Gas	1.5	310.0	103.5	0.963	0.037	1E-6	-	-
24	Gas	5.3	388.7	160.0	0.098	0.899	0.003	-	-
25	Liquid	60	375.7	160.0	0.044	0.842	0.114	-	-
26	Liquid	54.7	388.7	160.0	0.039	0.837	0.124	-	-
27	Gas	1.8	352.4	103.5	0.776	0.022	8E-4	-	-
28	Gas	1.5	310.0	103.5	0.963	0.037	1E-6	-	-
29	Liquid	0.4	310.0	103.5	0.043	0.953	0.004	-	-
30	Liquid	60	375.7	160.0	0.044	0.842	0.114	-	-
31	Gas	5.3	388.7	160.0	0.098	0.899	0.003	-	-
32	Liquid	54.7	388.7	160.0	0.039	0.837	0.124	-	-
33[a]	Liquid	110.1	314.0	103.5	0.039	0.838	0.123	-	-
34	Liquid	0.8	298.0	103.5	-	1	-	-	-
35	Liquid	0.002	298.0	103.5	-	-	1	-	-

[a] The lean loading is 0.32 whereas the rich loading is 0.52.

Table C.4 Key variables at the base case condition for an industrial-scale CO_2 capture plant (34 m absorber bed height plant)

Variable	Value
Power plant	
Power plant size	750 MWgross
Power generation at the base case condition	650 MWgross
Overall plant efficiency	40%
Pittsburgh#8 bituminous coal flow rate	52 kg/s
CO_2 emissions	790 $kgCO_2$/ kW
CO_2 emission rate (without CO_2 capture plant)	12,340 tCO_2/day
CO_2 emission rate (with CO_2 capture plant)	1,600 tCO_2/day
CO_2 capture plant	
Flue gas flow rate (entering CO_2 capture plant)	20 kmol/s (620 kg/s)
Energy required	4.1 GJ/tCO_2 captured
%CC	87%
CO_2 purity	96.3%
Lean MEA flow rate	110 kmol/s (2,500 kg/s)
L/G ratio (entering an absorber)	5.5 molLiquid/molGas
Lean loading	0.32 molCO_2/molMEA
Rich loading	0.52 molCO_2/molMEA
%flood in an absorber	65%
%flood in a stripper	62%
Reboiler temperature	388.7 K (116°C)
Condenser temperature	310 K (37°C)
Manipulated variables	
Q_{reb} per a reboiler	256.3 MW_{th}
Q_{tank}	407.6 MW_{th}
Q_{cond} per a condenser	17.8 MW_{th}
V13,23,33	45% opening
V42,52	37% opening
V60	30% opening